University of Alberta

Isotope Effects in High Temperature Superconductors and Related Materials

by

David Dickson Lawrie ©

A thesis
submitted to the Faculty of Graduate Studies and Research in partial fulfillment
of the requirements for the degree of
Doctor of Philosophy

Department of Physics

Edmonton, Alberta

Fall 1999

National Library of Canada
Acquisitions and Bibliographic Services
395 Wellington Street
Ottawa ON K1A 0N4
Canada

Bibliothèque nationale du Canada
Acquisitions et services bibliographiques
395, rue Wellington
Ottawa ON K1A 0N4
Canada

Your file Votre référence

Our file Notre référence

The author has granted a non-exclusive licence allowing the National Library of Canada to reproduce, loan, distribute or sell copies of this thesis in microform, paper or electronic formats.

L'auteur a accordé une licence non exclusive permettant à la Bibliothèque nationale du Canada de reproduire, prêter, distribuer ou vendre des copies de cette thèse sous la forme de microfiche/film, de reproduction sur papier ou sur format électronique.

The author retains ownership of the copyright in this thesis. Neither the thesis nor substantial extracts from it may be printed or otherwise reproduced without the author's permission.

L'auteur conserve la propriété du droit d'auteur qui protège cette thèse. Ni la thèse ni des extraits substantiels de celle-ci ne doivent être imprimés ou autrement reproduits sans son autorisation.

0-612-46870-4

Canada

University of Alberta

Library Release Form

Name of Author:	David Dickson Lawrie
Title of Thesis:	Isotope Effects in High Temperature Superconductors and Related Materials
Degree:	Doctor of Philosophy
Year this Degree Granted:	1999

Permission is hereby granted to the University of Alberta Library to reproduce single copies of this thesis and to lend or sell such copies for private, scholarly, or scientific research purposes only.

The author reserves all other publication and other rights in association with the copyright in the thesis, and except as hereinbefore provided, neither the thesis nor any substantial portion thereof may be printed or otherwise reproduced in any material form whatever without the author's prior written permission.

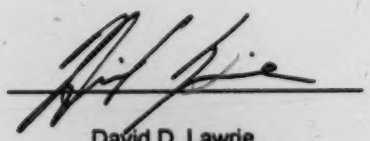

David D. Lawrie
301 10556 84 Ave.
Edmonton, Alberta
Canada T6E 2H4

Date: July 22, 1999

University of Alberta

Faculty of Graduate Studies and Research

The undersigned certify that they have read, and recommend to the Faculty of Graduate Studies and Research for acceptance, a thesis entitled **Isotope Effects in High Temperature Superconductors and Related Materials** submitted by David Dickson Lawrie in partial fulfillment of the requirements for the degree of Doctor of Philosophy.

Dr. J.P. Franck (Supervisor)

Dr. J.R. Beamish

Dr. P.C. Canfield

Dr. J. Jung

Dr. A. Mar

Dr. F. Marsiglio

Date: July 14, 1999

Acknowledgements

I wish to express my deep gratitude to all those who made it possible for me to complete this research. The two parties most responsible, and deserving of my greatest thanks, are; Professor Jurgen Franck for his continued support and direction (even after "retirement"); and my parents, Henry & Shirley Lawrie, for their unfailing support, and for (ultimately) making the entire endeavor possible in the first place.

I would like to thank Kevin Hewitt and Prof. J.C. Irwin of Simon Fraser University for their Raman work.

Special thanks are given for the invaluable technical support and assistance provided by the excellent technical staff at the University of Alberta. My deepest thanks to Mr. Don Mullin, Mr. Ken Marsh, Mr. Tony Walford, Mrs. Yolande Peske and Mr. Steve Rogers. A special thanks to Mr. Richard Tomski for his help with the borocarbide work.

During the course of this research, I received financial support in the form of Province of Alberta Graduate Fellowships and a Dissertation Fellowship. Acknowledgement is gratefully made, and much appreciated.

Finally, I would like to thank all those teachers, instructors and friends who, over the years, have made it all possible.

Abstract

This thesis examines isotope effects in four different materials. Two of the investigations deal with High Temperature Superconductors (HTSCs), specifically the copper isotope effect (^{63}Cu / ^{65}Cu) on T_c in oxygen deficient $YBa_2Cu_3O_{7-\delta}$ and the oxygen isotope effect (^{16}O / ^{18}O) on T_c in $Bi_2Sr_2CaCu_2O_{8+y}$ as a function of oxygen content, y. The importance of Cu-O planes and antiferromagnetic fluctuations in HTSCs leads to a search for isotope effects (both copper and oxygen) on the magnetic ordering temperatures of CuO. The fourth investigation concerns boron and carbon isotope effects on T_c in Ni and Pd based borocarbide superconductors.

A brief introduction outlines some of the common properties of HTSCs and a sketch of the conventional theory concerning isotope effects in superconductors is given. Practical aspects of isotope effect experiments are discussed. The importance of sample preparation and characterization are emphasized. Background information is given for each material followed by a description of the experimental process and a summary of results.

The investigation on the borocarbides shows clear evidence of a boron isotope effect in both YNi_2B_2C ($\alpha_B = 0.26 \pm 0.03$) and YPd_2B_2C ($\alpha_B = 0.32 \pm 0.04$). Results for a carbon isotope effect are suggestive for YNi_2B_2C ($\alpha_C = 0.07 \pm 0.06$), but essentially at the limit of experimental accuracy.

Isotopically enriched samples of ^{63}CuO, ^{65}CuO, $Cu^{16}O$ and $Cu^{18}O$ showed no difference in either Néel temperature within experimental uncertainty.

Results for $\alpha_{Cu}(\delta)$ in $YBa_2Cu_3O_{7-\delta}$ for $0.06 \leq \delta \lesssim 0.60$ show that it is zero at optimal doping ($\delta = 0.06$) and negative ($T_c(^{65}Cu) > T_c(^{63}Cu)$) for all other values of δ. It is a non-monotonic function of δ, showing large negative values away from the 60 K plateau and smaller values in the plateau ($0.35 < \delta < 0.45$).

Oxygen content (y) in $Bi_2Sr_2CaCu_2O_{8+y}$ was determined by iodometric titration. A wide variation was encountered in the data, but for several samples with identical y values, α_O is small (< 0.1) and positive, in both the over ($y \approx 0.24$) and under ($y \approx 0.10$) doped regions.

Table of Contents

Chapter 1	1.1	Introduction	1
	1.2	Organization of Thesis	4
Chapter 2	The Physics of the Isotope Effect in Superconductors		5
	2.1	Introduction	5
	2.2	BCS Theory and Extensions	7
	2.3	Summary for Chapter 2	10
Chapter 3	Practical Aspects of Isotope Effect Experiments		11
	3.1	Primary Considerations	11
	3.2	Sample Preparation	12
	3.3	Sample Measurement and Characterization	15
	3.4	Summary for Chapter 3	19
Chapter 4	Borocarbides		19
	4.1	Background	19
	4.2	Experiment	22
	4.3	Results	24
	4.4	Discussion	32
	4.5	Summary for Chapter 4	33
Chapter 5	Copper Oxide		34
	5.1	Background	34
	5.2	Experiment	36
	5.3	Results	37
	5.4	Discussion	40
	5.5	Summary for Chapter 5	41
Chapter 6	Cu Isotope Effect in Oxygen Deficient YBCO		42
	6.1	Background	42
	6.2	Experiment	45
	6.3	Results	47
	6.4	Discussion	56
	6.5	Summary for Chapter 6	60
Chapter 7	Oxygen isotope effect in $Bi_2Sr_2CaCu_2O_{8+y}$		61
	7.1	Background	61
	7.2	Experiment	65
	7.3	Results	71
	7.4	Discussion	77
	7.5	Summary for Chapter 7	80
Chapter 8	8.1	Final Discussion	81
	8.2	Conclusions	83
Bibliography			84
Appendix			90

List of Tables

Table	Title	Page
4.2.1	Borocarbide starting materials.	22
4.2.2	Isotopic composition of Ni borocarbide samples.	23
4.2.3	Isotopic composition of Pd borocarbide samples.	23
4.3.1	Average T_c values for YNi_2B_2C.	28
4.3.2	Average T_c values for YPd_2B_2C.	28
4.3.3	Isotope exponents in YNi_2B_2C.	29
4.3.4	Isotope exponents in YPd_2B_2C.	30
4.3.5	Lattice constants for YNi_2B_2C and YPd_2B_2C. All values in Ångstroms and are the average for 3 samples. Uncertainties are the maximum deviation from the mean.	30
4.4.1	Scaling of α_B with T_c.	32
4.4.2	Correlation between T_c and Bond Angle.	33
5.3.1	Observed values for T_{N1} and T_{N2}.	40
6.1.1	Cu and Ba Isotope Exponents in YBCO	44
6.3.1	Pair 2 $T_c(\infty)$ values for different storage temperatures.	47
6.3.2	Isotopic shifts for Pair 1.	54
6.3.3	Isotopic shifts for Pair 2.	54
6.4.4	Fitting parameters for $T_c(\delta) = a\delta^4 + b\delta^3 + c\delta^2 + d\delta + e$	57
7.1.1	Oxygen Isotope Effect results in the BSCCO system	62
7.2.1	BSCCO annealing conditions.	65
7.2.2	Isotopic substitution determined from Raman measurements.	69
7.3.1	BSCCO results after first oxygenation.	72
7.3.2	BSCCO results after second oxygenation.	73
7.3.3	BSCCO results after third oxygenation.	73
7.3.4	BSCCO results after first reduction.	73
7.3.5	BSCCO results after second reduction.	73

Table	Title	Page
7.3.6	HBO reduction results.	74
7.3.7	Averaged results for three identical oxygenations.	74
7.3.8	Summary of T_c and y values.	75
7.4.1	Observed values of Δy and ΔT_c.	77
7.4.2	Expected Δy and ΔT_c correlation.	77
7.4.3	Oxygen isotope exponents.	78
7.4.4	Fitting parameters.	79
A.1	Titration I – Raw Data	96
A.2	Titration II – Raw Data	96
A.3	Calculation of y.	97
A.4	CuO Standardization Data.	97

List of Figures

Figure	Caption	Page
1.1.1	Generalized HTSC Structure.	2
1.1.2	Phase Diagram for $YBa_2Cu_3O_{7-\delta}$ (adapted from Burns, 1992).	3
1.1.3	Schematic of Reduced $T_c = T_c/T_{c\,max}$ versus hole concentration.	3
3.2.1	Schematic of Oxygen Isotope Exchange System (OIES) (single channel).	14
3.2.2	4-Probe resistance set up.	16
3.2.3	Model of Raman peak for 60 % ^{18}O substitution. The total intensity curve has been shifted up slightly for clarity.	18
3.2.4	Raman measurements of BSCCO 2212 (sample set HBI – see chapter 7). Upper curve, ^{16}O, lower curve ^{18}O. Clearly there is no isotopic splitting observable in any of the shifted peaks.	18
4.1.1	Crystal structure of YNi_2B_2C. (Adapted from Lynn, 1997).	20
4.3.1	Typical susceptibility measurement for annealed YNi_2B_2C.	24
4.3.2	Enlargement of figure 4.3.1, showing the transition region.	24
4.3.3	Effect of annealing on the susceptibility of $YNi_2{}^{10}B_2C$.	25
4.3.4	Effect of annealing on the susceptibility of $YNi_2{}^{11}B_2C$.	25
4.3.5	Typical susceptibility measurement for YPd_2B_2C.	26
4.3.6	Enlargement of figure 4.3.5, showing the transition region.	26
4.3.7	Resistivity curves for $YPd_2{}^{10}B_2C$ and $YPd_2{}^{11}B_2C$.	27
4.3.8	Enlargement of figure 4.3.7, showing the transition.	27
4.3.9	Double logarithmic plot of Tc versus B mass for YNi_2B_2C. The lines are least squares fits to the data, with slopes equal to α_B. Upper points (squares) are annealed samples, lower (circles) are unannealed.	29
4.3.10	Double logarithmic plot of Tc versus B mass for YPd_2B_2C. The lines are least squares fits to the data, with slope equal to α_B.	30
4.3.11	Typical powder x-ray diffraction pattern for YNi_2B_2C showing peak assignments used in lattice constant determination.	31
4.3.12	Typical powder x-ray diffraction pattern for $YPd_5B_3C_{0.3}$ showing strong evidence of multiple phases.	31
5.1.1	Crystal structure of CuO (adapted from Yang *et al.*, 1989)	34

Figure	Caption	Page
5.1.2	Spin alignment in the commensurate (left) and incommensurate (right) phases. Projection is along the b axis, open (closed) circles are Cu in the ¼ b (3/4 b) plane. See text for an explanation of the arrows. Modified from Forsyth *et al.*, 1988)	35
5.3.1	Typical magnetic susceptibility for a sintered powder sample of CuO measured in 3 T.	37
5.3.2	Susceptibility of an oriented CuO single crystal measured in 3 T.	37
5.3.3	T_{N1} for oxygen isotope samples.	38
5.3.4	T_{N2} for oxygen isotope samples.	38
5.3.5	T_{N1} for Cu isotopes in 3 T.	39
5.3.6	T_{N2} for Cu isotopes in 3 T.	39
6.1.1	Structure of $YBa_2Cu_3O_{7-\delta}$ (YBCO). The structure shown has $\delta = 0$, see text. This figure neglects the buckling of the CuO planes.	42
6.1.2	Oxygen isotope ($^{16}O/^{18}O$) effect in YBCO as a function of T_c for various types of doping. References: Intrinsic (see text) – Zech *et al.* (1996); Fe – Bomnemann *et al.* (1991 & 1993); Zn – Franck *et al.* (1991 & 1992); Ni – Bomnemann *et al.* (1991); Pr – Franck *et al.* (1991); La – Bomnemann and Morris (1991).	43
6.3.1	Time dependence of T_c for Pair 2. The lines are fits to the relation of Veal et al., 1990.	47
6.3.2	Normalized Field Cooled Magnetization for Pair 1 prior to oxygen depletion. Upper – Full temperature range. Lower – Enlargement showing the transition.	48
6.3.3	Normalized Field Cooled Magnetization for Pair 1, oxygen depleted $\delta = 0.30$. Upper – Full temperature range. Lower – Enlargement showing the transition.	49
6.3.4	Normalized Field Cooled Magnetization for Pair 1 after re-oxygenation. Upper – Full temperature range. Lower – Enlargement showing the transition.	50
6.3.5	Normalized Field Cooled Magnetization for Pair 2 prior to oxygen depletion. Upper – Full temperature range. Lower – Enlargement showing the transition.	51
6.3.6	Normalized Field Cooled Magnetization for Pair 2, oxygen depleted $\delta = 0.44$. Upper – Full temperature range. Lower – Enlargement showing the transition.	52
6.3.7	Normalized Field Cooled Magnetization for Pair 2 after re-oxygenation. Upper – Full temperature range. Lower – Enlargement showing the transition.	53
6.3.8	T_c as a function of δ for both sample pairs. The lines are 4^{th} order polynomial fits to the data for the purpose of estimating $dT_c/d\delta$, see text. The solid square is the overlap of the two symbols.	55

Figure	Caption	Page
6.3.9	α_{Cu} as a function of δ for the two sample pairs. The solid square is the overlap of the two symbols.	55
6.4.1	α_{Cu} compared with $dT_c(\delta)/d\delta$. left – pair 1, right –pair 2. The solid lines $dT_c(\delta)/d\delta$ are (see text for units), derived from the polynomial fits of figure 6.3.8.	56
6.4.2	$\partial \ln T_c / \partial \ln \delta$ as a function of δ based on fits to $T_c(\delta)$.	58
6.4.3	Reproduction of figure 6.3.9 with data of Zhao *et al.* (1996) added for comparison.	59
7.1.1	Structure of BSCCO 2212 (Adapted from Martin and Lee, 1995)	61
7.1.2	T_c as a function of y in $Bi_2Sr_2CaCu_2O_{8+y}$. Data are from Allgeier *et al.*, (1990). The line is a fit to the data, see text.	63
7.1.3	Changes in T_c due to changes in y as a function of y in $Bi_2Sr_2CaCu_2O_{8+y}$.	63
7.2.1	X-ray powder diffraction spectra comparison of samples before (As received) and after oxygenation at 600 °C for 36 hours (HBG samples). Arrows indicate diffraction peaks appearing as a result of the treatment. All peaks in the as received spectra can be indexed to BSCCO 2212.	67
7.2.2	X-ray powder diffraction spectra comparison of samples before (As received) and after oxygenation at 350 °C for 48 hours (HBI samples). Arrows, indicating new peaks due to the high temperature treatment are in the same positions as in figure 7.2.1. In contrast to the 600 °C treatment, the 350 °C treatment does not cause any perceptible change to the diffraction spectra.	68
7.3.1	Typical BSCCO normalized FC susceptibility HBQ*02 samples).	71
7.3.2	T_c as a function of y in $Bi_2Sr_2CaCu_2O_{8+y}$, as measured in this investigation. Squares – ^{16}O samples, circles – ^{18}O samples. The solid line is the fit to the data of Allgeier *et al.* from figure 7.1.2.	76
7.4.1	Fits to the data of table 7.3.8. Upper curve and squares ^{16}O, lower curve and circles – ^{18}O.	78
A.1	Inert Atmosphere System (IAS) used for titrations.	91

Chapter I

1.1 Introduction

The term isotope effect in general refers to the change in a physical property of a material when one isotope is substituted for another. For example, both the boiling and freezing points of water change when deuterium is substituted for hydrogen. "Normal" water (H_2O) boils at 100.00 °C and freezes at 0.00 °C, while heavy water (D_2O) boils at 101.42 °C and freezes at 3.82 °C at standard atmospheric pressure (Handbook of Chemistry and Physics). The chemical properties are identical, but the physical properties differ slightly, simply due to the different mass of some of the constituent atoms. Any theory of the physical process involved (melting or freezing in this example) must account for this mass dependence. The reverse is also true; the existence of an isotope effect in a given property provides information about the physical processes responsible for that property. Isotope effects can thus be used as sensitive probes of the underlying physics of various phenomena.

A certain class of materials when cooled below a certain critical temperature (the transition temperature T_c – c for critical) undergo an abrupt change in their electromagnetic properties. The most dramatic perhaps being the complete loss of all electrical resistance, hence the name superconductor. Many (but not all) superconductors exhibit an isotope effect in T_c, most commonly the heavier isotope material having a lower T_c. The observation of an isotope effect in mercury (Maxwell, 1950 and Reynolds *et al.*, 1950) proved to be of crucial importance to the development of a theory of superconductivity. The isotope effect is now used as a probe of the underlying physics of superconductors, and one of the important questions to be answered about a newly discovered of a new superconductor is if there is an isotope effect, and if so, how large?

The field of superconductivity research has undergone remarkably explosive growth in the past 13 years. Prior to 1986, the Bardeen-Cooper-Schrieffer (BCS) and Ginzburg-Landau (GL) theories together provided a "remarkably complete and satisfactory picture" of superconductivity (Tinkham, 1996).

This changed with the 1986 paper by Bednorz and Müller suggesting the possibility of superconductivity in the La-Ba-Cu oxide system. Subsequent work (Bednorz *et al.* 1987, Takagi *et al.* 1987, Uchida *et al.* 1987) confirmed superconductivity in the compound $La_{(2-x)}Sr_xCuO_4$, with a transition temperature (T_c) of 38 K, more than 10 K higher than any material known to that time. New materials with even higher T_c values were soon found. The discovery of superconductivity in Y-Ba-Cu-O compounds (Wu *et al.* 1987, Hikami *et al.* 1987, Zhao *et al.* 1987) and other systems with T_c occurring above the boiling point of liquid nitrogen radically altered the situation and created intense interest. First, from a theoretical point of view, it was (and still is) unclear if these remarkably high transition temperatures are compatible with conventional BCS theory or its extensions. Second, a T_c at or above liquid nitrogen temperatures may allow the application of superconductivity in situations that would be totally impractical if liquid helium temperatures were required. Finally, if T_c values as high as 125 K can be obtained (Sheng *et al.* 1988), what is the upper limit? These "new" materials are collectively known as high temperature superconductors (HTSCs) and the field of HTSC research is currently one of the largest and most vigorous areas of condensed matter physics research.

Thirteen years after the original discovery a remarkably large number of new materials (with similar or even higher) transition temperatures have been discovered, but there are a surprising number of fundamental questions that remain unanswered. Perhaps the most basic is the question of the mechanism responsible for superconductivity at such high temperatures. Isotope effect studies are one method of probing this mechanism. A number of experimental

investigations have looked at isotope effects in HTSCs (See the extensive review by Franck, 1994), and it is generally found that there is a small but non-zero effect, at least for oxygen, in optimally doped materials. This thesis examines isotope effects in a number of HTSCs and related materials. Before discussing the goals of this investigation, it is worthwhile to mention some of the common properties of the HTSC materials.

The defining property of the HTSC materials is that they all contain copper and oxygen (Some recently discovered materials, such as the Sr-Ru-O superconductors (Maeno *et al.* 1994), which do not contain copper, may also fall into the HTSC category, but this is uncertain at present). As a result, they are often referred to as cuprate superconductors. In the simplest case, the copper atoms are arranged in a square planar configuration, surrounded by four oxygen atoms, and form distinct Cu-O sheets or planes. The Cu-O bond distance is relatively short (≈ 1.9 Å). These planes are parallel to the a–b plane, and there may be anywhere from one to three in the unit cell of a particular material (referred to as n = 1, 2 or 3). In materials with only one plane (i.e. $La_{(2-x)}Sr_xCuO_4$ or $Bi_2Sr_2CuO_{6+y}$) adjacent planes are separated by about 6.6 Å by a metal oxide layer (i.e. LaO_2), referred to as the charge reservoir layer. Materials with two (i.e. $YBa_2Cu_3O_{7-\delta}$) or three (i.e. $Bi_2Sr_2Ca_2Cu_3O_{10+y}$) Cu-O planes have adjacent planes separated by about 3.2 Å by a sparsely populated Y or Ca layer. These structures are shown schematically in figure 1.1.1. This is a simplified description and numerous complications occur, the most common being an orthorhombic distortion with b > a. In addition, the planes need not be flat, but may be slightly buckled (O atoms displaced along the c direction).

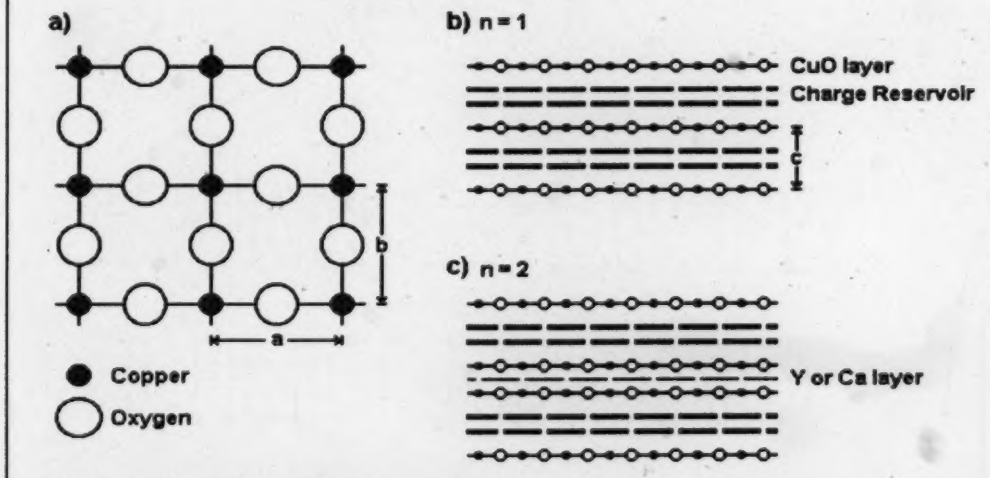

Figure 1.1.1 Generalized HTSC Structure.

a). Cu-O Plane. b). n = 1 structure ($La_{(2-x)}Sr_xCuO_4$) c). n = 2 structure ($YBa_2Cu_3O_{7-\delta}$).

A significant feature of superconductivity in these materials is that it shows a limited existence range in terms of composition. It is generally necessary to dope the starting material in some way in order to induce superconductivity. The parent or undoped materials are antiferromagnetic insulators. Hole doping, for example the replacement of La^{3+} by Sr^{2+} in La_2CuO_4, results in a deficiency of positive charge required for electrical neutrality (assuming the oxygen content and valence remains unchanged). The result is the creation of Cu^{3+} (hole) in the Cu-O layers. This positive charge is not localized to any particular Cu site and the Cu-O planes therefore become conducting. The Sr is located in the metal oxide layer separating the Cu-O planes, and electrons are transferred from the Cu-O planes into these layers. These metal oxide layers are therefore referred to as charge reservoirs.

Doping may also be achieved by alteration of the total oxygen content. For example, strict charge balance in $Bi_2Sr_2CaCu_2O_{8+y}$ (with Bi^{3+}) requires y =0, and this material is an AF insulator. The incorporation of a slight oxygen excess ($y \approx 0.15$) gives a superconductor with $T_c \approx$ 90 K. This excess oxygen is incorporated into the Bi-O layers separating the CuO planes (Bordet *et al*, 1988). A similar situation occurs in $YBa_2Cu_3O_{7-\delta}$ but the situation is more complicated in this case as the charge reservoir layer also includes Cu. There are two crystallographically inequivalent Cu sites, the usual plane sites[1] and "chain" sites (so named because these Cu, located in the charge reservoir layers, form one dimensional Cu-O chains parallel to the b-axis). Excess oxygen is still found only in the charge reservoir layer.

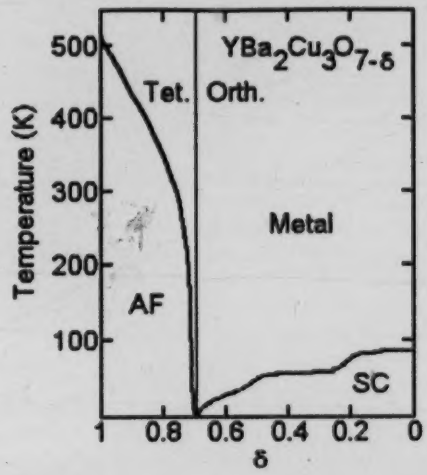

Figure 1.1.2 Phase diagram for $YBa_2Cu_3O_{7-\delta}$ (adapted from Burns (1992)).

These features are illustrated in the phase diagram shown in figure 1.1.2 for $YBa_2Cu_3O_{7-\delta}$. The abbreviations Tet. (tetragonal) and Orth. (orthorhombic) refer to the crystal structure. AF indicates the antiferromagnetic insulating phase and SC the superconducting phase. As can be seen from the figure, the boundary between the normal and superconducting states is not a simple function of doping. T_c is a maximum for δ = 0.06 (not apparent in the figure due to the scale) drops rapidly around δ = 0.2 to around 60 K, and remains at this value over a relatively large range of δ. Further increases in δ beyond about 0.5 lead to a second drop, and the material becomes an insulator for $\delta \geq 0.7$ or so. The cause of this behaviour is believed to be related to oxygen ordering in the material. More will be said in this regard in chapter 6, where the Cu isotope effect as a function of δ is discussed.

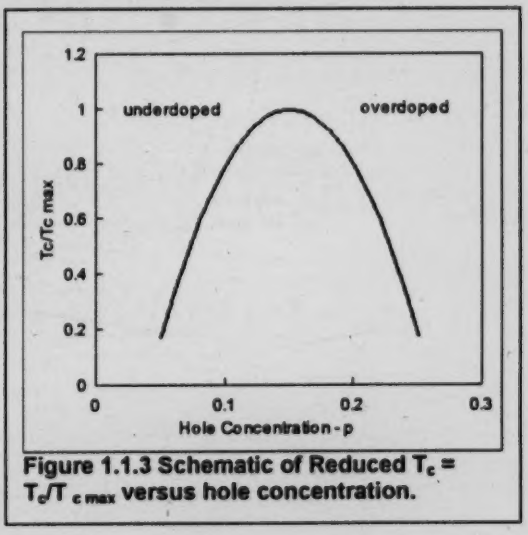

Figure 1.1.3 Schematic of Reduced T_c = $T_c/T_{c\,max}$ versus hole concentration.

The highest values of T_c are obtained at a particular level of doping. Materials with doping levels above or below this optimum value are referred to as over and under doped respectively. It has been shown by a number of workers (e.g. Tallon

[1] There are actually 3 crystallographically inequivalent Cu sites in YBCO, the chain sites and 2 different plane sites. The difference between the two plane sites is minimal compared to the chain site and is neglected here for simplicity.

et al. (1995)) that there is a universal relationship between T_c and the hole concentration (p) in the Cu-O planes, with optimum T_c values occurring at $p \approx 0.15$. The situation is illustrated schematically in figure 1.1.3. This may appear inconsistent with figure 1.1.2, where T_c does not appear to decrease noticeably with increasing δ, but it is not. In YBCO, it is not experimentally possible to introduce oxygen into the structure much above $\delta = 0$ (i.e. negative δ values), hence the overdoped region cannot be reached simply by increasing the O content. Replacement of Y(3+) by Ca (2+) is believed to be equivalent to overdoping (Tokura *et al.* 1988) and increasing amounts of Ca do result in a drop of T_c, giving a parabolic dependence (neglecting the "60 K plateau" on the underdoped side) (Tallon *et al.* 1995). See also figure 7.1.2, T_c as a function of y in $Bi_2Sr_2CaCu_2O_{8+y}$, where this dependence is more clearly shown.

There is no consensus at present as to why this hole concentration ($p = 0.15$) produces the highest T_c values, but this universal dependence seems to be a tantalizing clue to the underlying physics of these materials. As a result, a number of properties have been investigated as a function of doping in a number of different materials. (See the series "Physical Properties of High Temperature Superconductors" edited by D.M. Ginsburg for a number of review articles concerning these investigations). The isotope effect on T_c has been investigated as a function of doping for only a few materials. (See the review by Franck in Physical Properties of High Temperature Superconductors IV (1994)).

This investigation examines four different materials. The primary goal of the investigation is the elucidation of the behaviour of the copper isotope effect ($^{63}Cu/^{65}Cu$) in $YBa_2Cu_3O_{7-\delta}$ and the oxygen isotope effect ($^{16}O/^{18}O$) in $Bi_2Sr_2CaCu_2O_{8+y}$ as a function of hole concentration. In both cases, the hole concentration is controlled by variation of the total oxygen content (δ or y), rather than chemical substitution of some species (i.e. Y for Ca in YBCO (Tokura *et al.* 1988)). An additional goal of the investigation is the determination of B ($^{10}B/^{11}B$) and C ($^{12}C/^{13}C$) isotope effects in the recently discovered (Nagarajan *et al.* (1994) and Cava *et al.* (1994)) borocarbide superconductors. At the time this portion if the investigation was begun (February 1994) there had been no isotope work done on these materials and the existence of an isotope effect was an open question. Finally, the investigation the possibility of copper or oxygen isotope effects in the fourth material, CuO, was undertaken due to the importance of Cu-O planes in the HTSC materials.

1.2 Organization of Thesis

Physically this thesis is divided into 8 chapters. In terms of content, it may be divided into four main sections. In the first I will outline the physics underlying the isotope effect in superconductors (chapter 2). In the second I will discuss some of the practical subtleties involved in isotope effect experiments (chapter 3). The third section presents the specific experimental investigations of the four materials examined (chapters 4 to 7). Each chapter in this section begins with a short background of the material and a review of previous isotope effect work. This is followed by an outline of the experimental procedure, typical data, results and discussion and ends with a brief summary. The order chosen is semi-chronological, but also reflects the increasing complexity of the investigations. In the final chapter I present an overall summary of results and a discussion of their similarities and differences. An appendix is included that discusses the use of iodometric titrations for the determination of oxygen (hole) content.

Chapter 2

Physics of the Isotope Effect in Superconductors

2.1 Introduction

In this chapter I first give a brief historical overview of the development of BCS theory and its extensions, showing the importance of the observation of isotope effects. Definitions relevant to the discussion of isotope effects are then given. The second section examines various theoretical predictions for isotope exponents.

Although H. Kamerlingh Onnes first discovered superconductivity in 1911, more than 40 years passed before a thorough theoretical understanding of the phenomenon was achieved. Progress was made in 1950 with the suggestion of Fröhlich, and independently Bardeen, that lattice vibrations might play a significant role in superconductivity. Experimental work by Maxwell and independently by Reynolds *et al.* in the same year demonstrated an isotope effect in T_c for mercury, confirming this suggestion. Fröhlich's model involved the exchange of virtual phonons by electrons moving through the crystal lattice. This exchange leads to an interaction between electrons that can be attractive. In 1956, Cooper showed that a Fermi sea of electrons is unstable with regard to the formation of bound pairs of electrons (Cooper Pairs) if there is some type of attractive interaction, regardless of how weak, between the electrons.

These ideas culminated in 1957 with the theory of Bardeen, Cooper and Schrieffer. In this theory, electrons are considered to interact via the exchange of virtual phonons, and this leads to pairing. These pairs condense to form a ground state that is separated by an energy gap from excited states. It is this ground state that is identified with the superconducting state. The BCS theory was a triumph. It provided a microscopic picture of superconductivity and a number of predictions that were in excellent agreement with experimental observations. It accounts for the observed isotope effects in many materials. A principal reason for the success of BCS theory is its use of the weak coupling assumption (see below), which allowed predictions of material independent properties of the superconducting state.

Deviations from BCS were soon found for several materials, for example the critical field of mercury and lead (Phillips, 1959 and Finnemore *et al.*, 1960) and the absence of an isotope effect in ruthenium (Geballe *et al.*, 1961) and zirconium (Bucher *et al.*, 1965). These observations combined with work on the electron-phonon interaction in the normal state (Migdal, 1958) led to the development of the theory of strong-coupled superconductors.

Eliashberg theory (1960, 1961) treats the retarded nature of the electron phonon interaction and the damping (finite lifetime) of quasi-particle excited states. The phonon density of states enters explicitly in this formulation. This theory, while much more complicated than the original BCS approach, can convincingly account for a number of the observed deviations. Unfortunately, due to the specific inclusion of the phonon structure, theories which try to go beyond the weak coupling approximation do not allow general predictions of superconducting properties, as in weak coupled BCS (which is derivable as a limiting case). The best one can do is to make predictions for given classes of closely related materials.

Before discussing the aspects of the BCS theory and its extensions relevant to isotope effects, some definitions are needed. As noted, it has been shown experimentally that T_c is proportional to the isotopic mass, M, and is conventionally expressed as

$$T_c \propto M^{-\alpha}, \tag{2.1.1}$$

where α is known as the isotope exponent. α is therefore defined as

$$\alpha = -\frac{d(\ln T_c)}{d(\ln M)} = -\frac{\Delta(\ln T_c)}{\Delta(\ln M)}. \tag{2.1.2}$$

The final term in 2.1.2 is the experimental definition of α, where Δ refers to finite differences in T_c and M. This expression is appropriate only for elemental superconductors, where there is only one chemical species. If more than one isotope is present in a sample, M is interpreted as the average atomic mass.

Partial isotope exponents, α_i, are defined for componds or alloys as

$$\alpha_i = -\left(\frac{\partial(\ln T_c)}{\partial(\ln m_i)}\right)_{m_j \neq m_i} = -\left(\frac{\Delta(\ln T_c)}{\Delta(\ln m_i)}\right)_{m_j \neq m_i}. \tag{2.1.3}$$

Here m_i refers to the isotopic mass of chemical species i. The individual exponents are defined for variations in mass i with all other masses held constant. A total isotope exponent can be expressed by rewriting 2.1.1 as

$$T_c = T_c(m_i), \tag{2.1.4}$$

so that

$$dT_c = \sum_i \left(\frac{\partial T_c}{\partial m_i}\right)_{m_j \neq m_i} dm_i. \tag{2.1.5}$$

Using 2.1.3,

$$\alpha_i = -\left(\frac{\partial(\ln T_c)}{\partial(\ln m_i)}\right)_{m_j \neq m_i} = -\frac{m_i}{T_c}\left(\frac{\partial T_c}{\partial m_i}\right)_{m_j \neq m_i}, \tag{2.1.6}$$

this becomes

$$dT_c = \sum_i \frac{T_c}{m_i}\frac{m_i}{T_c}\left(\frac{\partial T_c}{\partial m_i}\right)_{m_j \neq m_i} dm_i = -T_c \sum_i \alpha_i \frac{dm_i}{m_i}, \tag{2.1.7}$$

or

$$d(\ln T_c) = -\sum_i \alpha_i \, d(\ln m_i). \tag{2.1.8}$$

With the condition that all mass changes are made by the same relative amount, $d(\ln m_i) = \text{const.}$, this gives

$$\alpha_{Total} = -\frac{d(\ln T_c)}{d(\ln m)} = \sum_i \alpha_i. \tag{2.1.9}$$

2.2 BCS Theory and Extensions

The simplest result of BCS theory concerning isotope effects arises from the weak coupling expression for T_c

$$k_B T_c = 1.13 \hbar\omega_D e^{-1/(N(0)V)}. \quad (2.2.1)$$

The terms in the exponential, N(0), the single spin electronic density of states at the Fermi surface and V, the interaction potential, are independent of the ionic mass. The only ionic mass dependence enters through the phonon cutoff frequency ω_D, commonly taken as the Debye frequency. In the harmonic approximation,

$$\omega_D \propto \sqrt{\frac{K}{M}} \quad (2.2.2)$$

where K is some force constant of the lattice and M is the ionic mass. This leads to the result

$$\alpha = -\frac{d\ln T_c}{d\ln M} = \frac{1}{2} \quad (2.2.3)$$

It is important to remember that 2.2.3 is derived from 2.2.1 and a number of assumptions go into 2.2.1. BCS theory in its simplest form makes use of the weak coupling assumption, namely that the pairing energy is negligible compared to both the phonon energies and the Fermi energy, ε_F. Specifically, if Δ is the superconducting pairing energy, the weak coupling assumption is that $\Delta/\varepsilon_F \ll \Delta/\omega_D \ll 1$. They assumed an effective interaction in the form of a constant attractive interaction (-V) for electrons within a cutoff energy (usually taken as the Debye energy) of the Fermi energy and zero otherwise. This ignores details of the phonon structure, and the only way in which phonons enter is in terms of the cutoff energy. Coulomb repulsion between interacting electrons is incorporated into V, but not treated explicitly. Given these approximations, deviations from 2.2.3 are perhaps not unexpected.

Eliashberg theory deals with the electron-phonon interaction explicitly in terms of the electron-phonon spectral function $g(\omega) = \alpha^2(\omega)F(\omega)$, where $\alpha^2(\omega)$ is an effective electron-phonon coupling function averaged over the Fermi surface and $F(\omega)$ is the phonon density of states. $g(\omega)$ can be obtained from tunneling measurements. It enters the theory in terms of the electron-phonon coupling parameter λ, defined by

$$\lambda = 2\int_0^\infty \alpha^2(\omega)F(\omega)\frac{d\omega}{\omega} \quad (2.2.4)$$

λ is analogous to the term N(0)V in 2.2.1, but specifically includes the frequency dependence of the coupling.

Coulomb repulsion between interacting electrons is dealt with using the effective Coulomb repulsion μ^* (Morel and Anderson, 1962)

$$\mu^* = \frac{\mu}{1 + \mu\ln\left(\frac{\varepsilon_F}{\hbar\omega_c}\right)} \quad (2.2.5)$$

The screened Coulomb repulsion μ is reduced by the presence of other electrons because the time scales of the Coulomb and electron-phonon interactions are quite different (Scalapino,

1969). The ratio of the Fermi energy ε_F to a phonon cutoff energy (typically in the range $5\omega_D \lesssim \omega_c \lesssim 10\omega_D$) measures this difference.

Perhaps the best-known equation for Tc utilizing 2.2.4 and 2.2.5 is McMillan's result (1968):

$$T_c = \frac{\Theta_D}{1.45} \exp\left[-\frac{1.04(1+\lambda)}{\lambda - \mu^*(1+0.62\lambda)}\right] \qquad (2.2.6)$$

Here, Θ_D is the Debye temperature. This expression was obtained by numerically solving the Eliashberg equations, using the phonon spectrum for niobium to determine λ in 2.2.4.

McMillan has shown that λ can be expressed as

$$\lambda = \frac{\eta}{m\langle\omega^2\rangle} \qquad (2.2.7)$$

where η is a strictly electronic property. This means that λ is mass independent in the harmonic approximation. The only mass dependence in 2.2.6 other than Θ_D ($\propto m^{-1/2}$) therefore enters through the phonon cutoff frequency in 2.2.5 for μ^*, so that

$$\frac{d\mu^*}{dm} = \left[\frac{\mu}{1+\mu\ln\left(\frac{\varepsilon_F}{\hbar\omega_c}\right)}\right]^2 \frac{1}{\omega_c}\frac{d\omega_c}{dm}. \qquad (2.2.8)$$

In the harmonic approximation, this can be written

$$\frac{d(\ln\mu^*)}{d(\ln m)} = \frac{1}{2}\mu^* \qquad (2.2.9)$$

The isotope exponent is then

$$\alpha = \frac{1}{2}\left[1 - \frac{1.04(1+\lambda)(1+0.62\lambda)}{[\lambda - \mu^*(1+0.62\lambda)]^2}\,\mu^{*2}\right] \qquad (2.2.10)$$

It can be seen from 2.2.10 that reductions from $\alpha = ½$ are only possible for $\mu^* > 0$, and that 2.2.3 is recovered in the case $\mu^* = 0$. An important point is that 2.2.10 shows that α can assume negative values. Generally α is negative for $\mu \lesssim \lambda \lesssim 2.3\,\mu^*$,[1] although this varies somewhat with the value of μ^*. μ^* is usually in the range 0 ~ 0.2 (Burns, 1992), with 0.13 typical for the transition metals considered by McMillan. λ values below 0.25 are considered to be in the weak coupling regime (Scalapino, 1969) and $\lambda = \mu^*$ values are probably physically unrealistic.

[1] Consider the simpler strong coupling result $T_c \propto \omega_c \exp[-1/(\lambda-\mu^*)]$, giving $\alpha = ½\{1-[\mu^*/(\lambda-\mu^*)]^2\}$. Here α is easily seen to be negative for $0 < \lambda < 2\mu^*$, but physically λ must be greater than μ^*. A similar argument gives the mentioned condition.

The discussion in this section so far has been concerned with elemental superconductors ie. only one mass is present. The generalisation of 2.2.3 to the case of more than one mass is not readily apparent, since it is unclear what relation to use for 2.2.2. Similarly, generalizations of McMillan's and similar formulas face problems in determining the mass dependence of μ^* for multiple masses.

An alternative approach was used by Rainer *et al.* (1973 and 1979). Using a functional derivative approach they were able to directly calculate changes in Tc resulting from changes in the spectral function:

$$\Delta T_c = \int_0^\infty \Delta[\alpha^2(\omega)F(\omega)] \frac{\delta T_c}{\delta[\alpha^2(\omega)F(\omega)]} d\omega \qquad (2.2.11)$$

Here ΔT_c is the change in T_c corresponding to the change $\Delta[\alpha^2(\omega)F(\omega)]$ in the spectral function. It was found that $\delta T_c/\delta[\alpha^2(\omega)F(\omega)]$, the functional derivative of Tc with respect to the spectral function, is a fairly universal function for a variety of spectral functions. This led to the idea of defining partial isotope exponents as a function of frequency (β is used to avoid confusion with $\alpha^2(\omega)$):

$$\beta(\omega) = \frac{d}{d\omega}\left(\frac{1}{2}\frac{\omega}{T_c}\frac{\delta T_c}{\delta[\alpha^2(\omega)F(\omega)]}\right)\alpha^2(\omega)F(\omega) \qquad (2.2.12)$$

with the condition that all phonon frequencies are changed by the amount $\Delta\ln\omega = -1/2\ \Delta\ln m$, this leads to a total isotope exponent

$$\alpha_{Total} = \int_0^\infty \beta(\omega)\, d\omega \qquad (2.2.13)$$

The coefficients defined in 2.2.12 can only be identified with experimentally observed partial isotope exponents defined by 2.1.3 if each individual mass is uniquely assosciated with only a certain portion of the phonon spectrum. This is unlikely unless there is a large difference in the masses of the various constituent atoms. Even in this case it is probably necessary to integrate $\beta(\omega)$ over a certain range of phonon frequencies to obtain the experimentally observed α_i.

A more direct approach suggested by Franck (1994) would be to define the α_i directly from 2.2.11:

$$\alpha_i = -\int_0^\infty \frac{\partial[\alpha^2(\omega)F(\omega)]}{\partial(\ln m_i)}\left(\frac{1}{T_c}\frac{\delta T_c}{\delta[\alpha^2(\omega)F(\omega)]}\right)d\omega \qquad (2.2.14)$$

While this relation gives a direct connection between observed isotope effects and the spectral function, calculation of the first derivative is hampered by the difficulty of any calculation of $\alpha^2(\omega)$.

The discussion given in this section relies heavily on the reviews of Franck (1994) and Carbotte (1990) and is intended as a brief sketch of some of the theoretical basis of isotope effects. The original reviews should be consulted for a more complete picture. The main point of this section is that a wide range of isotope exponents are compatible with Eliashberg theory.

There is some debate over the existence of negative isotope exponents within the framework of this theory however. This was pointed out in a paper by Marsiglio (1992) where he studied the effects of bandwidth, band filling and direct Coulomb repulsion on calculated values for T_c and α, using Eliashberg theory. He used a Hamiltonian consisting of two terms. The first is based on the Holstein model (Holstein, 1959) and treats the electron-phonon interaction. The second is a Hubbard model type term (Hubbard, 1963) and accounts for direct Coulomb interactions. This model can, in principle, produce small values of isotope exponents. Negative exponents are ruled out. The model parameters required to produce both a large T_c and small α are probably physically unrealistic however. This is in disagreement with the work of Akis and Carbotte (1990) who were able to produce both hight T_c and negative α values. There is some question as to the use of a certain approximation in a region in which it may not apply.

It should be pointed out that these models seem to be concerned only with total rather than partial isotope effects. It is an unanswered question if partial isotope exponents may be negative, while the total isotope exponent is positive.

2.3 Summary

In this section I have briefly described the physics behind the isotope effect. It arises due to the coupling of electrons through the electron phonon interaction. The classic BCS result is presented and reasons for deviations are briefly mentioned. Eliashberg theory is shown to be able to account for small and possibly even negative isotope exponents, although there is debate over this last point. Consideration is also given to partial isotope exponents.

The fundamental purpose of this section is to show that a wide range of isotope exponents are possible within the framework of electron-phonon mediated superconductivity. In short, small (even zero, as observed in certain transition metal elemental superconductors such as Ru and Zr) isotope exponents do not rule out the electron-phonon interaction as the mechanism responsible for superconductivity.

Chapter 3

Practical Aspects of Isotope Effect Experiments

3.1 Primary Considerations

The goal of any isotope effect experiment is to determine how (or even if) a given physical property is related to the mass of the constituent atoms of the material. By their very nature, these are extremely subtle experiments. Atomic masses are decreed by nature, and the mass range of stable isotopes of a given element is fairly narrow. The largest possible mass change for stable isotopes occurs in the substitution of deuterium for hydrogen, a factor of two (Experiments using tritium (giving a factor of 3) are possible, but are greatly complicated by the radioactive decay of tritium.) This is the best case scenario and is the extreme case; the relative mass change is less for any other element. Properties that show an isotope effect are usually related to the frequency of atomic vibrations, so that, in the harmonic approximation, the expected change in the property of interest is related to the square root of the mass ratio. Generally this is roughly equivalent to half the relative mass change[1]. Experimental investigations are therefore faced with the fact that the controlled variable may be varied by a factor of two at most, and the response is expected to change by less than half this amount. Typically mass changes on the order of 10 % are feasible, at least for the lighter elements. The practical difficulties involved in achieving 100 % substitution are another question. This investigation examines isotope substitutions for $^{10}B/^{11}B$ ($\Delta M \approx 9$ %), $^{12}C/^{13}C$ ($\Delta M \approx 8$ %), $^{16}O/^{18}O$ ($\Delta M \approx 11$ %) and $^{63}Cu/^{65}Cu$ ($\Delta M \approx 3$ %). Other isotopes of possible interest in this investigation have smaller mass changes and/or are not available in sufficiently high chemical purity.

Any experiment faces the signal to noise question. The signal in an isotope experiment is a change in the physical property of interest. In order to observe this change, a minimum of two samples are required, each with a different isotopic composition. Comparisons are made and any difference between the samples is attributed to the effects of isotopic substitution. The noise is any factor, other than the alteration of atomic mass that causes a similar change (or any other alteration) in the property of interest. As such, there is a large potential for noise in isotope experiments. Preparing a large number of comparison samples and treating the results statistically may reduce noise, but this is generally impractical due to the extremely high cost of well-separated isotopes. Careful preparation of a pair of comparison samples is the usual route.

The physical property of most interest in isotope experiments on superconductors is the transition temperature, and a number of factors may affect it. For discussion purposes, they may be roughly divided into two groups. The first group is any actual or real difference in T_c not due to isotopic substitution. A difference in the chemical composition of comparison samples is the most common cause, although ordering effects[2] may also play a role. This group represents the most significant source of noise, but can be controlled by careful sample preparation and

---

[1] For a property $X = X(\omega)$, where $\omega \propto M^{-1/2}$, the relative change in X is $\Delta X/X = (X_2-X_1)/X_1 = (1+\Delta M/M_1)^{1/2}-1$, where $\Delta M = M_2-M_1$. For small ΔM, $M_1 \approx M_2 \approx M$, this becomes $\Delta X/X = (1+\Delta M/M)^{1/2}-1 \approx \frac{1}{2}\,\Delta M/M$.

[2] For example, there are four crystalographically inequivalent oxygen sites in YBCO, and it is possible to selectively substitute certain positions with ^{16}O or ^{18}O (Nickel, 1992). Thus two samples with identical chemical composition and levels of isotopic substitution may have different T_cs due to the physical location of the various isotopes. See also chapter 6, where "room temperature annealing" is discussed.

characterization. The second group can be described as apparent differences in T_c due to variations in the measurement process and the determination of T_c. A thorough understanding of the measurement process can reduce errors in this area.

This chapter discusses various aspects of these considerations as applied to the isotope effect experiments conducted in this investigation. It is divided into three sections, the first dealing with sample preparation, the second with measurement and characterization.

3.2 Sample Preparation

Ideal samples for isotope effect experiments differ only in the mass of certain atomic species. The preparation procedure is therefore of crucial importance. The production of HTSC samples is an exercise in solid state chemistry and a number of techniques are available (See Cheetham and Day, 1995). A number of routes have been explored but the most common, and the one used in this investigation, is the solid-state reaction of well-mixed oxides and/or carbonates. The intended isotope substitution determines the preparation method. The majority of isotopic species of interest are solids and the direct reaction of either the element or a suitable stable compound is the only choice available. Isotopically pure gasses represent a special case. High purity, highly enriched $^{16}O_2$ and $^{18}O_2$ are available and high levels of substitution can be achieved in some cases by thermally activated diffusion in a controlled atmosphere of the pure gas. Both methods were used in this investigation. The first part of this section discusses solid state reactions and the second describes gas phase substitution methods, including the specialized equipment required.

In general, any chemical reaction (neglecting back reactions, or considering only those with a large equilibrium constant) may be written

$$A + B \rightarrow C + D$$

Where A and B are the starting reagents, C is the desired product and D any byproducts. A useful synthesis of C requires that either the amount of D produced is very small compared to the production of C, or that is readily separated from C. A practical synthesis also requires that both A and B are commonly available or simple to produce.

The synthesis of HTSC compounds generally proceeds by the high temperature reaction of suitable starting reagents. For example, YBCO is produced according to the reaction (above 900 °C, in the presence of O_2):

$$\tfrac{1}{2}\, Y_2O_{3(s)} + 2\, BaCO_{3(s)} + 3\, CuO_{(s)} + \tfrac{1}{4}(1-\delta)\, O_{2(g)} \rightarrow YBa_2Cu_3O_{7-\delta(s)} + 2\, CO_{2(g)} \qquad (3.2.1)$$

For the purposes of discussion, the first three solid reagents may be considered as A; gaseous oxygen as B; the desired YBCO as C and the CO_2 as D. This example provides numerous points of interest. First, the solid reagents are all reasonably stable stoichiometric compounds that can be easily manipulated to provide the required metals ratio. Basically A is relatively easy to prepare, and B is also readily available. The presence of carbon in $BaCO_3$ is an undesirable impurity, but since it is released as CO_2 under the reaction conditions, the use of $BaCO_3$ more than offsets the difficulties of trying to work with BaO or BaO_2. In short, D readily separates from the desired product. Second, the level of doping (δ) is obviously a function of the amount of gaseous O_2 available, in short the oxygen partial pressure[3]. Reaction 3.2.1 indicates that isotopic substitution of the cations is relatively straightforward. For a given cation, one need only use an appropriately enriched compound as the starting material. It is also clear that oxygen presents special difficulties. Four different enriched starting materials are required for full substitution.

---

[3] In YBCO, δ is a function of T in an atmosphere of excess O_2, so this is not strictly correct. In general, equilibrium values of δ depend on both T and oxygen partial pressure.

Fortunately, YBCO, and the other HTSCs, are readily amenable to gas phase substitution, as discussed below. In either case, a suitable preparation procedure must be followed.

Given a suitable synthesis route such as reaction 3.2.1, a practical procedure must be developed. This includes such factors as pretreatment of required reagents (e.g. drying or heating in an O_2 atmosphere to ensure correct starting stoichiometry) and the thermal sequence followed (how much time at what temperature), slow cooling or quenching, etc. The process should be optimized to minimize differences in T_c between samples produced with identical starting materials but different production trials. Careful work has shown that samples with $\Delta T_c \leq 0.015$ K are possible (Culletto and Pobel, (1978)) at least in the Chevrel-phase Mo_6Se_8 superconductors ($T_c \approx 6.3$ K, $\Delta T_c/T_c \approx 0.2$ %). The situation for the HTSCs is less satisfactory, due to their variable oxygen composition. Differences for identically prepared samples in different preparation runs (thermal treatments) are often of the order of 0.1 K or more. Identical samples, prepared separately, but subject to the same thermal treatment show much smaller variations, on the order of 0.05 K, at least for optimum doping. The variations seen in different runs are probably due to slight differences in O_2 content, but the exact cause of this variation is not clear. In order to achieve maximum sensitivity for determination of isotopic shifts, it is essential that comparison samples of the HTSCs undergo the same thermal treatment.

Materials that form well-defined stoichiometric compounds are much less sensitive to slight variations in the production process. Examples include Nb_3Sn and the Ni borocarbide materials (Chapter 4).

Master mixes are used to reduce variations in the stoichiometry of non-isotopic species. In this process, a stoichiometric mixture of the non-substituted compounds is first prepared and this mix is then combined with the required amount of the isotopic species. For example, the production of $La_{(2-x)}Sr_x{}^{63}CuO_4$ and $La_{(2-x)}Sr_x{}^{65}CuO_4$ is carried out by preparing a single mixture of La_2O_3 and $SrCO_3$ in the correct ratio. Portions of this mixture are then combined with appropriate amounts of enriched CuO. This greatly reduces the likelihood of variations in the La:Sr ratio of the comparison samples (Franck, 1993). This is crucial as T_c in this material varies appreciably with small changes in Sr content.

The use of master mixes is carried to the limit in investigations of oxygen isotope effects where substitution can be achieved by gas phase diffusion. In this case a suitable amount of the desired material is produced without any isotopic enrichment. Portions of this sample are then treated in atmospheres of either $^{16}O_2$ or $^{18}O_2$. The starting material for the comparison samples is therefore identical. Identical thermal treatment requires specialized apparatus allowing close physical proximity of the samples (to reduce the possibility of thermal variations due to temperature gradients), but the maintenance of separate atmospheres. The atmosphere may be circulated or stagnant. A circulated atmosphere has the advantage that adsorbed gasses such as H_2O or CO_2 may be easily trapped out and uniformity of the atmosphere is assured. A schematic of the circulating atmosphere system used in this study is shown in figure 3.2.1 (hereafter referred to as the Oxygen Isotope Exchange System, OIES). Note that the figure shows only one line or channel of the system. The work on YBCO used a three channel system developed by Drs. J.P. Franck and J.J. Jung. Later I was involved in the construction of a four line system for work on BSCCO. The oven is a vertical tube furnace with a diameter of about 5 cm. The sample holder is constructed of fused quartz and consists of a large outer tube (4 cm dia.) containing three or four u-tubes surrounding a central thermocouple. Samples are wrapped in Pt mesh or Au foil and lowered to the bottom of the insert on fine Pt wires. In the final configuration, samples are separated by at most 2 cm. Oven temperature is determined by the thermocouple located between the samples. The oven and insert are capable of temperatures up to 1200 °C and a microprocessor-based controller regulates the temperature. Various automated temperature programs are possible.

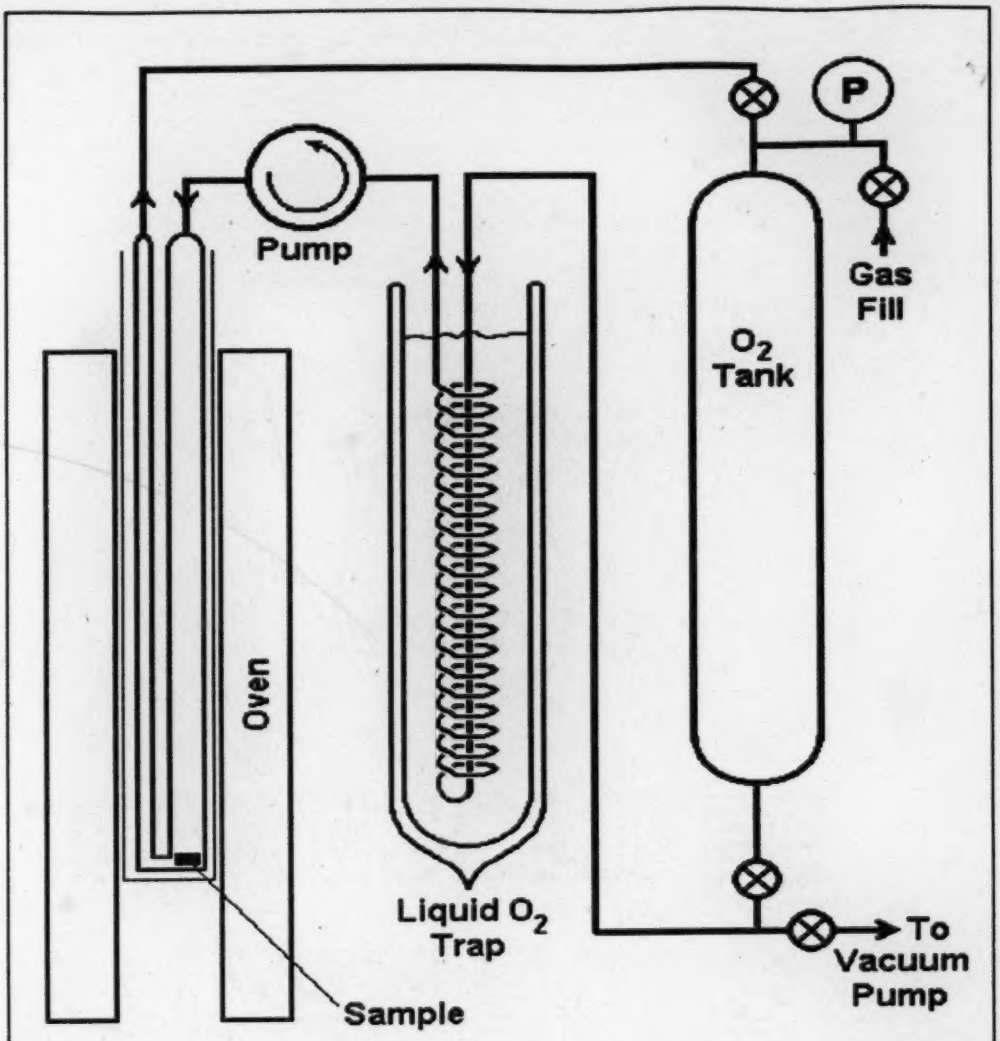

Figure 3.2.1 Schematic of the Oxygen Isotope Exchange System (OIES) (single channel).

Pieces of the same starting material (YBCO, BSCCO, LSCO) treated in different lines in the same atmosphere generally showed virtually identical magnetization curves, with a difference in T_c of less than 5 mK. These results confirm that the multi-channel system is very effective at ensuring the identical parallel processing conditions required for isotope work.

3.3 Sample Measurement and Characterization

Having produced suitable samples, the first requirement is to determine T_c. The two most common methods are measurements of the magnetic susceptibility or resistance. The two methods are complimentary, as they measure different properties.

Magnetic susceptibility probes the bulk or average properties of a sample. Determination of T_c relies on the diamagnetic shielding or Meissner effect of the superconducting state. The magnetic induction in the interior of a superconductor in an external field (less than H_{c1}) is zero. The relationship between applied field H_A, magnetization M and magnetic induction B in the interior is

$$\mathbf{B} = \mathbf{H}_A + 4\pi\mathbf{M} = 0, \tag{3.3.1}$$

so that

$$\mathbf{M} = -\frac{1}{4\pi}\mathbf{H}_A. \tag{3.3.2}$$

The magnetic susceptibility is defined as $\chi = \mathbf{M}/\mathbf{H}$, so that the susceptibility (per unit volume) is $\chi = -1/4\pi \approx 0.08$ cm^{-3} (cgs units, $\chi = -1$ m^{-3} in MKS units). χ varies with temperature due to the temperature dependence of the penetration depth λ. The value of $-1/4\pi$ is therefore an idealization, but for a bulk specimen with dimensions much larger than λ, it is closely approached at low temperatures ($T << T_c$). The ideal transition for a bulk sample is sharp and the magnetization saturates at low temperatures.

The diamagnetic susceptibility is much larger than typical paramagnetic susceptibilities, so that small amounts of non-superconducting phases usually have no effect on measurements. Conversely additional superconducting phases will be detected, giving either a broader transition or steps in the transition, depending on the amount and T_c of the extra phase(s). Broadening may also occur due to penetration depth effects in smaller grains. Degmagnetizing effects must also be considered. These two factors require that comparison samples should have similar grain sizes and a similar overall shape. Good comparison samples typically have low temperature magnetization values within a few percent of each other. Large differences are often an indication of a problem in the synthesis procedure, and such samples are not used for comparison.

All magnetization measurements in this study were made using a Quantum Design SQUID magnetometer. The sample is mounted at the end of a long rod in a temperature-controlled chamber. A superconducting magnet provides an applied field and the sample magnetization is determined by moving the sample in a set of detection coils. These coils are coupled to an RF SQUID and the magnetic moment is determined from the induced voltage in the coils. The entire system is computer controlled. Temperature accuracy is on the order of 0.01K. Sensitivity is on the order of 10^{-7} emu.

Magnetic measurements have the advantage that they are non-contact, meaning that samples may be treated after measurement with no danger of contamination from contact materials. In general, magnetic determinations of T_c are simpler and cleaner than resistance methods. All determinations of T_c in this investigation were made magnetically with only a few resistance measurements being made.

The few resistance measurements that were made used the 4-probe technique. A schematic of the experimental set up is given in figure 3.2.2. A current source is used to drive a known current through the sample and the voltage developed between 2 points on the sample is monitored with a high impedance voltmeter. Since a negligible current is drawn by the voltmeter, contact resistance effects are eliminated. The resistance between the points is then $R = V/I$. If the sample has a constant cross sectional area A, and the voltage contacts are separated by a distance ℓ, the resistivity is then $\rho = RA/\ell$.

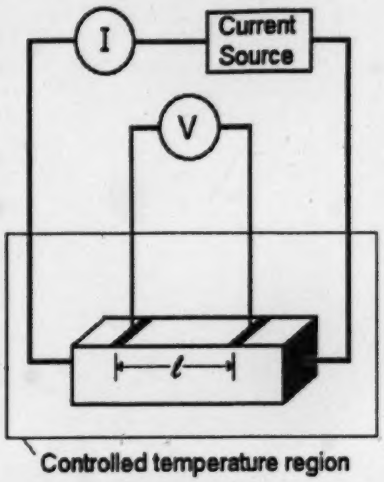

Figure 3.2.2 4-Probe resistance set up.

Samples were usually cut in the form of narrow rectangular bars and contact was made by pressing indium onto the samples as shown by the black areas on the sample in figure 3.2.2.

The prime criterion for superconductivity in resistance measurements is a zero resistance state. Measurements showing zero voltage between the contacts simply indicate that there is a superconducting path between the contacts. It does not indicate bulk superconductivity. Grain boundaries can also have a significant effect, and it is possible for samples showing a large superconducting fraction from magnetic measurements to not show a zero resistance state. These grain boundary effects probably account for the broadness of resistance transitions observed in polycrystalline samples.

The second important question involved in sample measurement is the determination of sample quality. Sharp magnetic and resistive transitions are indicative of good single-phase samples, however they are not exclusive. Powder samples or weakly sintered samples may show quite broad transitions, even though they are single-phase. Powder x-ray diffraction measurements can be used to determine phase purity. This should be done both before and after substitution treatments, at least in the preliminary stages of an investigation, to ensure that the thermal treatment used does not alter the material (see chapter 7 on BSCCO). Measurements were made using a Rigaku Rota-Flex RU-200B machine, with Cu-α radiation (typically running at 50 kV and 100 mA), primarily to confirm phase purity although lattice constants were determined in a number of cases.

Finally, it is important to be certain of the isotopic exchange. A number of methods are available and two were used in this investigation. Inductively Coupled Plasma Mass Spectrometry (ICPMS) can be used to obtain isotopic abundance for certain isotopes, but is unsuitable for oxygen as the sample is carried as an aqueous solution and O from the water would interfere. It can also be used to check the cation composition of comparison samples if quantitative measurements are carried out. In the investigations discussed here, ICPMS was used primarily to ensure that samples contained the expected isotope (samples had not been mixed up) and as a check of trace impurities.

The second method is Raman Spectroscopy. In order to be of use, there must be at least one Raman active mode associated primarily with the isotopic species. Measurements are made on the comparison samples and the shift in mode frequency due to isotopic substitution can be used as an estimate of the level of isotopic enrichment. In the harmonic approximation, the mode frequencies are inversely proportional to the square root of the atomic mass, $\nu \propto m^{-1/2}$, so that

$$\nu(m_j) = \sqrt{\frac{m_i}{m_j}}\,\nu(m_i) \qquad (3.3.3)$$

for 2 different isotopic masses i and j. The experimentally observed frequency of a given mode can be approximated as an average of the two isotopic frequencies

$$\nu_{exp} = x\,\nu(m_j) + (1-x)\,\nu(m_i) \qquad (3.3.4)$$

where the material is composed of a fraction x of m_j and (1-x) m_i. Using 3.3.3, this can be inverted to give the fraction x,

$$x = \frac{1 - \dfrac{\nu_{exp}}{\nu(m_i)}}{1 - \sqrt{\dfrac{m_i}{m_j}}}. \qquad (3.3.5)$$

Here, $\nu(m_i)$ is the observed frequency of the comparison sample having only a single isotope. 3.3.5 is most useful for oxygen isotope substitutions, and in this case i = ^{16}O and j = ^{18}O, and can be written

$$x \approx 17.5\left(1 - \frac{\nu_{18\ exp}}{\nu_{16\ exp}}\right) \qquad (3.3.6)$$

where x is the fraction of ^{18}O in the sample, and the frequencies are the experimentally observed peak positions.

It should be remembered that 3.3.5 and 3.3.6 are approximations since 3.3.4 does not accurately describe the situation. A large amount of work has been done on the modeling of isotopic substitution as applied to Raman shifts (see for example Altendorf *et al.* (1991) and the review by Thomsen and Cardona (1989)).

Consider the limiting case of a collection of non-interacting simple harmonic oscillators, all of frequency $\omega_i = (K/m_i)^{1/2}$. This case corresponds to a shortwavelength Raman mode dominated by the motion of a single atomic species. As one isotope is substituted for another ($m_i \rightarrow m_j$) the frequency of the peak does not shift continuosly, as suggested by 3.3.4. Rather two peaks appear, at the expected positions for the pure isotopes (i.e. at ω_i and $\omega_j = (m_i/m_j)^{1/2}\,\omega_i$), and there is a gradual transfer of intensity from one peak to the other as one isotope is replaced by the other. If the peaks are sufficiently broad, so that the isotopic splitting cannot be observed, the effect is a continuous shift in frequency, and 3.3.4 is a reasonable approximation. In the case of a long wavelength mode, where a large number of atoms (but still all of a single type) contribute to a particular phonon mode, the situation is far more complicated. Introduction of a second mass results in line broadening (due to disorder effects) and a possible non-linear shift in peak postition as a function of isotopic content (Altendorf *et al.* (1991)).

In either case, IF the experimentally observed peaks can be identified principally with the motion of a single atomic species AND there is no isotopic splitting observed of the peaks, then equation 3.3.4 and the following are useful estimates of the degree of isotopic substitution (Schwarz *et al.* (1992)). The situation is modelled in figure 3.2.3 for 60 % substitution of a short wavelength mode. Experimental data for a pair of BSCCO 2212 samples (sample set HBI – see chapter 7) is shown in figure 3.2.4. It is clear from this figure that no isotopic splitting of any of the peaks can be observed, and therefore that the above equations offer a reasonable estimate of ^{18}O content in the sample.

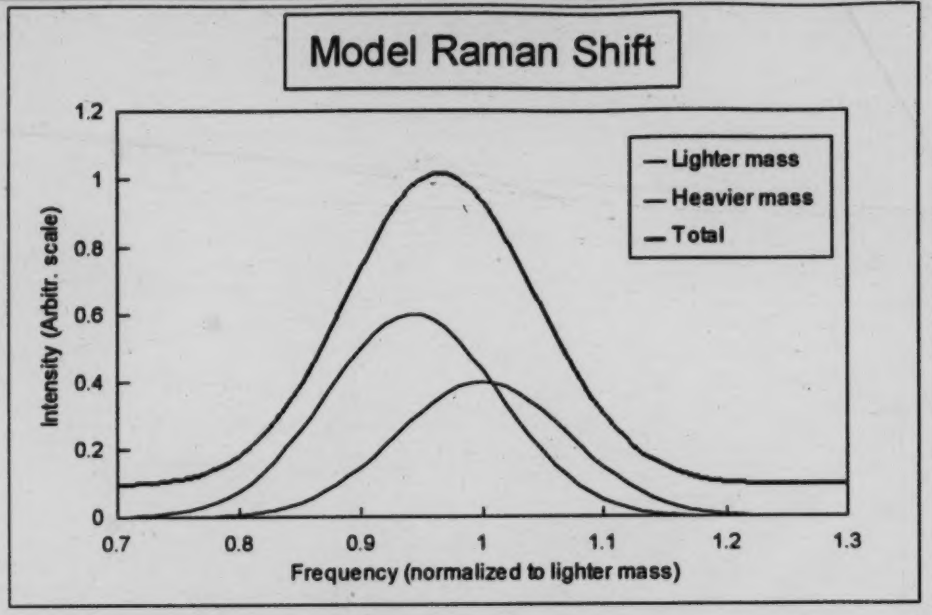

Figure 3.2.3 Model of Raman peak for 60 % ^{18}O substitution. The total intensity curve has been shifted up slightly for clarity.

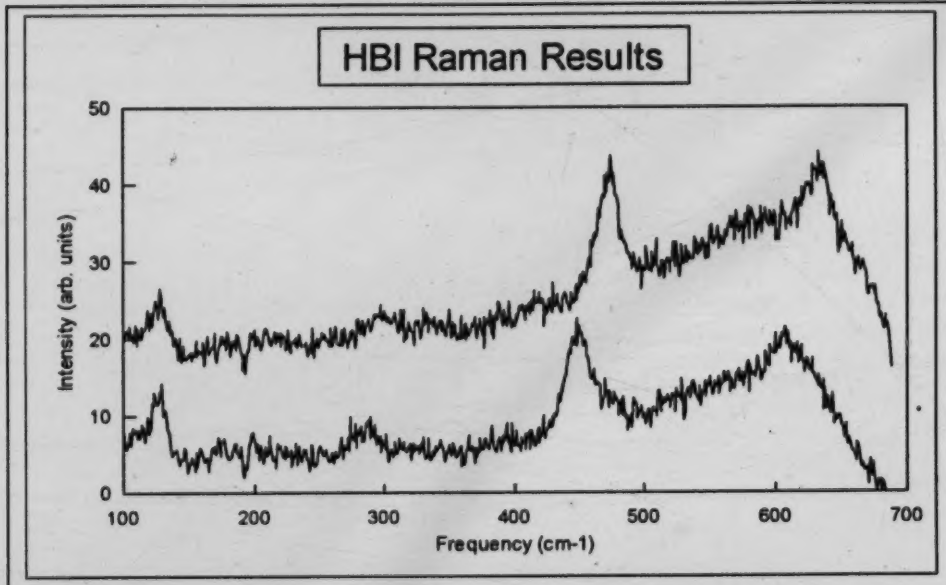

Figure 3.2.4 Raman measurements of BSCCO 2212 (sample set HBI – see chapter 7). Upper curve, ^{16}O, lower curve, ^{18}O. Clearly, there is no isotopic splitting observable in any of the shifted peaks.

3.4 Summary for Chapter 3

This chapter discusses the preparation and measurement of superconducting samples for isotope effect measurements. General comments have been made concerning preparation methods and additional details are given in the following chapters for specific materials.

The most important consideration concerning samples used for the investigation of isotopic effects is that the samples be as identical as possible in every way with the exception of isotopic composition. There are a number of criteria to be satisfied and these are summarized below.

Preparation:	Identical parallel processing must be used. The use of master mixes is essential.
Measurement of T_c:	Measurement conditions must be as identical as possible. Transitions for all samples should be similar and parallel in the comparison region. Measurements of susceptibility should show similar values for the low temperature magnetization. Likewise, resistance measurements should show similar R(T) curves and have similar room temperature resistance values. Samples showing major differences should not be used for comparison.
Characterization:	X-ray diffraction measurements should be used to confirm the material structure and phase purity. Mass spectrometry is useful for confirmation of isotopic identity in some cases, and as a check on trace impurities. Raman measurements can be used for the determination of ^{18}O content.

Chapter 4[1]

Borocarbides

4.1 Background

Superconductivity in quaternary borocarbide systems was first reported in early 1994. The first material YNi_2B_2C (Nagarajan *et al.*, 1994;Cava *et al.*, 1994) has a T_c around 15 K, and numerous related compounds were soon found. Replacement of Ni by Pd (Cava *et al.*, 1994) or Pt (Cava *et al.*, 1994) also give superconductors ($T_c \approx 23$ and 11 K, respectively). Replacement of Y by various lanthanides also yield superconductors, many with quite unusual magnetic properties (Many references, see Lynn *et al.*, 1997 for a good overview). The relatively high T_c's at first prompted speculation that these materials might be a new type of HTSC, but band structure calculations (Mattheiss, 1994; Picket *et al.*, 1994; Lee *et al.*, 1994; Mattheiss *et al.*, 1994; Coehoorn, 1994; Singh, 1994) and specific heat measurements (Carter *et al.*, 1994) quickly suggested that these were fairly conventional materials (at least those with Y or non-magnetic rare earth elements). In a paper by Mattheiss, Siegrist and Cava (1994), superconductivity is attributed to an electron-phonon mechanism in which high frequency boron optical modes are of particular importance. The authors state "... a large isotope effect is predicted, especially for the B and C constituents."

The crystal structure for YNi_2B_2C is illustrated in Figure 4.1.1 (adapted from Lynn, 1997). The Pd and Pt materials are isostructural, the Pd or Pt replacing Ni. The unit cell is body centered tetragonal, space group I4/mmm. Lattice parameters vary somewhat with composition, but are typically of order $a \approx 3.5$ Å and $c \approx 10$ Å. The structure consists of alternating layers of YC and Ni_2B_2 stacked along the c-axis. This layered structure was one of the principal reasons for considering these materials to be similar to the layered cuprate materials.

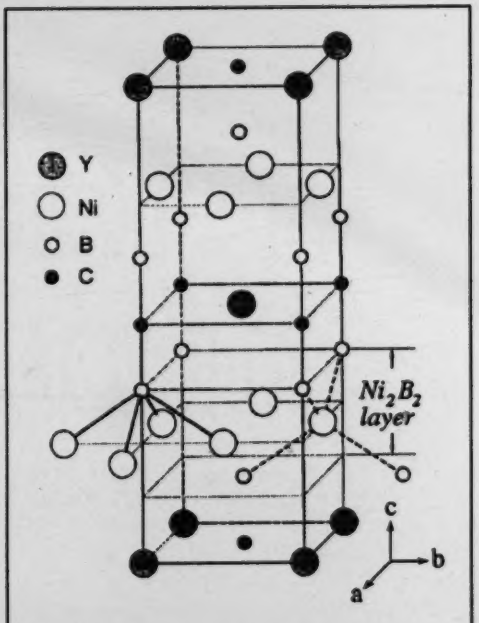

Figure 4.1.1 Crystal structure of YNi_2B_2C. (Adapted from Lynn, 1997).

I began work on the borocarbides in late February 1994, shortly after news of their discovery. A number of factors contributed to the decision to pursue isotope investigations. The major factor was that such investigations had not yet been made and such a study would provide valuable information for the understanding superconductivity in these materials. A second factor was the ease of synthesis and the availability of suitable equipment. The materials are made by direct reaction of the elements, in the molten state. The borocarbides are very refractory and the high temperatures required are difficult, if not impossible, to achieve in a conventional furnace. The alternative is arc-melting in which a high current electric arc is used to heat the material

[1] A version of this chapter has been published. D.D. Lawrie and J.P. Franck 1995. Physica C. 245: 159-163.

directly. A very similar process is used in arc welding and a special type of welding machine known as a plasma torch is often used in the welding of refractory metals. In this device an electric arc is established between a tungsten electrode and the metal. A flowing argon atmosphere prevents oxidation, and a dense, extremely high temperature argon plasma carries the current. Using such a device, a skilled operator can melt a few hundred mg of tungsten (mp. = 3400 °C) in essentially ambient conditions with virtually no oxidation. Using a plasma torch in the physics machine shop, I had produced superconducting samples of YNi_2B_2C by March 8, 1994. The final consideration was the ready availability of B and C isotopes in high purity form. ^{10}B has a number of industrial uses and is readily available commercially, while ^{11}B, ^{12}C and ^{13}C isotopes are commonly used in a number of research applications. This ready availability translates into relatively low cost ($/g for B isotopes as compared to $/mg for Cu isotopes), meaning that a much larger number of samples could be prepared, allowing a more statistical treatment of variations.

The ease of borocarbide preparation must be contrasted with difficulties associated with the HTSCs. I often found it possible to begin a preparation in the morning and have a good measurement of T_c by the following day. As a consequence, preliminary results for the B isotope effect in both the Ni and Pd borocarbides were presented at the M^2S IV (Grenoble) conference in July of 1994, less than a year after the discovery of superconductivity in these compounds. The production of good quality HTSC samples involves several thermal treatments with regrinding of the material between treatments. Typical thermal treatments were often of 12 to 24 hours (or more) duration. The result is that one to two weeks were often required for the production of a single set of HTSC isotope samples.

This chapter concerns isotope investigations of borocarbide superconductors having the formula YM_2B_2C, where M = Ni or Pd. It should be remembered that there is a fundamental difference between the two types of samples. Sample preparation conditions result in essentially pure (single phase) YNi_2B_2C, while the Pd material is multiphase, with average bulk composition $YPd_5B_3C_{0.3}$. At the time of writing, the only known superconducting phase is YPd_2B_2C, and has not been isolated in pure form. Since this investigation is concerned only with the superconducting phase, the samples are referred to as YPd_2B_2C, regardless of the bulk composition.

4.2 Experiment

The Ni and Pd borocarbide superconductors were prepared by arc melting an appropriate mixture of powders of the pure elements. Samples of a given initial composition were pressed into 6 mm diameter pellets of approximately 330 mg each, and arc-melted using a Linde "Plasma Needle Arc Welder™" plasma torch under a flowing argon atmosphere in a water cooled molybdenum crucible. The pellet was melted 3 times and the sample inverted between melting operations. The result was a roughly spherical bead, approximately 4 mm in diameter with a dull black (Ni) or gray (Pd) surface. The surface layer was extremely thin, but quite durable. Bulk material was polycrystalline with a bright silvery metallic luster.

Mass losses of on the order of 1 to 5 % were observed as a result of the melting process. In order to account for this variation, a series of three identical pellets were prepared from a 1 g master mix for each composition. Starting materials were of high chemical purity, as summarized in Table 4.2.1.

Table 4.2.1 Borocarbide starting materials

Material	Chemical Purity (%)	Isotopic Enrichment (at.%)	Source
Y	99.99	Natural	Aldrich Chemical Co.
Ni	99.995	Natural	Aldrich Chemical Co.
Pd	99.999	Natural	Aldrich Chemical Co.
B	99.7	Natural	Aldrich Chemical Co.
^{10}B	99.7	99.8	Eagle Picher Industries Inc.
^{11}B	99.999	99.71	Eagle Picher Industries Inc.
C	99.8	Natural	Aldrich Chemical Co.
^{12}C	99.9	91.9	Isotec Inc.
^{13}C	99.9	98.9	Isotec Inc.

The B isotopes were received in the form of large crystalline lumps and it was necessary to grind the material prior to use. Crystalline B is extremely hard, so special procedures were required (grinding in an agate mortar would have caused abrasion of the mortar, introducing impurities, principally SiO_2). It is also chemically quite inert (at room temperature) and this fact was employed in the final procedure. Crystalline lumps were crushed between two aluminum plates, and the resulting powder (B + Al) was washed repeatedly with dilute HCl to dissolve any aluminum, then washed with distilled H_2O, acetone and air dried.

A total of 24 Ni based samples were used in the isotope investigation. Four different boron isotopic compositions were used: pure ^{10}B, a 1:1 mix of ^{10}B and ^{11}B, natural B (18.8 at.% ^{10}B, 81.2 at.% ^{11}B), and pure ^{11}B using natural C. Four additional sets were prepared using pure B isotopes and ^{12}C or ^{13}C isotopes. Starting composition in all cases was stoichiometric (Y:Ni:B:C ratio = 1:2:2:1). After arc melting, all samples were annealed in a Ta container (used to react with any oxygen present) in vacuum ($<10^{-1}$ Pa) at 1050 °C for 24 hours, followed by slow (2 °C/min) oven cooling to room temperature. Nine samples were also measured prior to annealing.

The Pd superconductor cannot be synthesized from a stoichiometric mix as reported by Cava *et al* (1994). Samples were prepared using Y:Pd:B:C ratios of 1:2:2:1 and 1:2:2:1.5, and were not superconducting above 5 K. A suitable starting composition was found to be 1:5:3:0.3, as used by Cava *et al*. The pellet obtained after melting is a mixture of phases, but was found to have a reasonably large amount of the superconducting phase. The Pd based samples showed a wider variation in T_c than the Ni samples, perhaps due to the presence of additional phases, so two separate series (giving 6 samples) of each composition were prepared. A total of 24 Pd based samples were investigated, two identical series of varying B mass using natural C. Annealing of these samples was found to destroy superconductivity, as reported by Cava *et al*. A single set of

three identical pellets was prepared using ^{13}C, but the variation in T_c of the three samples was so large[2] that a more detailed investigation of the C isotope effect was considered impractical in the Pd based compounds.

Tables 4.2.2 and 4.2.3 give a summary of the Ni and Pd sample series used in the investigation. Each series consists of three identical samples. N refers to starting material with a natural (unenriched) isotopic composition. 10+11 refers to a 1:1 mixture of ^{10}B and ^{11}B – average MW is ≈ 10.5 g/mol. Series not listed in the tables (eg. YB-1 etc.) represent "learning experiences" and were not used in the final investigation.

Table 4.2.2 Isotopic composition of Ni Borocarbide samples

Sample Series	B Isotope	C Isotope
YB-5	10	N
YB-6	11	N
YB-7	10+11	N
YB-8	11	13
YB-9	11	12
YB-10	10	12
YB-11	10	13
YB-12	N	N

Table 4.2.3 Isotopic composition of Pd borocarbide samples

Sample Series	B Isotope	C Isotope
YPB-4	N	N
YPB-5	10	N
YPB-7	11	N
YPB-8	10	N
YPB-9	11	N
YPB-10	10+11	N
YPB-11	10+11	N
YPB-12	N	N

Magnetic susceptibility for all samples was measured in a Quantum Design SQUID Magnetometer from 5 K to above T_c in a field of 3 Gauss. Measurements were made on warming for both zero field and field cooling. Powder x-ray diffraction (Cu K-α radiation) measurements were also made on several samples. Resistance measurements were made in a closed cycle refrigerator for several of the Pd samples. The lowest temperature consistently attainable in this system (around 15 K) did not allow a clear observation of the superconducting transition in the Ni based samples, and so no resistance measurements were attempted on them.

It was observed that the transition widths (10-90 % of low temperature value) for both resistivity and susceptibility were generally of order 2 K or less, but that the lower temperature behavior showed a much more gradual change. T_c was therefore taken as the first onset of diamagnetic shielding in susceptibility measurements[3], and the first abrupt[4] drop in resistivity.

---

[2] The largest difference for three "identical" samples was 1.3 K.

[3] Effectively the temperature at which χ reached approximately 0.5 % of the low temperature value.

[4] A drop of more than 1% in less than 0.3 K

4.3 Results

Representative data for susceptibility and resistivity measurements are presented in figures 4.3.1 to 4.3.8, followed by analysis. X-ray diffraction results and analysis are presented at the end of this section.

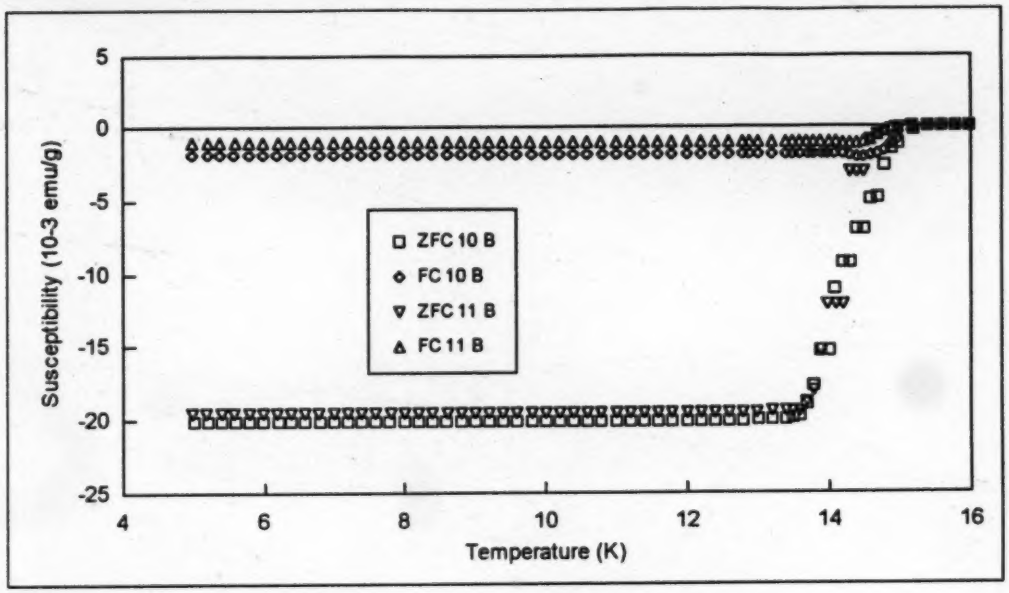

Figure 4.3.1 Typical susceptibility measurement for annealed YNi_2B_2C.

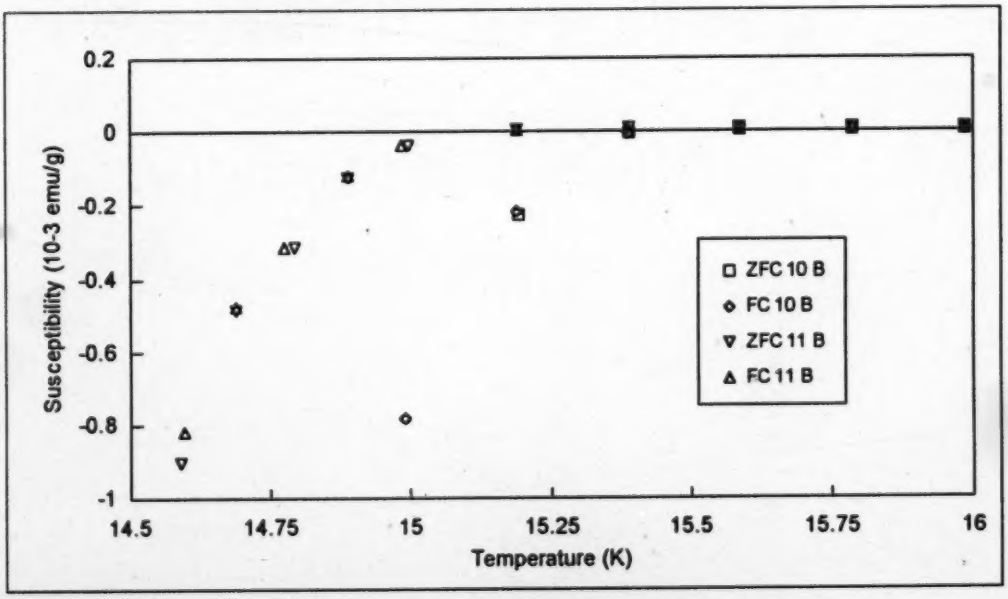

Figure 4.3.2 Enlargement of Figure 4.3.1, showing the transition region.

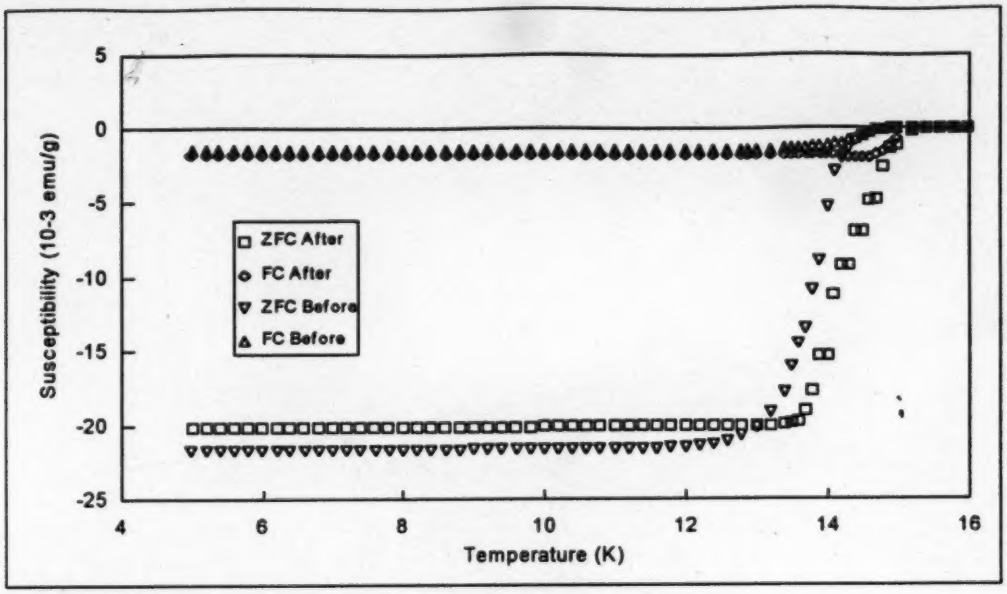

Figure 4.3.3 Effect of annealing on susceptibility of $YNi_2{}^{10}B_2C$.

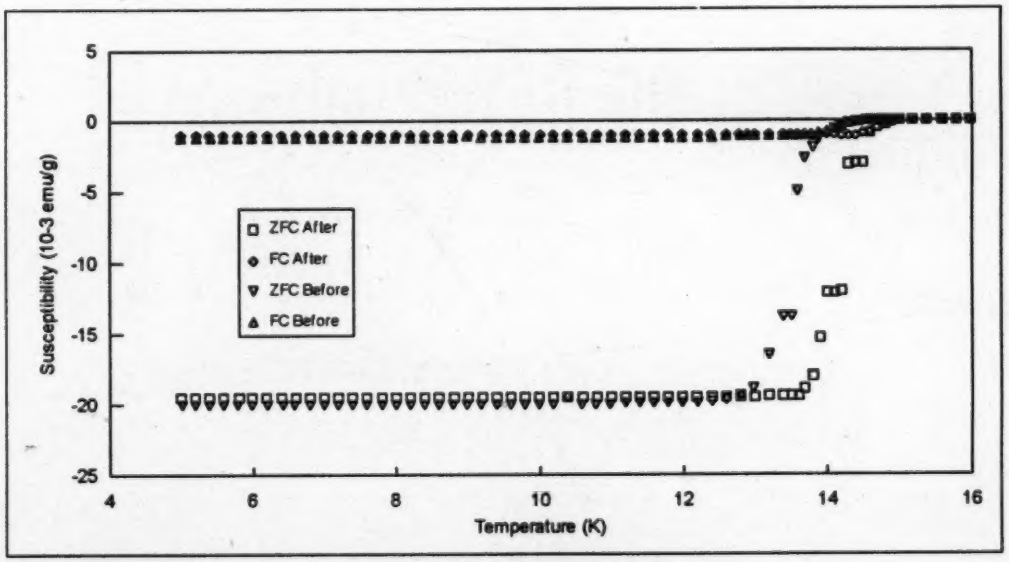

Figure 4.3.4 Effect of annealing on susceptibility of $YNi_2{}^{11}B_2C$.

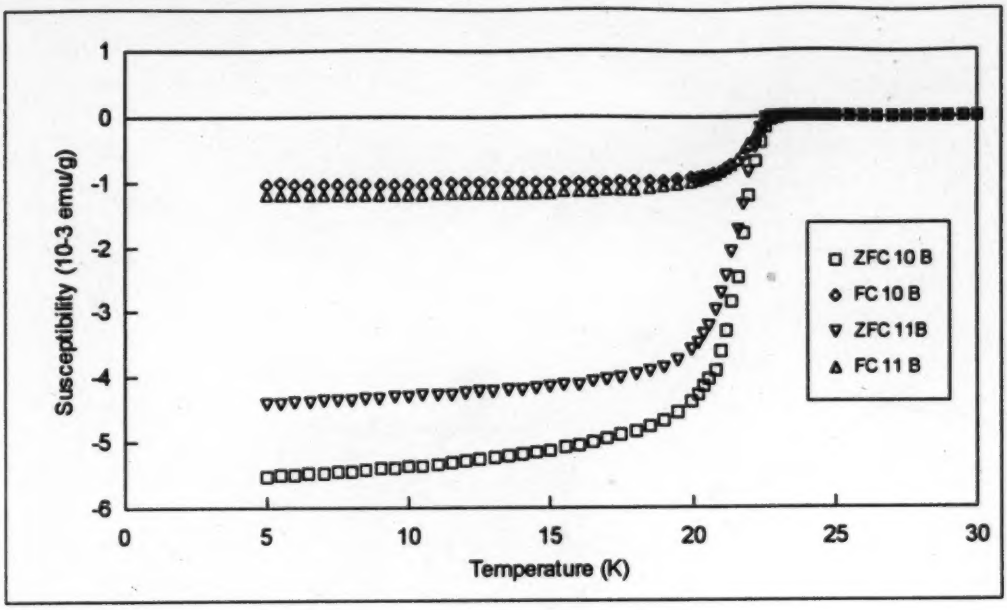

Figure 4.3.5 Typical susceptibility measurement for YPd_2B_2C.

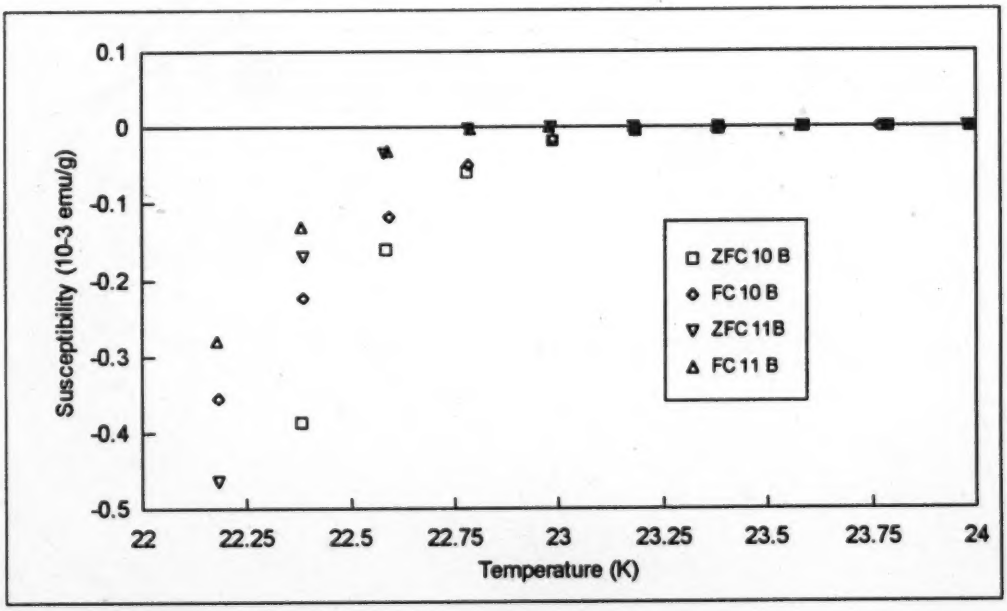

Figure 4.3.6 Enlargement of Figure 4.3.5, showing the transition region.

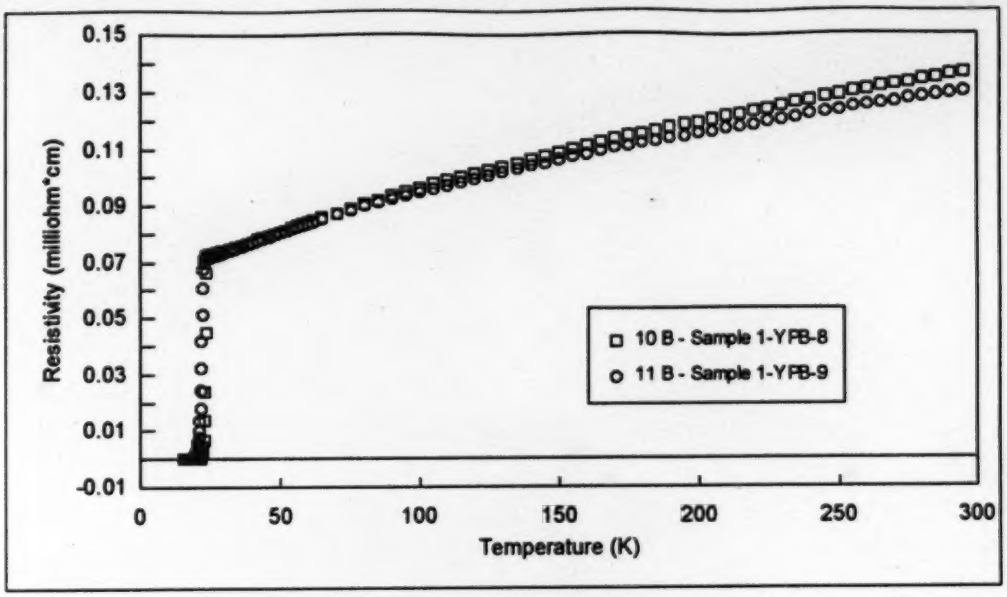

Figure 4.3.7 Resistivity curves for $YPd_2{}^{10}B_2C$ and $YPd_2{}^{11}B_2C$ samples.

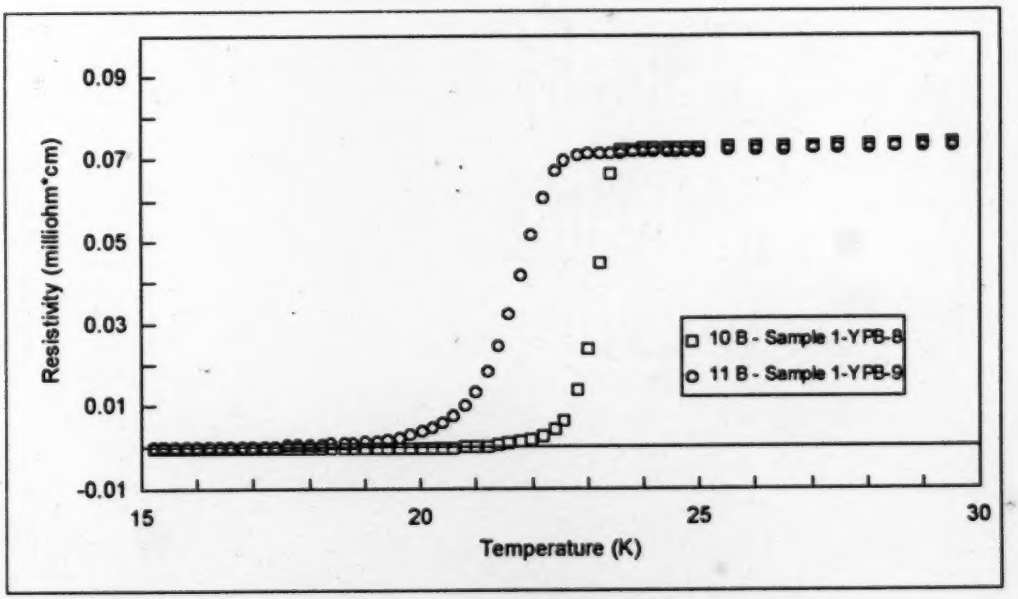

Figure 4.3.8 Enlargement of Figure 4.3.7, showing the transition.

T_c values as determined from susceptibility measurements for the Ni and Pd samples are summarized in Tables 4.3.1 and 4.3.2 respectively. The listed values are the average of all samples (3 for Ni, 6 for Pd) of a given composition (series). The uncertainty is the maximum deviation from the mean.

Table 4.3.1 Average T_c values for YNi_2B_2C.

Sample Series	Boron Mass (g/mol)	Carbon Mass (g/mol)	T_c (unannealed) (K)	T_c (annealed) (K)
YB-5	10.013	12.011	15.04 ± 0.07	15.48 ± 0.03
YB-7	10.511	"	14.90 ± 0.13	15.35 ± 0.05
YB-12	10.811	"	/	15.24 ± 0.06
YB-6	11.009	"	14.66 ± 0.15	15.10 ± 0.10
YB-10	10.013	12.000	/	15.46 ± 0.17
YB-9	11.009	"	/	15.07 ± 0.07
YB-11	10.013	13.003	/	15.36 ± 0.07
YB-8	11.009	"	/	14.99 ± 0.05

Table 4.3.2 Average T_c values for YPd_2B_2C.

Sample Series	Boron Mass (g/mol)	T_c (K)
YPB-5 & -8	10.013	23.32 ± 0.16
YPB-10 & -11	10.511	22.89 ± 0.07
YPB-4 & -12	10.813	22.63 ± 0.23
YPB-7 & -9	11.009	22.63 ± 0.40
Resistivity	10.013	23.36 ± 0.27
Resistivity	11.009	22.66 ± 0.40

The final two entries in the Pd table are the averages of T_c determined from resistivity measurements. Three samples of each isotope were measured, but usable data was obtained for only two of the three ^{11}B samples. The uncertainty in this case is simply the difference in the two measured temperatures.

The isotope exponents were obtained from this data in two ways. In the case of materials prepared with unenriched C, 4 different B masses are available for consideration, and so a double logarithmic plot of T_c versus mass should yield a straight line with slope equal to $-\alpha_B$. Least squares fits are shown in Figures 4.3.9 and 4.3.10 for the Ni and Pd results respectively. When only two masses are available, the only recourse is to direct calculation using equation 2.1.2. Tables 4.3.3 and 4.3.4 summarize the values obtained by both methods for the two materials.

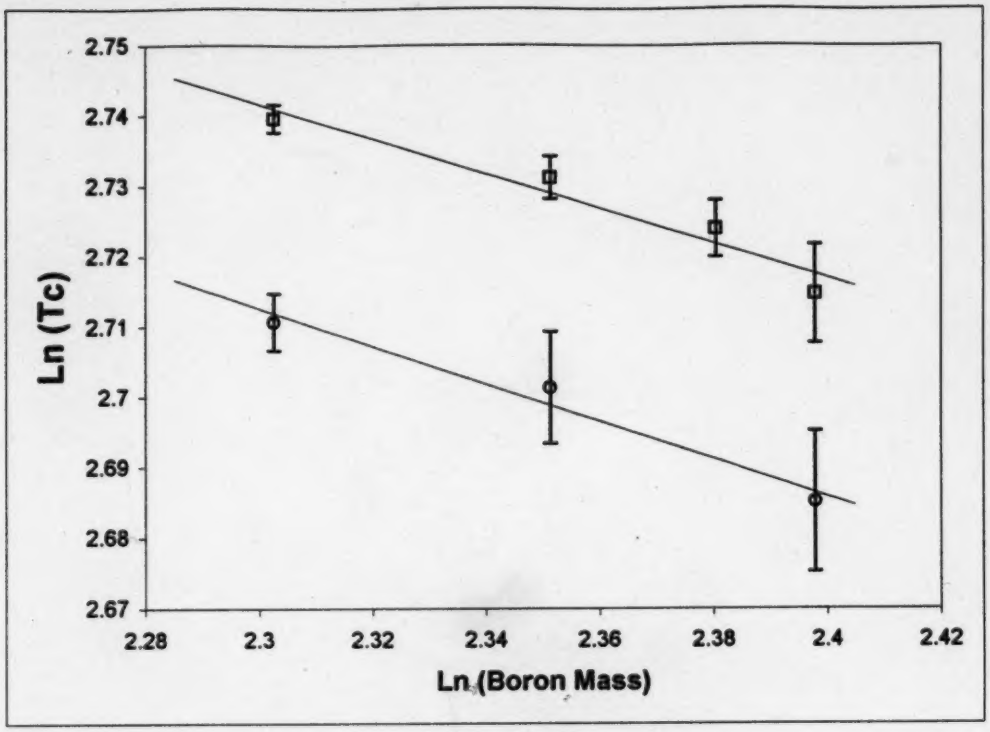

Figure 4.3.9 Double logarithmic plot of Tc versus B mass for YNi_2B_2C. The lines are least squares fits to the data, with slopes equal to $-\alpha_B$. Upper points (squares) are annealed samples, lower (circles) are unnanealed.

Table 4.3.3 Isotope Exponents in YNi_2B_2C

Method	α_B	α_C
Least squares – annealed samples	0.25 ± 0.04	
Least squares – unannealed samples	0.27 ± 0.05	
Direct – ^{12}C samples	0.27 ± 0.13	
Direct – ^{13}C samples	0.26 ± 0.06	
Direct – ^{10}B samples		0.08 ± 0.14
Direct – ^{11}B samples		0.07 ± 0.07

The values above were determined more or less independently, so a best estimate for the isotope exponents may be found by taking a weighted average. The result is

For YNi_2B_2C, $\alpha_{B\,Best} = 0.26 \pm 0.03$ $\alpha_{C\,Best} = 0.07 \pm 0.06$

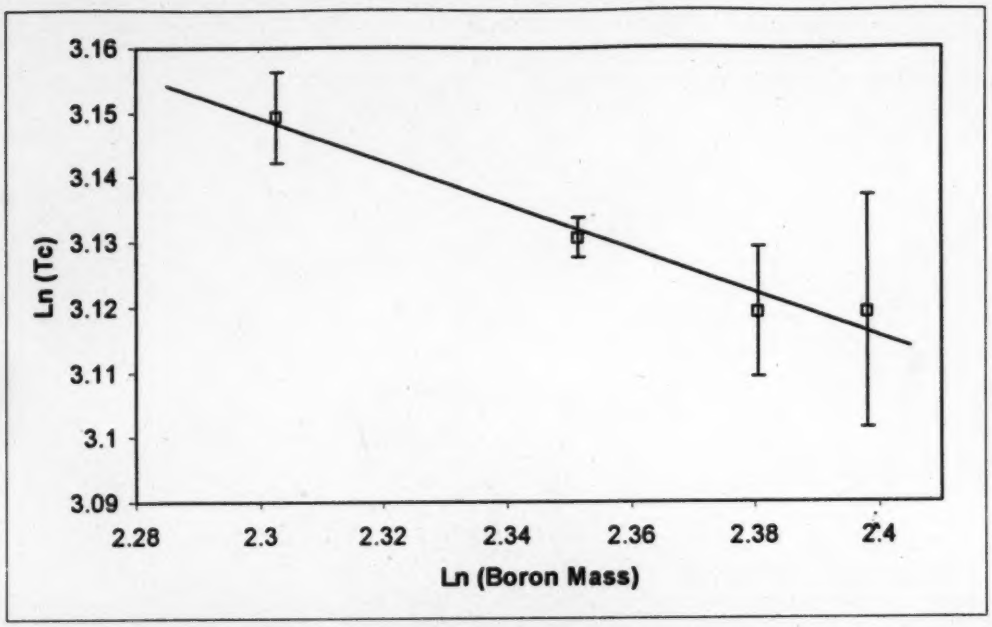

Figure 4.3.10 Double logarithmic plot of Tc versus B mass for YPd_2B_2C. The lines is a least squares fits to the data, with slope equal to $-\alpha_B$.

Table 4.3.4 Isotope Exponents in YPd_2B_2C

Method	α_B
Least squares	0.32 ± 0.04
Direct – Resistivity	0.32 ± 0.22

For YPd_2B_2C, $\alpha_{B\ Best} = 0.32 \pm 0.04$

Typical x-ray diffraction patterns for the two materials are shown in figures 4.3.11 and 4.3.12. Lattice parameters were determined by a least squares fitting procedure using the assignments shown in figure 4.3.11. This was straightforward for the Ni samples, but more difficult for the Pd samples due to the presence of additional phases. This difficulty in resolving certain Pd peaks probably means that the uncertainties for the lattice parameters are somewhat underestimated. Results are summarized in table 4.3.5.

Table 4.3.5 Lattice constants for YNi_2B_2C and YPd_2B_2C. All values are in Ångstroms and are the average for 3 samples. Uncertainties are the maximum deviation from the mean.

Material	a = b	c
$YNi_2{}^{10}B_2C$	3.529 ± 0.001	10.539 ± 0.004
$YNi_2{}^{11}B_2C$	3.529 ± 0.001	10.534 ± 0.005
$YPd_2{}^{10}B_2C$	3.714 ± 0.003	10.741 ± 0.008
$YPd_2{}^{11}B_2C$	3.712 ± 0.002	10.737 ± 0.005

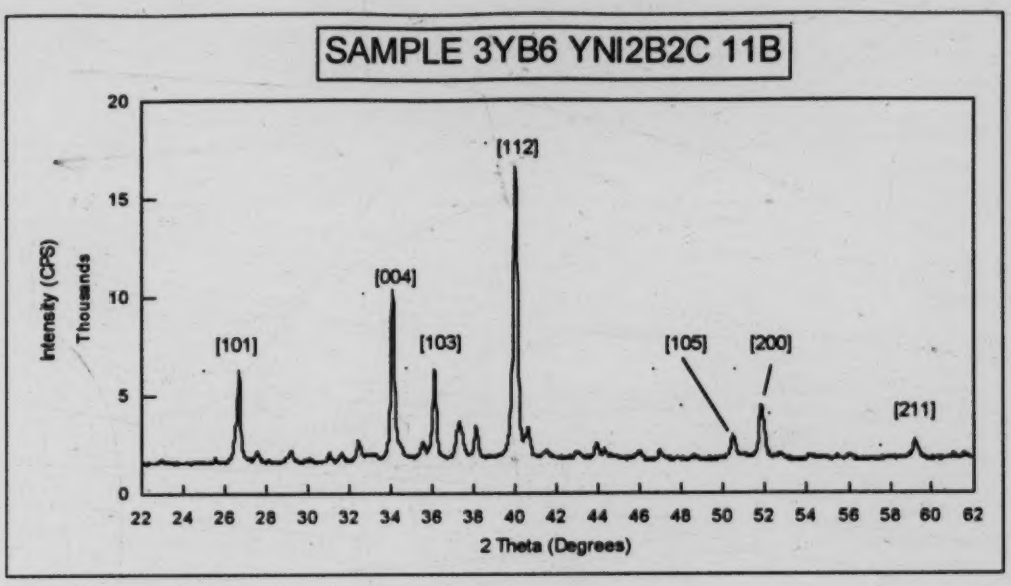

Figure 4.3.11 Typical powder x-ray diffraction pattern for YNi_2B_2C showing peak assignments used in lattice constant determination.

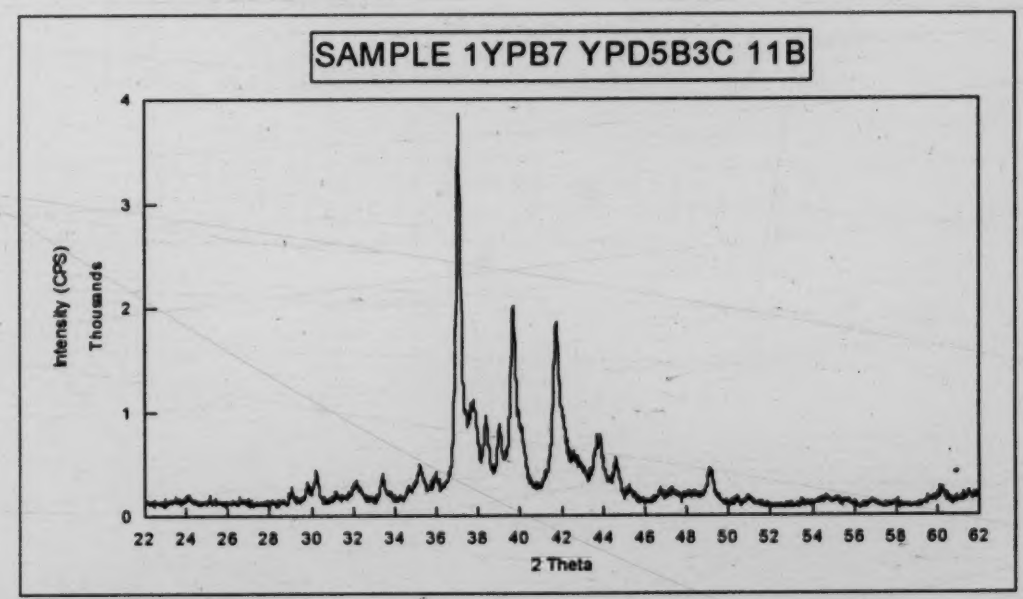

Figure 4.3.12 Typical powder x-ray diffraction pattern for $YPd_5B_3C_{0.3}$ showing strong evidence of multiple phases.

4.4 Discussion

The results show a clear dependence of T_c on isotopic mass, at least for B isotopes, confirming the prediction of Mattheiss, Siegrist and Cava (1994). Recently, the B isotope effect has been investigated in single crystals of YNi_2B_2C and $LuNi_2B_2C$ (Cheon *et al* 1999). They also find a dependence of T_c on isotopic mass. Values of $\Delta T_c = 0.29 \pm 0.08$ K and $\alpha_B = 0.21 \pm 0.07$ for YNi_2B_2C are in excellent agreement with values found in this investigation. Values for $LuNi_2B_2C$ are $\Delta T_c = 0.16 \pm 0.07$ K and $\alpha_B = 0.11 \pm 0.05$.

In order to extract some physical understanding of these results, it is interesting to compare the sizes of the observed α_B for the three materials for which data is now available. The largest effect is seen in the Pd material and the smallest in $LuNi_2B_2C$. Starting from YNi_2B_2C, it is instructive to consider the expected change in α_B when a). Pd is substituted for Ni and b). Lu is substituted for Y. Note that α_B does not scale with T_c, as shown in the table 4.4.1.

Table 4.4.1 Scaling of α_B with T_c.

Material	T_c (K) (^{10}B samples)	α_B	α_B / T_c
YNi_2B_2C	15.48	0.26	0.0168
$LuNi_2B_2C$	16.20	0.11	0.0068
YPd_2B_2C	23.32	0.32	0.0137

A first approximation in the Pd case is to neglect any change in the electronic structure of the material due to the substitution and simply consider the change Ni → Pd to be an increase in the Ni mass. In this approximation, no changes occur in the electronic density of states, or in the Fermi energy. There are changes in the phonon spectrum however. Modes involving primarily Ni (Pd) vibrations will be shifted to lower frequencies, while collective modes will also show a lowering of frequency. The frequency of modes involving primarily B will remain relatively unaffected, but there will be a greater decoupling of relative motions of the ions. The amplitude of B vibrations would then be expected to increase[5]. The paper by Matheiss *et al.* (1994) attributes superconductivity in the borocarbides to an electron-phonon mechanism in which high frequency boron a_{1g} optical phonons are of primary importance. These phonons dynamically modulate the tetrahedral B-Ni-B bond angles. The change from Ni to Pd should result in larger B amplitudes and greater modulation of the bond angles. A larger isotope effect would then be expected for the Pd material than the Ni, since the relative change in the amplitude of motion on isotopic B substitution is greater in the Pd material. Using these arguments, a naive first approximation would be to estimate α_B in the Pd material as

(4.4.1)

where as the experimental results give . These arguments remain valid if changes in the electronic structure are included, but a number of complications arise. The most significant effect is a change in the electronic density of states (DOS) at the Fermi surface (Coehoorn, 1994). As a result, exact agreement with equation 4.4.1 should not be expected, but the principal explanation of the larger α_B in YPd_2B_2C is probably due to the effect discussed.

The Lu case is less clear. Here, as a first approximation, similar arguments about changes to the phonon spectrum can also be made. Y (Lu) dominated modes will be shifted to

---

[5] Consider the optical modes of a diatomic cubic crystal, the ratio of atomic displacements (x_i) is, at K = 0, $x_1/x_2 = -M_2/M_1$ (Kittel, 1986). Increasing one mass increases the relative amplitude of motion of the other.

lower frequencies. In this case however, the decoupling of the amplitude of B motion is from Y (Lu) modes, and not Ni modes. If anything, there may be a reduction of B amplitude relative to Ni since the Ni will also undergo a (smaller) degree of decoupling from Lu modes. This reduction could be responsible for the significantly smaller α_B observed by Cheon et al. in $LuNi_2B_2C$. Changes in the electronic density of states at the Fermi surface may also play a role.

If these suggestions are qualitatively correct in accounting for the observed sizes of α_B, then the following predictions can be made: 1. α_B should be large in YPt_2B_2C (greater decoupling of B modes due to heavier mass of Pt), perhaps even greater than 0.3; 2. α_B should be approximately the same size for the various lanthanide borocarbide superconductors (relatively small mass changes on changing the lanthanide), at least for those materials not showing unusual magnetic ordering effects.

The order of transition temperatures in these three materials ($T_c(Pd) > T_c(Lu) > T_c(Ni)$) can be understood from the theory of Matheiss *et al.* (1994). In addition to dynamic B motions, they find that the electronic DOS at the Fermi surface is strongly affected by the static (average) B-Ni-B angle. Optimal conditions for superconductivity occurring when the angle is 109.47°, i.e. the coordination of the Ni-B groups is exactly tetrahedral. In YNi_2B_2C, it is 107.2° (Belger *et al.* 1998). In YPd_2B_2C it is about 109°, estimated from data in table 4.3.5, assuming the relative positions of Pd and B are the same, i.e. Ni and Pd are located at (0,1/2,1/4) and B at (0,0,0.123) (adapted from Belger *et al.*). In $LuNi_2B_2C$, it is 108.7° (Matheiss *et al.* 1994). This is summarized in the table below.

Table 4.4.2 Correlation between T_c and Bond Angle

Material	T_c (K) (^{10}B samples)	B-M-B bond angle
YNi_2B_2C	15.48	107.2°
$LuNi_2B_2C$	16.20	108.7°
YPd_2B_2C	23.32	≈ 109°

The results presented here for α_C are suggestive, but unsatisfactory. Samples prepared using enriched C isotopes showed much larger variations in T_c, and it is not clear why. One possibility is mass losses and inhomogeneity during the melting process. The C isotopes were of a more granular form than the unenriched C, and gave pellets with much poorer physical coherence. More controlled melting conditions would probably reduce this effect. A second possibility is the production of enriched C single crystals using the method of Cheon *et al.*

4.5 Summary for Chapter 4

There is a boron isotope effect in both YNi_2B_2C and YPd_2B_2C, with values of the isotope exponent α_B of 0.26 ± 0.03 and 0.32 ± 0.04 respectively. These results are in good agreement with those of Cheon *et al.* (1999). Results for a carbon isotope effect in YNi_2B_2C are at best inconclusive. There is a suggestion of a small effect $\alpha_C = 0.07 \pm 0.06$, but it is essentially at the level of the experimental uncertainty. Experimental limitations prevented an examination of α_C in YPd_2B_2C. No variation in lattice constants as a function of atomic mass was observed within experimental uncertainty.

These results support the idea that the non-magnetic borocarbide materials are fairly conventional superconductors.

Chapter 5[1]

Copper Oxide

5.1 Background

As was noted in the introduction, a characteristic feature of HTSC materials is that they are antiferromagnetic insulators for zero doping, the antiferromagnetic ordering taking place in the CuO planes. Similarly CuO itself is an insulator that undergoes antiferromagnetic ordering, the ordering taking place in two stages (Brockhouse, 1954; Yang *et al*, 1988; Yang *et al*, 1989; Forsyth *et al*, 1988). At temperatures above about 230 K, the material is paramagnetic and shows no magnetic ordering. As the material is cooled, a second order phase transition at the first Neél temperature ($T_{N1} \approx 230$ K) leads to incommensurate antiferromagnetic (ICAF) ordering. Further cooling results in a first order transition to commensurate antiferromagnetic (CAF) order at the second Neél temperature ($T_{N2} \approx 210$ K).

In order to understand the changes that take place on cooling, it is necessary to understand the material structure. CuO is monoclinic with a = 4.684 Å, b = 3.423 Å, c = 5.129 Å and $\beta = 99.5°$(Åsbrink *et al*, 1970) and the structure is shown in figure 5.1.1. The structure can be described as CuO planes parallel to the ac plane, stacked along the b axis, located at ¼ b and ¾ b and offset by ½ b. Each Cu atom in one of these planes is surrounded by four coplanar O atoms in a nearly rectangular configuration. O atoms are shared along the diagonal, resulting in essentially 1 dimensional Cu-O chains oriented in the [10$\bar{1}$] direction. These chains are indicated by the lighter lines in figure 5.1.2, O atoms are not shown, but are located approximately midway between the Cu, the Cu-O-Cu bond angle being 146°.

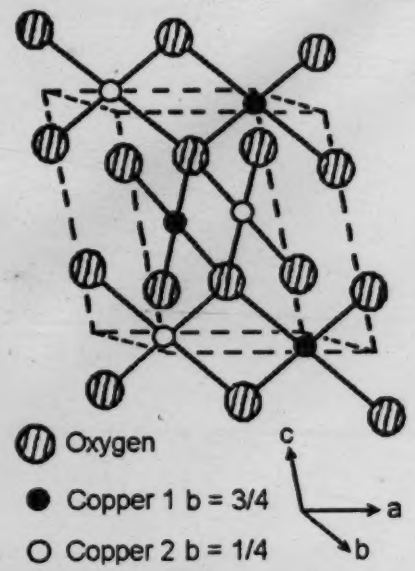

Figure 5.1.1 Crystal structure of CuO (Adapted from Yang *et al*. 1989).

Magnetic ordering in the chains occurs as a result of super exchange along these bonds. In the commensurate phase, spins in a chain are antiferromagnetically aligned, with spins along the b-axis. Adjacent chains are antiferromagnetically aligned. This is shown schematically in the left-hand portion of figure 5.1.2, up arrows indicating spins parallel to b and down antiparallel (the b-axis is perpendicular to the plane of the figure).

The situation is more complicated in the incommensurate phase. In this case, spins in a given chain are approximately antiferromagnetically ordered, however they are no longer oriented only along the b-axis, but have components in the a-c plane. In addition the relative orientation of spins on adjacent chains (in a given plane) shows a helical modulation. The arrows in the right-

[1] A version of this chapter has been published. D.D. Lawrie, J.P. Franck and Cheng-Tian Lin 1998. Physica C. 297: 59-63.

hand part of figure 5.3.2 are thus semi-schematic representations of the spin vectors projected onto the a-c plane. There is no coherent relationship between spins on different a-c planes. This description and figure 5.3.2 are based on the work of Forsyth *et al* (1988).

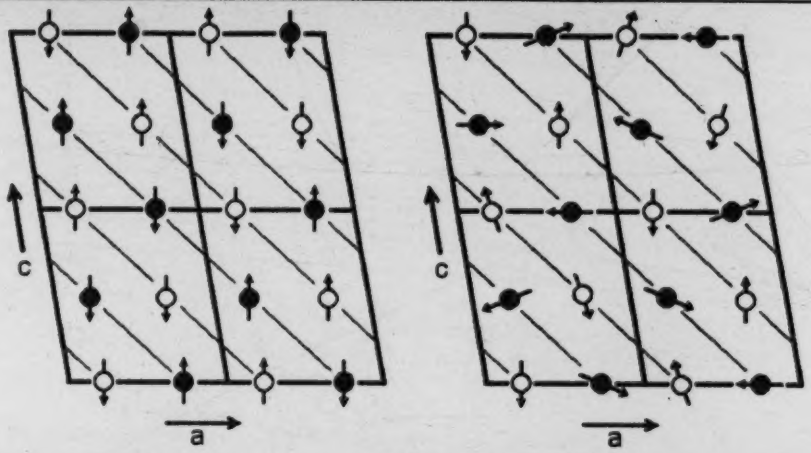

Figure 5.1.2 Spin alignment in the commensurate (left) and incommensurate (right) phases. Projection is along the b axis, open (closed) circles are Cu in the ¼ b (¾ b) plane. See text for an explanation of the arrows (Modified from Forsyth *et al.*, 1988).

The exchange interaction has been determined using spin wave measurements in neutron diffraction (Yang *et al*, 1989) and from magnetic susceptibility measurements (Kondo *et al*, 1988). The values are similar J_0 = 67 meV (spin) and 69 meV (susceptibility) and rather large. The ordered Cu moment, 0.68 μ_B, is smaller than the expected spin only value of 1 μ_B for Cu^{2+}.

Raman scattering measurements have been used to identify phonon and magnon peaks (Irwin *et al.*,1991). In particular, a strong spin-phonon interaction has been identified in a copper mode at about 240 cm^{-1} (Chen *et al.*, 1995). This mode is unobservable above T_{N2}, and becomes Raman active as a result of the magnetic ordering effectively increasing the size of the unit cell in the commensurate phase, resulting in Brillouin zone folding. Just below T_{N2}, this feature is weak and appears at about 230 cm^{-1}. As the temperature is lowered, the mode becomes sharper, increases in intensity and hardens in frequency to 240 cm^{-1} for $T \lesssim 60$ K. This behavior is in contrast to that usually observed in zone-folding situations, where new features appear abruptly below the transition temperature and remain fairly constant in frequency as the temperature is lowered. The observed behavior was explained in terms of a strong interaction between the magnetic sublattice and zone-folded phonons. The spin-phonon coupling coefficient, λ, was estimated to be on the order of 50 cm^{-1}, much larger than values of $\lambda \lesssim 1$ cm^{-1} reported for other antiferromagnetic materials such as MnF_2 (Lockwood *et al.*, 1988).

The importance of Cu-O planes in the HTSCs and this large spin-phonon interaction suggested that it might be worthwhile to search for an isotope effect in either T_{N1} or T_{N2}. The only previous investigation of the possibility of an isotope effect in either Neél temperature was conducted by Zhao *et al.* (1994), and concerned only the oxygen ($^{16}O/^{18}O$) effect on T_{N1}. No effect was found. Facilities and materials (isotopically enriched CuO) were available for an investigation of both the oxygen and copper ($^{63}Cu/^{65}Cu$) isotope effects on both T_{N1} and T_{N2}. Since the investigation was concerned with pure CuO, these samples would not be chemically modified and could be used in future isotope investigations. This was an important factor in deciding to proceed with the investigation. There is no conventional theoretical reason to expect an isotope effect, but

the large spin-phonon interaction observed in Raman studies suggests at least the possibility of an effect.

This investigation should be viewed as a case of simply being thorough and investigating all possibilities. Even though an isotope effect was very unlikely, the existence of such an effect would have had a number of implications for the HTSC materials. Even so, this investigation would not have been attempted had it meant the isotopically enriched samples would be unavailable for future investigations (preparation of isotopic HTSC samples). The principle purpose of this investigation was therefore to experimentally confirm that there are no observable isotope effects (copper or oxygen) on either T_{N1} or T_{N2} in CuO.

5.2 Experiment

Measurements were carried on sintered powder pellets of isotopically enriched CuO. Samples of ^{63}CuO and ^{65}CuO powder were obtained from Oak Ridge National Laboratory. Enrichment was very high (99.67 at. % ^{63}Cu, and 99.72 at. % ^{65}Cu) and chemical impurities for both materials were below the 0.01 at. % level. $Cu^{16}O$ and $Cu^{18}O$ powders were obtained from Merck-Frosst (Montreal) and were synthesized directly from pure Cu and $^{16}O_2$ or $^{18}O_2$, giving very high isotopic enrichment (greater than 99 at. %)[2]. Chemical purity was 99.9 at. % or better.

Approximately 120 mg of each powder was pressed into a 6 mm diameter pellet and fired at 950 °C for 24 hours. Cu isotope samples (2 pairs) were fired together in air and an unenriched high purity (99.99 %) CuO sample was also prepared in this way. O isotope samples (1 pair) were fired in separate lines of the OIEA in atmospheres of pure $^{16}O_2$ or $^{18}O_2$. This firing procedure was followed for two reasons. First, it ensures that the samples have stoichiometric amounts of oxygen and second, it improves the physical stability of the pellets, making them easier to handle. Finally, measurements were also made on a single crystal of CuO (unenriched) grown by Cheng-Tian Lin at the Max Planck Institut für Festkörperforschung, Stuttgart.

The two transitions were observed in measurements of the magnetic susceptibility as a function of temperature. Measurements were made using a Quantum Design SQUID magnetometer in a field of 3 T, on warming from 60 K to 300K.

---

[2] This is the best method for obtaining high ^{18}O levels in CuO. The gas phase exchange, firing CuO in $^{18}O_2$, is relatively ineffective, indicating that O is quite tightly bound in CuO.

5.3 Results

A typical plot of the susceptibility from 60 K to 300 K for one of the sintered pellets is shown in figure 5.3.1. In sintered powder samples the first transition (ICAF → P) appears as a slight kink in the susceptibility at T_{N1}. The second transition (CAF → ICAF) appears as a shift in the susceptibility over a range of temperature, and is somewhat difficult to observe. This is at first surprising as the transition is first order and is expected to give a sharp step in the susceptibility.

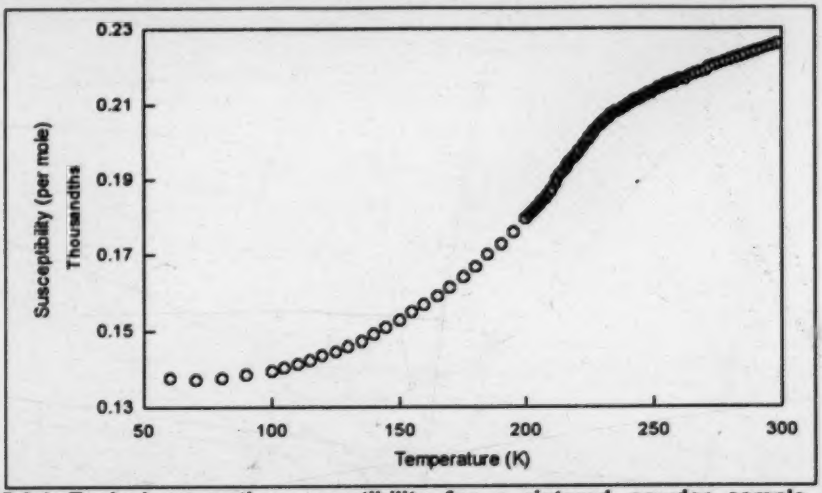

Figure 5.3.1 Typical magnetic susceptibility for a sintered powder sample of CuO measured in 3 T.

It can be explained by examining the results shown in figure 5.3.2, where the susceptibility of an oriented single crystal is shown. The change from commensurate to incommensurate order results in a sharp drop in magnetization along the [001] direction, while at the same time an abrupt jump is seen along the [100] and [010] directions. The two effects nearly cancel in a powder sample due to the random grain orientation.

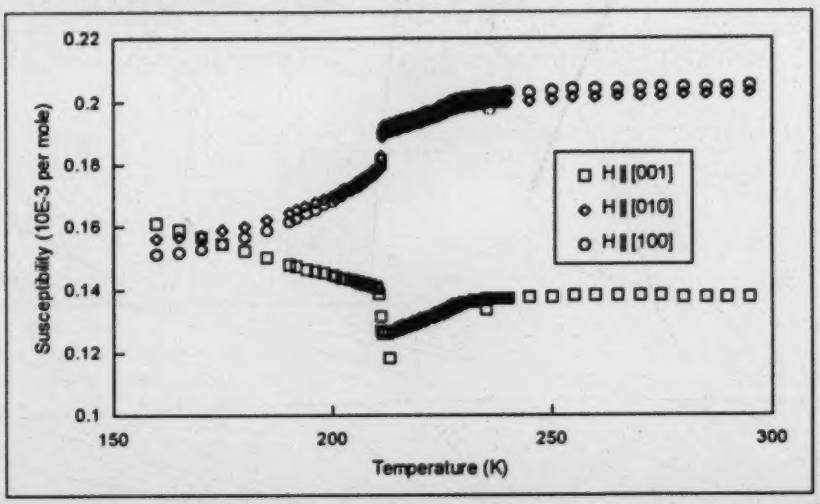

Figure 5.3.2 Susceptibility of an oriented CuO single crystal measured in 3 T.

Over a small range around both transitions, the susceptibility is approximately linear. T_{N1} was determined by fitting straight lines to the data from 220K to 227K and 234K to 240 K. The intersection of the lines gives T_{N1}. Similarly straight lines were fitted to data from 200 K to 206 K and 214 K to 220 K. The first deviation from these lines is referred to as T_{N2} low and high, and T_{N2} is taken as the average of the two values. The difference between them is a measure of the width of the transition and is referred to as ΔT_{N2}. Figures 5.3.3, 5.3.4 show T_{N1} and T_{N2} for the oxygen isotope samples, and figures 5.3.5 and 5.3.6 show the same for a pair of Cu isotopes.

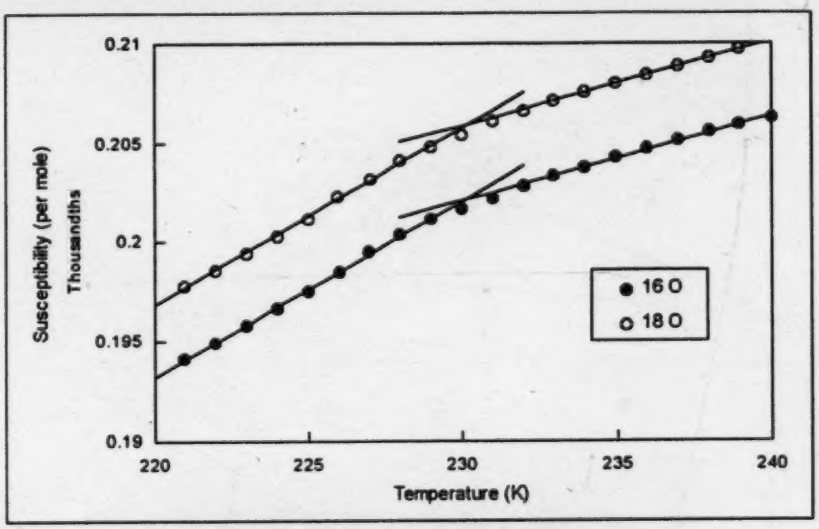

Figure 5.3.3 T_{N1} for oxygen isotope samples.

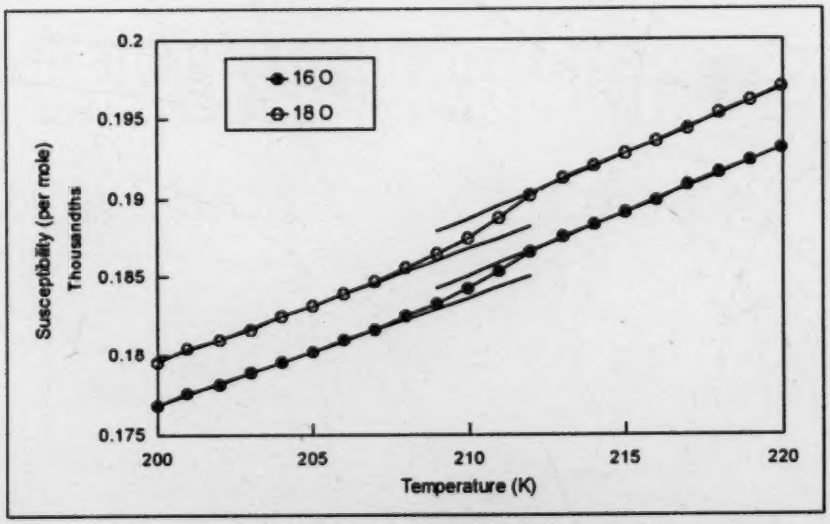

Figure 5.3.4 T_{N2} for oxygen isotope samples.

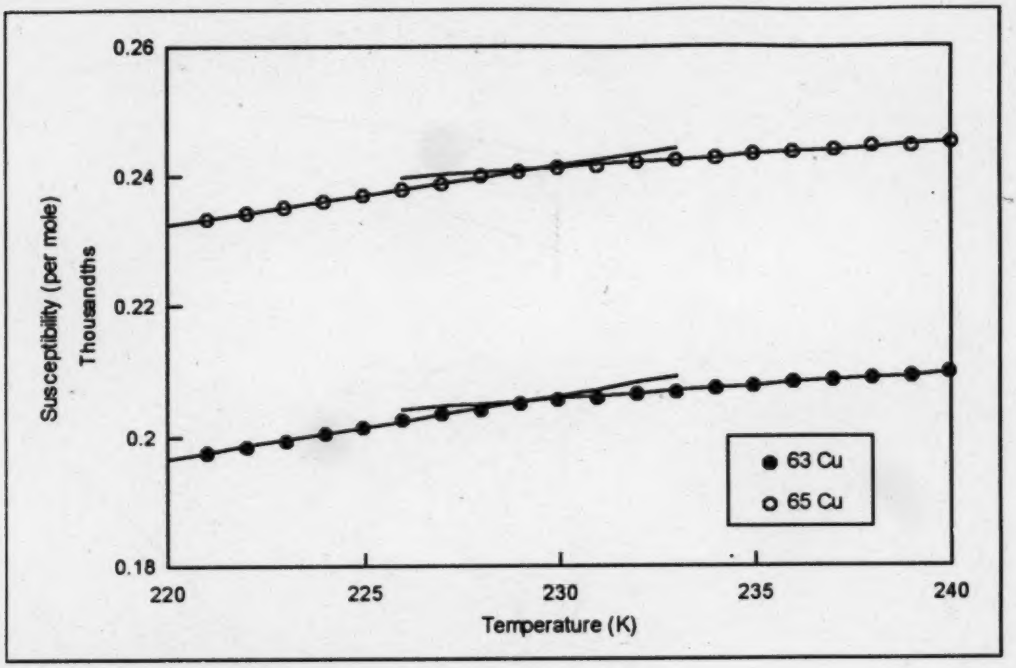

Figure 5.3.5 T_{N1} for Cu isotopes in 3 T.

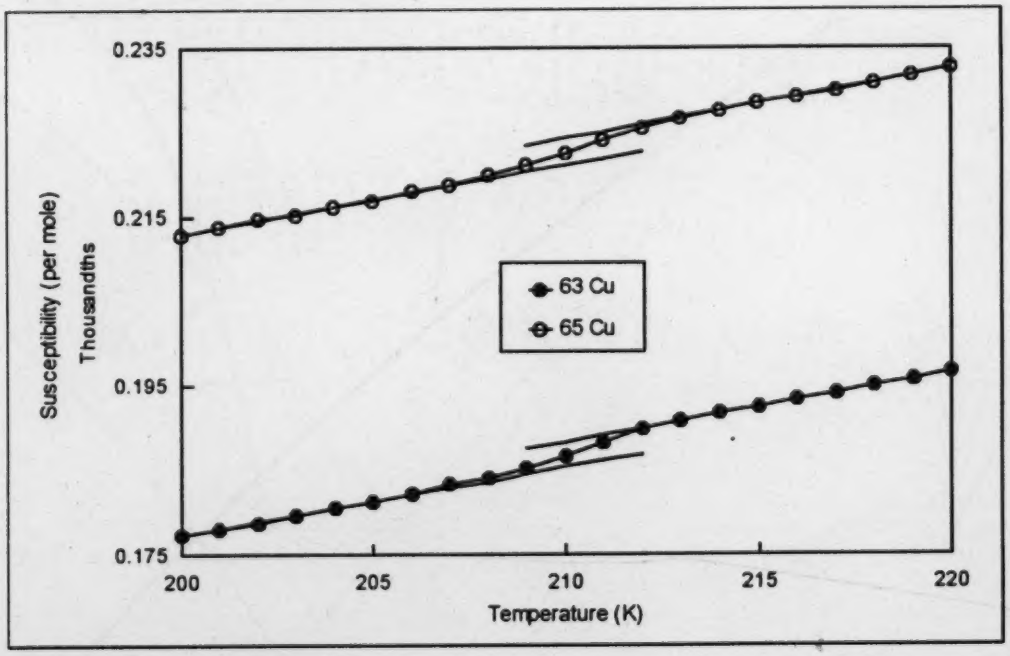

Figure 5.3.6 T_{N2} for Cu isotopes in 3 T.

Results of all measurements are summarized in table 5.3.1, along with values reported by other investigators. Overall, the agreement is quite good. The small differences may be attributed to slight differences in samples and measurement conditions. There is no observable dependence of either transition temperature on isotopic mass.

Table 5.3.1 Observed values for T_{N1} and T_{N2}.

Sample	T_{N1} (K)	T_{N2} (K)	ΔT_{N2} (K)
$Cu^{16}O$	231.07	211.06	3.9
$Cu^{18}O$	230.38	210.77	3.9
^{63}CuO-1	229.80	209.25	3.1
^{65}CuO-1	229.46	209.35	4.7
^{63}CuO-2	228.96	209.95	3.5
^{65}CuO-2	230.06	210.15	4.7
CuO (nat.)	229.72	209.65	4.1
CuO (single crystal)	228.0	211.0	/
Junod *et al.* (1989)	229.5	212.6	/
Loram *et al.* (1989)	230.0	212.0	/
Gmelin *et al.* (1990)	231.0	209.5	/
Zhao *et al.* (1994)	229.5 (^{16}O)	/	/
"	229.7 (^{18}O)	/	/
Roden and Freimuth (1987)	230.0	/	/
Chattopadhyay *et al.* (1990)	229.0	213	/
Köbler *et al.* (1991)	231.0	212	/

5.4 Discussion

As can be seen from table 5.3.1, there is rather good overall agreement with previously reported data. Two points deserve comment however.

The first concerns the absence of an isotope effect in the transitions. Given that the ordering is magnetic in origin, it is perhaps not surprising that there is no observed isotope effect. This raises questions about the strong spin-phonon interaction mentioned in the background to this chapter. The relative contribution of the spin-phonon coupling ($\lambda = 50\ cm^{-1}$) to the total superexchange interaction (≈ 70 meV) is small, $\hbar\lambda/J_o \approx 1.4$ %. The model used by Chen *et al.* (1995) shows $\lambda \propto m_{Cu}^{-1/2}$ (in the harmonic approximation). This allows the shift in T_N due to copper isotope substitution to be estimated as

$$\frac{\Delta T_N}{T_N} \approx \frac{\lambda}{J_o}\left(1 - \sqrt{\frac{65}{63}}\right) \approx 0.022\% \qquad (5.4.1)$$

Taking $T_N = 230$ K, this gives an expected shift of only 0.05 K. If the same value of the spin-phonon coupling is assumed to apply to oxygen modes, the expected shift is still small, ~ 0.20 K. Both of these possible shifts are much smaller than the variation shown in table 5.3.1, and, at least for copper substitution, are probably below the level of experimental detection. It should be noted that the model does not account for the two stage ordering and as a result, the shift in either T_{N1} or T_{N2} is likely to be smaller than these estimated shifts.

The second point concerns the observed 3 – 4 K width of T_{N2} in the powder samples. This width is unexpected in a first order transition in constant field. Figure 5.3.2 clearly shows that the transition is quite sharp in an oriented single crystal. The most likely explanation is local inhomogeneities in the powder samples. Variations in the oxygen content could be responsible,

but a second possibility is smearing of the transition due to randomly aligned grains coupled with the anisotropy in magnetization shown in figure 5.3.2. A possibility would be to magnetically align powder samples prior to measurement. This was considered, but most likely would have meant immersing powder samples in some type of medium that would then harden and preserve the alignment. This risked chemical contamination of the isotopically enriched samples and this was unacceptable, given that they were to be used in future investigations.

5.5 Summary for Chapter 5

There are no copper or oxygen isotope effects in either magnetic ordering temperature T_{N1} or T_{N2} of CuO within experimental uncertainty. This agrees with the previous work by Zhao et al., (1994) on the possibility of an oxygen isotope effect in T_{N1}. An estimate based on the relative strength of the spin-phonon coupling to the total superexchange interaction suggest that any effect is at, or below the level of experimental detection.

Chapter 6[1]

Copper Isotope Effect in $YBa_2Cu_3O_{7-\delta}$

6.1 Background

$YBa_2Cu_3O_{7-\delta}$ (YBCO) is probably the best known and most studied of the HTSCs. The structure of YBCO is shown in figure 6.1.1. There are four oxygen and two copper chemically inequivalent sites in the structure. The two copper sites, usually designated as Cu(1) and Cu(2) are labeled in the figure as chain and plane coppers respectively (there are actually two different plane copper sites, but the difference is minimal and is neglected here). Three of the four oxygen sites are indicated (chain – O(1), plane – O(3) and apical – O(4)). The O(2) site is the O located mid-way along the a-axis in the CuO plane.

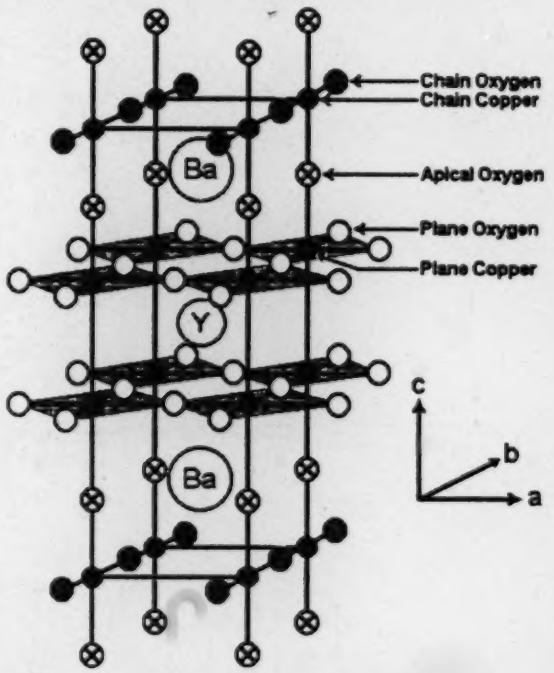

Figure 6.1.2 Structure of $YBa_2Cu_3O_{7-\delta}$ (YBCO). The structure shown has $\delta = 0$, see text. This figure neglects the buckling of the Cu-O planes.

As described in the introduction, YBCO is an n = 2 HTSC material. The charge reservoir layer is made up of linear CuO chains aligned along the b-axis. The figure shows the idealized, fully occupied ($\delta = 0$) structure. As the value of δ increases, vacancies occur in the chain oxygen positions. $\delta = 1$ corresponds to the absence of all chain oxygen. T_c is a maximum ($\approx$ 92 K) for a slight oxygen deficiency, $\delta = 0.06$, decreases slowly with increasing δ ($0<\delta<0.2$) then rapidly decreases ($0.2<\delta<0.35$) to around 60 K at which point it is relatively stable for $0.35 < \delta < 0.5$. Tc drops rapidly with further increases in δ and superconductivity is destroyed for $\delta \gtrsim 0.65$ (Jorgensen *et al.*, 1990). The plateau regions (relatively constant $T_c(\delta)$) are believed to be related to oxygen ordering in the CuO chains. Specifically, in the 60 K plateau chain oxygens may order in such a way that every other chain has a full oxygen occupation while intervening chains are unoccupied. This condition is believed to give rise to the most defined plateau structure. Disorder in the form of partial occupation of all chains is thought to smear out this plateau behaviour.

A large number of isotope studies have been made (See the review by Franck, 1994), and the results are generally consistent, but show some variation. Overall, a small effect is observed for oxygen at optimal doping ($\alpha_O \approx 0.02$ to 0.05, $T_c \approx 92$ K), and no effect is seen for

[1] A version of this chapter has been published. J.P. Franck and D.D. Lawrie 1995.Journal of Superconductivity. 8: 591-594.

other isotopes ($\alpha_{Cu} \approx \alpha_{Ba} \approx 0$ within the limit of detection; there is only one stable Y isotope). This changes quite drastically for doped samples, with values greater than $\alpha_O \approx 0.5$ in Pr doped YBCO (Franck 1991) being reported. Clearly, the oxygen isotope effect is a strong function of doping. It must be stressed that the chemical doping (replacement of Y by isovalent Pr or Cu by isovalent Fe, Ni or Zn) is not expected to alter the hole concentration in the Cu-O planes, while changing δ does. T_c changes in both cases however. Measurements of an isotope effect in materials with isovalent chemical substitution are therefore fundamentally different from measurements where T_c is changed simply by changing δ. For the purposes of future discussion, I will refer to the substitution of an isovalent, but different element as chemical doping, and the alteration of hole content by changes in the total oxygen content as intrinsic doping. Chemically doped samples are generally produced in a manner that ensures optimal oxygen content ($\delta \lesssim 0.06$). The results for the oxygen isotope effect ($^{16}O/^{18}O$) for a number of different chemically doped materials are shown in figure 6.1.1. Chemical doping is of the form $YBa_2M_xCu_{(3-x)}O_7$, where M = Fe, Ni or Zn; $Y_{(1-x)}Pr_xBa_2Cu_3O_7$ (Pr doping) and $YBa_{(2-x)}La_xCu_3O_7$ (La doping). The figure also includes the results of Zech *et al.* (1996), for the oxygen effect in oxygen deficient samples (i.e. intrinsically doped).

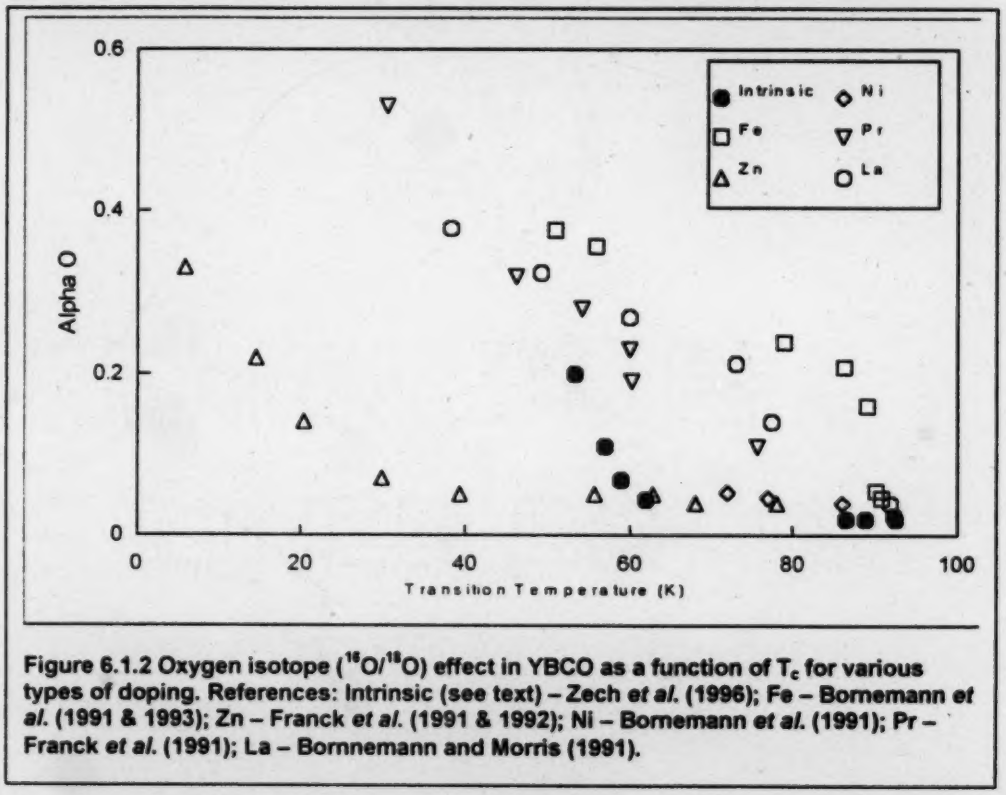

Figure 6.1.2 Oxygen isotope ($^{16}O/^{18}O$) effect in YBCO as a function of T_c for various types of doping. References: Intrinsic (see text) – Zech *et al.* (1996); Fe – Bornemann *et al.* (1991 & 1993); Zn – Franck *et al.* (1991 & 1992); Ni – Bornemann *et al.* (1991); Pr – Franck *et al.* (1991); La – Bornnemann and Morris (1991).

Values of α_O are plotted as a function of T_c in figure 6.1.1 since T_c is far from a universal function of doping, and plotting versus T_c allows a number of separate results to be placed on the same graph for comparison. The original papers should be consulted for the various $T_c(x)$ relations. In general, T_c decreases monotonically with increasing x (the exception is Zn doping (Lawrie *et al.*, 1997). The behaviour of $T_c(\delta)$ has been described above and results are given later in this chapter (figure 6.3.8). The principle point to be drawn from figure 6.1.1 is that as T_c decreases, α_O increases. A similar situation occurs in $La_{(2-x)}Sr_xCuO_4$ (LSCO). Results (Franck, 1993) for α_{Cu} in LSCO also show a similar trend.

Investigations have been made of the Cu and Ba isotope effects on T_c for optimally doped $YBa_2Cu_3O_{7-\delta}$, and table 6.1.1 lists a number of results. No studies examining either isotope effect as a function of doping (intrinsic or chemical) had been made at the time this investigation was begun. One (copper) has since been made by Zhao *et al.* 1996.

Table 6.1.1 Cu and Ba Isotope Exponents in YBCO

Isotopes	α_{Cu} or α_{Ba}	Reference
$^{63}Cu/^{65}Cu$	0	Katayama- Yoshida et al. (1987)
"	0 ± 0.07	Bourne et al. (1987)
"	0	Liu et al. (1988)
"	0.01 ± 0.03	Vasiliev et al. (1988)
"	0	Mascarenhas et al. (1989)
"	0	Franck et al. (1991)
$^{135}Ba/^{138}Ba$	0 ± 0.10	Bourne et al. (1987)
$^{134}Ba/^{135}Ba$	-0.10	Inyushkin et al. (1988)
$^{134}Ba/^{137}Ba$	0	Hidaka et al. (1988)

A major reason for the lack of Cu or Ba isotope studies as a function of doping relates to the high cost of Ba or Cu isotopes ($/mg). Chemical substitution studies typically require a fairly large amount of enriched starting material (on the order of one to two grams) to prepare a series of chemically substituted samples. Ba presents unique difficulties in that it has a number of stable isotopes and is also chemically quite reactive. As a result it is extremely difficult to obtain well separated and chemically pure isotopically enriched Ba compounds.

Intrinsic doping by varying the total oxygen content offers the possibility of using a single set of isotopically enriched samples and subjecting that set to a sequence of thermal treatments to produce a series of different total oxygen contents. The isotope effect for a number of different hole concentrations (oxygen contents) can then be examined. It is, of course, essential to ensure that the various thermal treatments do not irreversibly alter the sample. Repeating a given treatment, specifically the treatment that gives optimal oxygen content for T_c, can check this. This approach has been followed here. This investigation looks at the copper isotope ($^{63}Cu/^{65}Cu$) as a function of oxygen deficiency (δ).

The primary reason for conducting this investigation is to determine the behavior of α_{Cu} as a function of oxygen content (δ). This experiment is unique for two reasons. First, it is the first attempt to measure α_{Cu} as a function of δ. Second, it is a uniquely "clean" investigation. Isotopic substitution is achieved in a single initial preparation step. Changes in doping may then be achieved by treatment of the isotopic pair in the same atmosphere under identical conditions.

6.2 Experiment

Two sets of YBCO samples were prepared using ^{63}CuO and ^{65}CuO. The Cu isotopes were obtained from Oak Ridge National Laboratories. The materials were of high chemical purity (≥ 99.99 %) and were from the same separation run, so any impurities were likely to be very similar for the two isotopes. Separation was achieved using mass spectrometry methods and the same systems were used for the separation of a number of chemically different isotopes. The main source of trace impurities is contamination from previous runs on different elements (although this is minimal). Isotopes obtained from the same separation run are therefore much more likely to have similar trace impurities than those obtained from different runs.

. Enrichment was very high (99.67 % ^{63}Cu and 99.72 % ^{65}Cu). The same material was used in the examination of the antiferromagnetic transitions in CuO (Chapter 5). In order to ensure a consistent Y:Ba ratio, a master mix of high purity Y_2O_3 and $BaCO_3$ (both 99.999 % purity) was first prepared (Y:Ba = 1:2, per mole) and thoroughly ground in an agate mortar. Appropriate amounts of ^{63}CuO and ^{65}CuO were added to produce a final metals ratio of Y:Ba:Cu = 1:2:3 per mole. In order to reduce errors in weighing and subsequent grinding, relatively large amounts of the CuO isotopes were used (130 to 150 mg). Final sample masses were about 200 mg.

Parallel processing was adhered to at all times. Calcining (preliminary reaction of the mixed powders, in powder form) was performed twice in air at 910 °C for a total of 48 hours. Pellets (6 mm diameter, 1 mm thick) were prepared by pressing at approximately 200 bar for a few minutes. Two pairs of pellets were made. Pair 1 was sintered at 925 °C and 475 °C (36 h), and pair 2 at 940 °C and 475 °C (36 h). Both were treated in pure flowing oxygen in the OIES. Magnetic susceptibility was measured for each sample before any additional treatment was undertaken. Results showed T_c was virtually identical for each pair, with pair 1 T_c = 91.4 K and T_c = 91.5 K for pair 2, $\Delta T_c < 0.04$ K in both cases.

Two different approaches were used in making the samples oxygen-deficient. The first followed the method of Jorgensen *et al.* (1990). Pair 1 was treated at 520 °C in a mix of Ar and O_2 in the same line of the OIES. The final oxygen content of the samples was controlled by adjusting the oxygen partial pressure, while the annealing temperature was held constant. Typical annealing times were around 96 hours. At the end of the annealing period the samples were quenched into liquid nitrogen.

Pair 2 was treated at various temperatures ranging from 530 °C to 685 °C, in air (i.e. Constant O partial pressure, variable annealing temperature) again followed by quenching in liquid nitrogen. This is a commonly used process, see for example the pressure effect studies of Metzger *et al.* (1993).

T_c was determined by magnetic susceptibility measurements in a field of 3 G using a Quantum Design SQUID magnetometer, and was defined as the temperature at which the FC magnetization reached 1 % of its low temperature (5 K) value. 1% was chosen as the criteria since this portion of the magnetization curve is relatively insensitive to penetration depth effects in smaller grains. Franck (1994) gives a detailed discussion of the choice of T_c criteria in his review. Based on previous measurements in our lab, this definition of T_c is expected to be within 0.02 K of the actual value, or equivalently the uncertainty in T_c defined in this way is 0.02 K.

In both cases, samples were stored for a minimum of five days, under Ar, before final measurements of T_c. This storage time is essentially an annealing process, carried out at room temperature. It has been shown (Veal *et al.*, 1990, Claus *et al.*, 1990) that there is a gradual increase of T_c in oxygen-deficient YBCO as a function of time and a steady state value is reached a few days after quenching. A similar effect was observed in both pairs of samples.

The oxygen deficiency, δ, was determined by careful monitoring of mass changes due to thermal treatment with a microbalance. At $T_c = T_{c\,MAX}$, it is known that $\delta = 0.06$ (Jorgensen *et al.* 1990, many others), and subsequent values were calculated based on mass changes, using this as the starting value. This method is usable only if mass losses from other sources (physical loss of sample, desorption of water, etc.) are negligible. Repeated treatments under identical conditions showed mass changes of only 5 – 7 μg. This translates to an uncertainty in δ of 0.004 to 0.006. Typical mass changes in the 200 mg samples were on the order of a 100 μg to 1 mg, corresponding to changes in δ of 0.02 to 0.2 respectively. A range of δ values were investigated by successive treatments. After a large series had been investigated, both sample pairs were again treated in pure oxygen, as a check to ensure that no irreversible changes had occurred in the samples. The original T_c was recovered for both pairs.

6.3 Results

Figure 6.3.1 shows the transition temperature as a function of time for pair 2. The samples were stored at room temperature (293 K) between measurements.

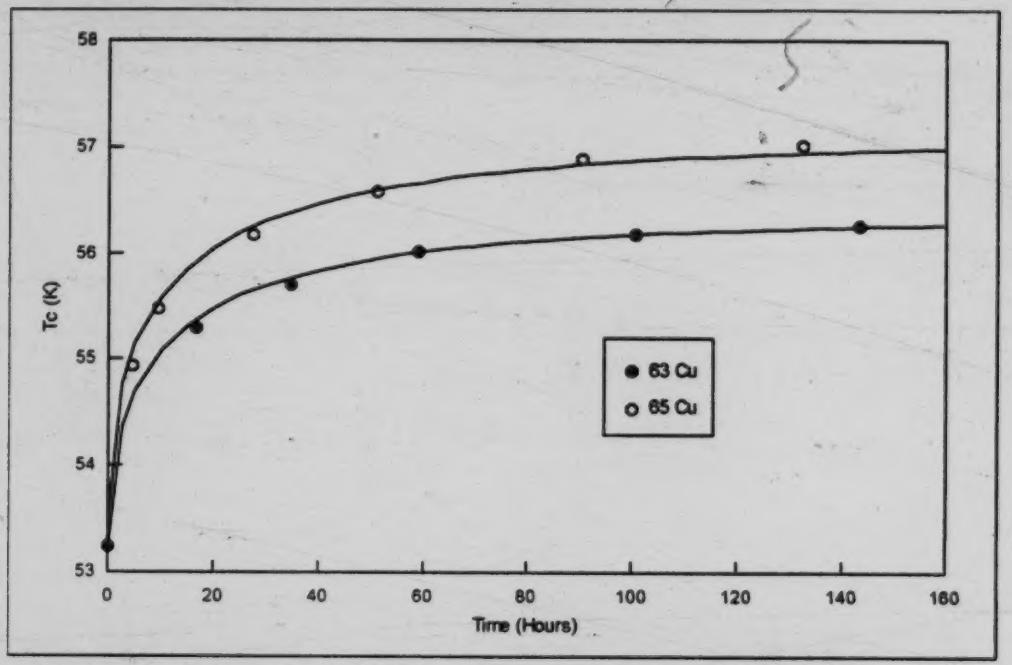

Figure 6.3.1 Time dependence of T_c for Pair 2. The lines are fits to the relation of Veal *et al.*, 1990.

The time dependence was fitted to the relation (Veal *et al.*, 1990):

$$T_c(t) = T_c(\infty) - [T_c(\infty) - T_c(0)]e^{-\sqrt{t/\tau}} \qquad \textbf{(6.3.1)}$$

Values of the relaxation times obtained from the fit are τ = 740 and 800 minutes and $T_c(\infty)$ = 56.15 K and 56.76 K respectively for the ^{63}Cu and ^{65}Cu samples. This pair was also stored at a number of different temperatures and although the time evolution was not followed, $T_c(\infty)$ values were obtained. Results are summarized in Table 6.3.1.

Table 6.3.1 Pair 2 $T_c(\infty)$ values for different storage temperatures.

Storage Temperature (K)	^{63}Cu $T_c(\infty)$ (K)	^{65}Cu $T_c(\infty)$ (K)
273	56.24	57.17
293	56.15	56.76
313	55.82	56.54
333	55.49	56.15

Typical normalized FC magnetic data for both pairs is shown in figures 6.3.2 to 6.3.7. Data are shown for the original fully oxygenated pair, a typical depleted pair and finally for the fully re-oxygenated pair.

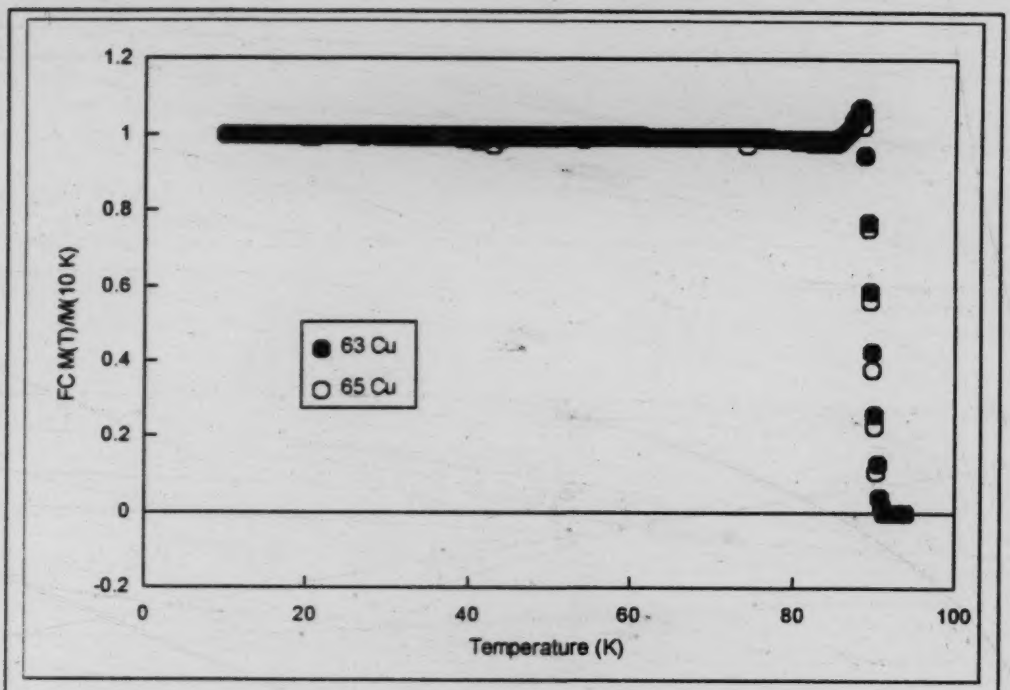

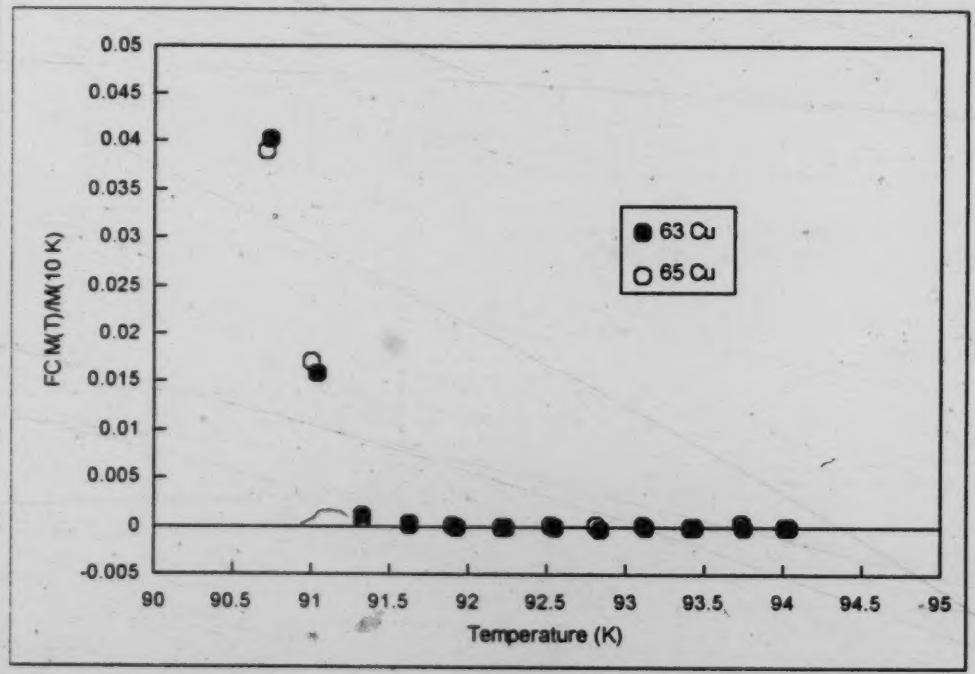

Figure 6.3.2 Normalized Field Cooled Magnetization for Pair 1 prior to oxygen depletion. Upper – Full temperature range. Lower – Enlargement showing the transition.

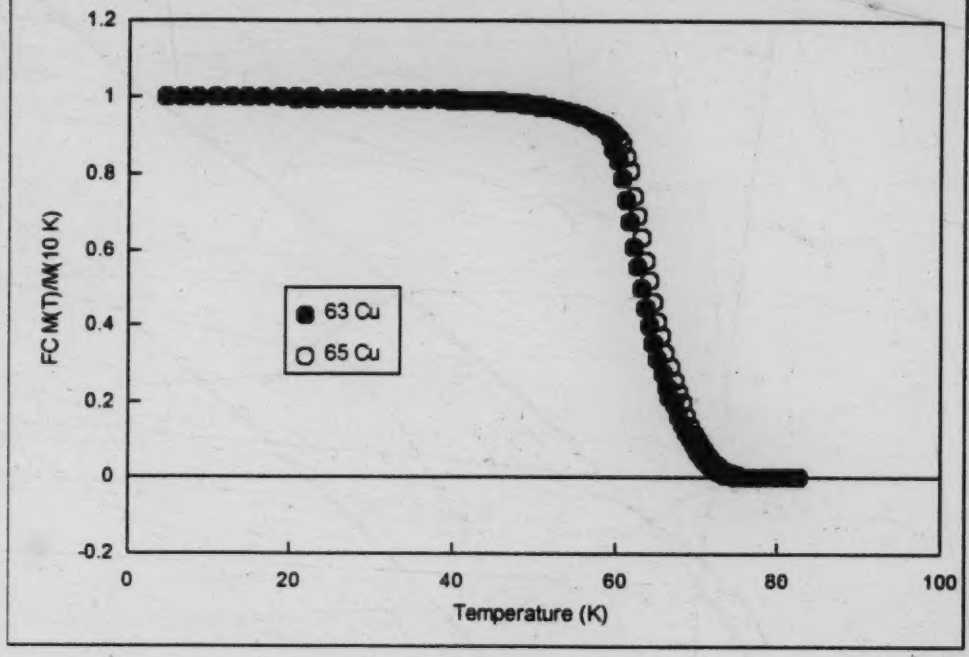

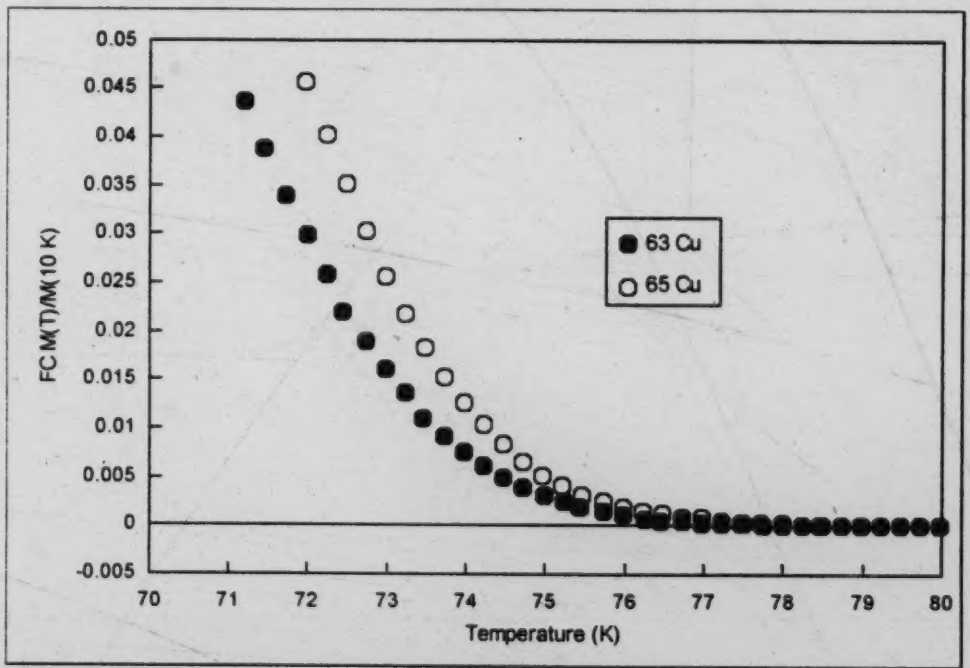

Figure 6.3.3 Normalized Field Cooled Magnetization for Pair 1, oxygen depleted δ = 0.30. Upper – Full temperature range. Lower – Enlargement showing the transition.

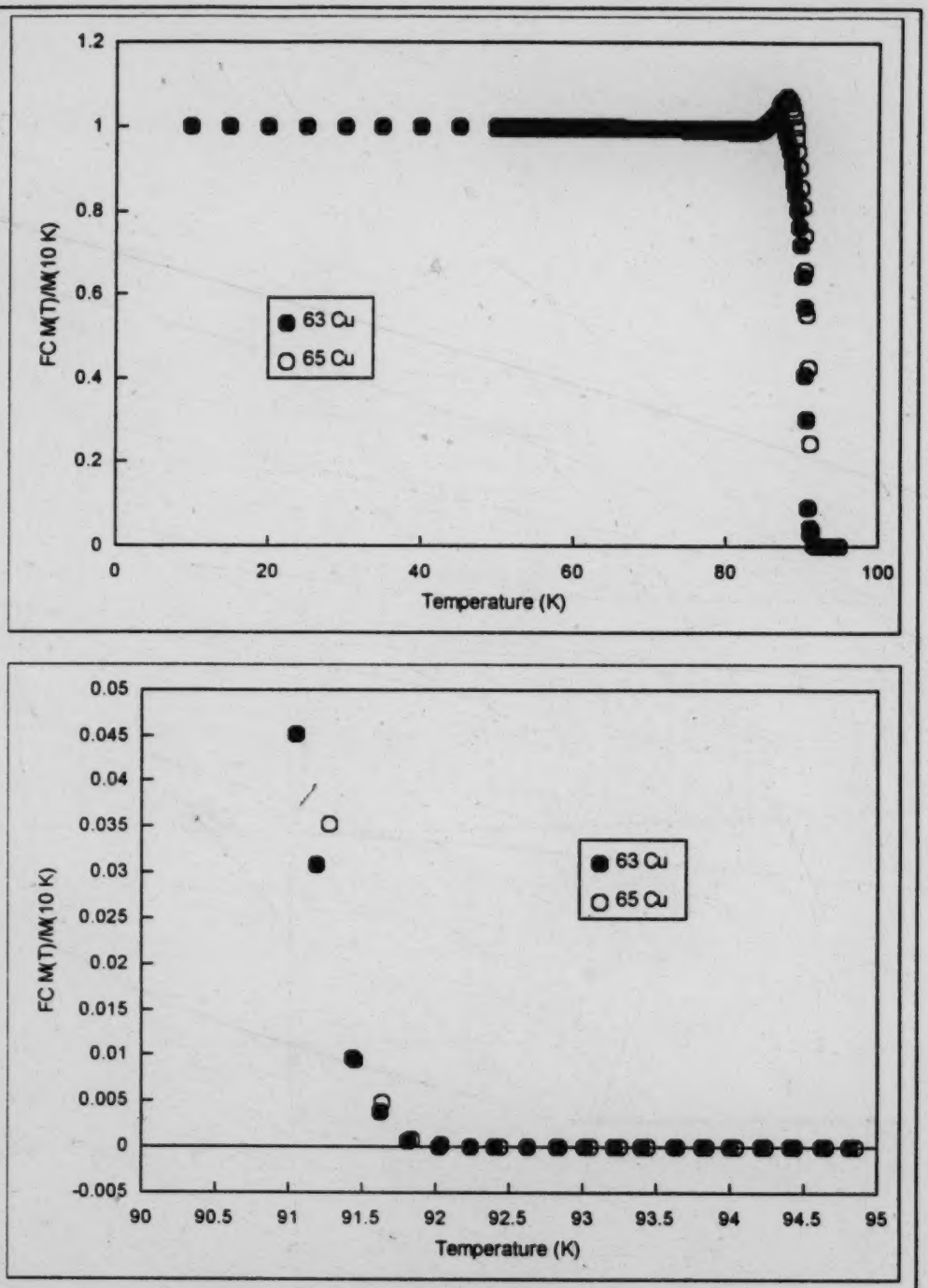

Figure 6.3.4 Normalized Field Cooled Magnetization for Pair 1, after re-oxygenation. Upper – Full temperature range. Lower – Enlargement showing the transition.

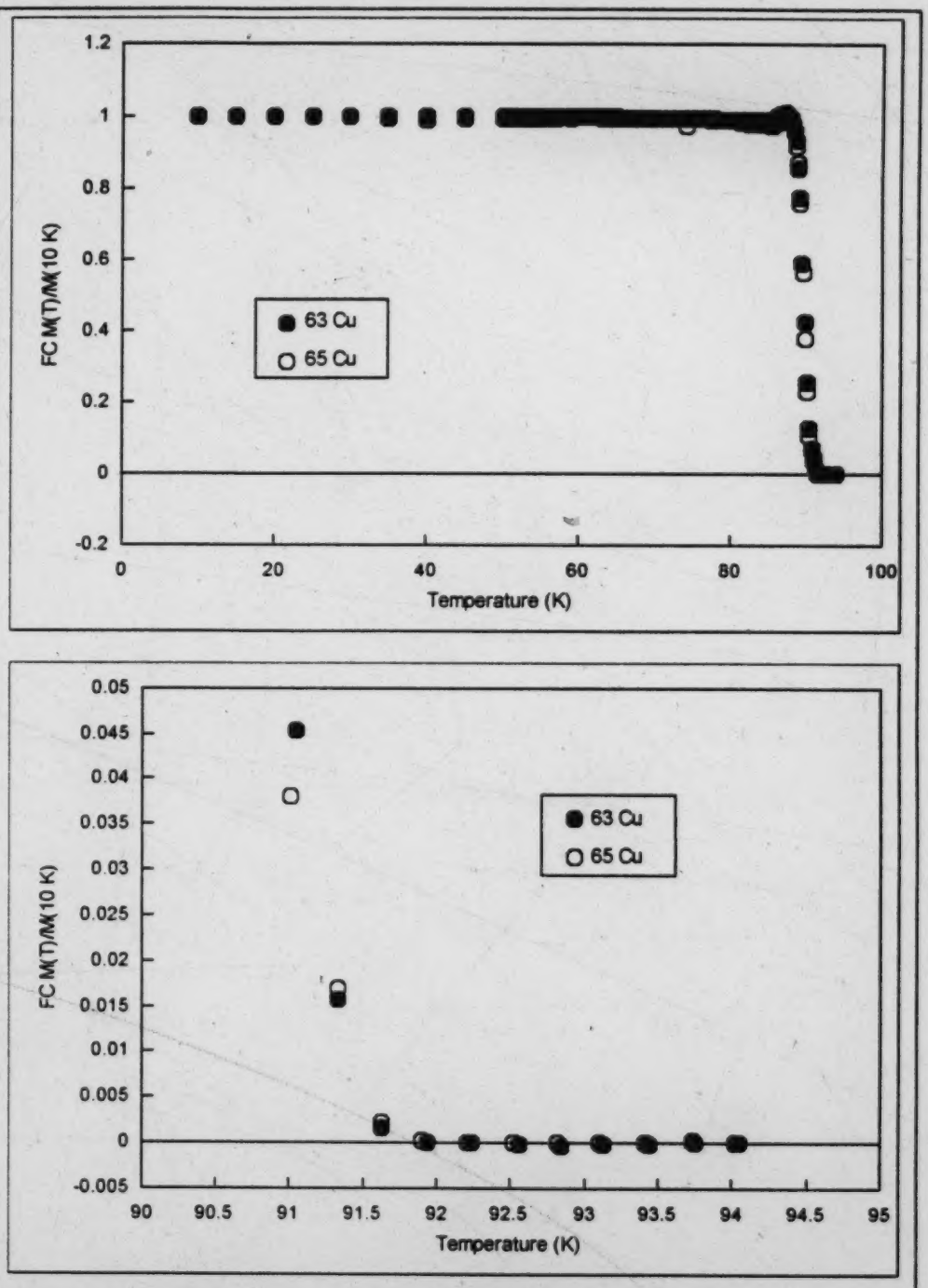

Figure 6.3.5 Normalized Field Cooled Magnetization for Pair 2 prior to oxygen depletion. Upper – Full temperature range. Lower – Enlargement showing the transition.

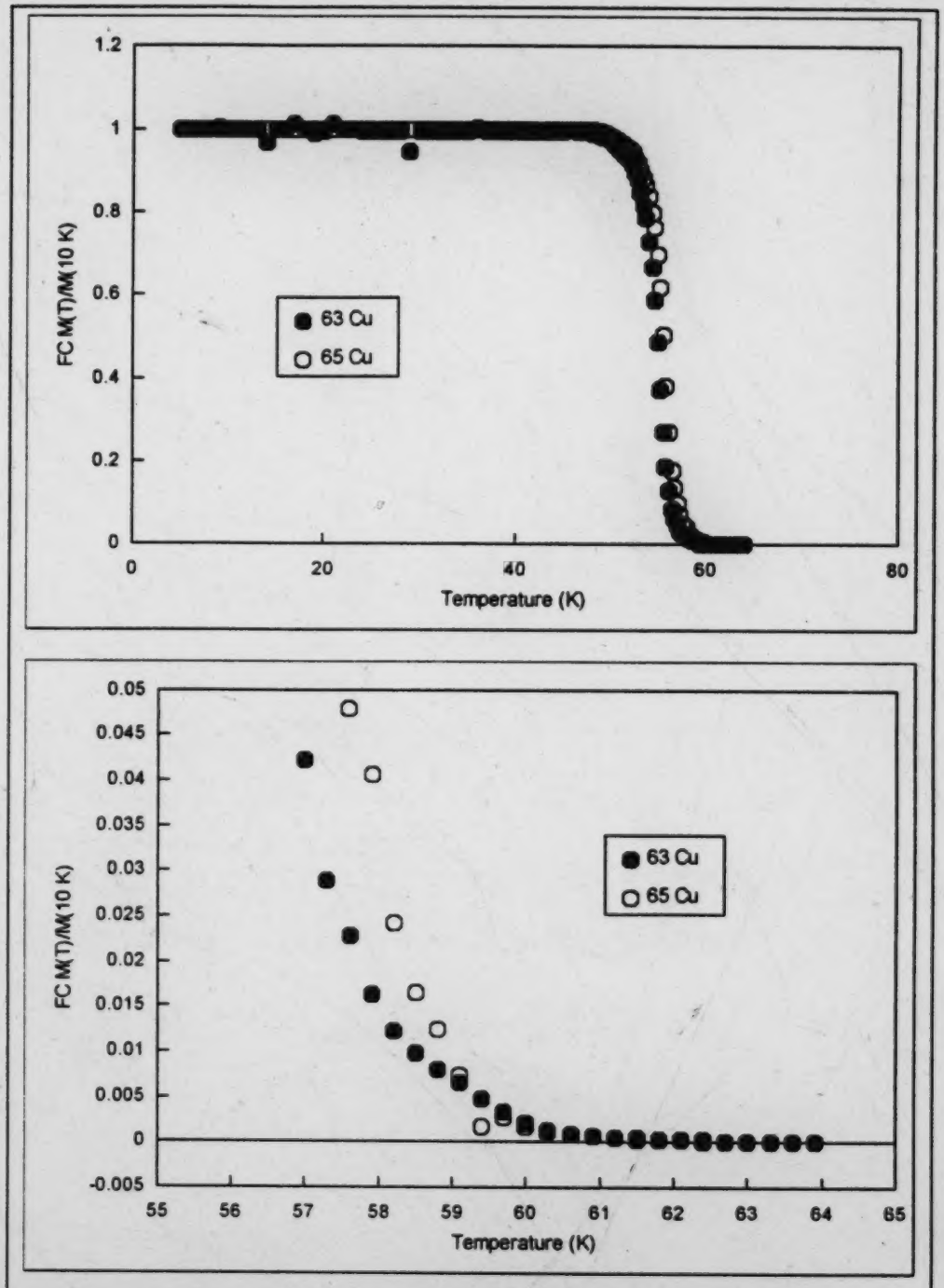

Figure 6.3.6 Normalized Field Cooled Magnetization for Pair 2, oxygen depleted $\delta = 0.44$. Upper – Full temperature range. Lower – Enlargement showing the transition.

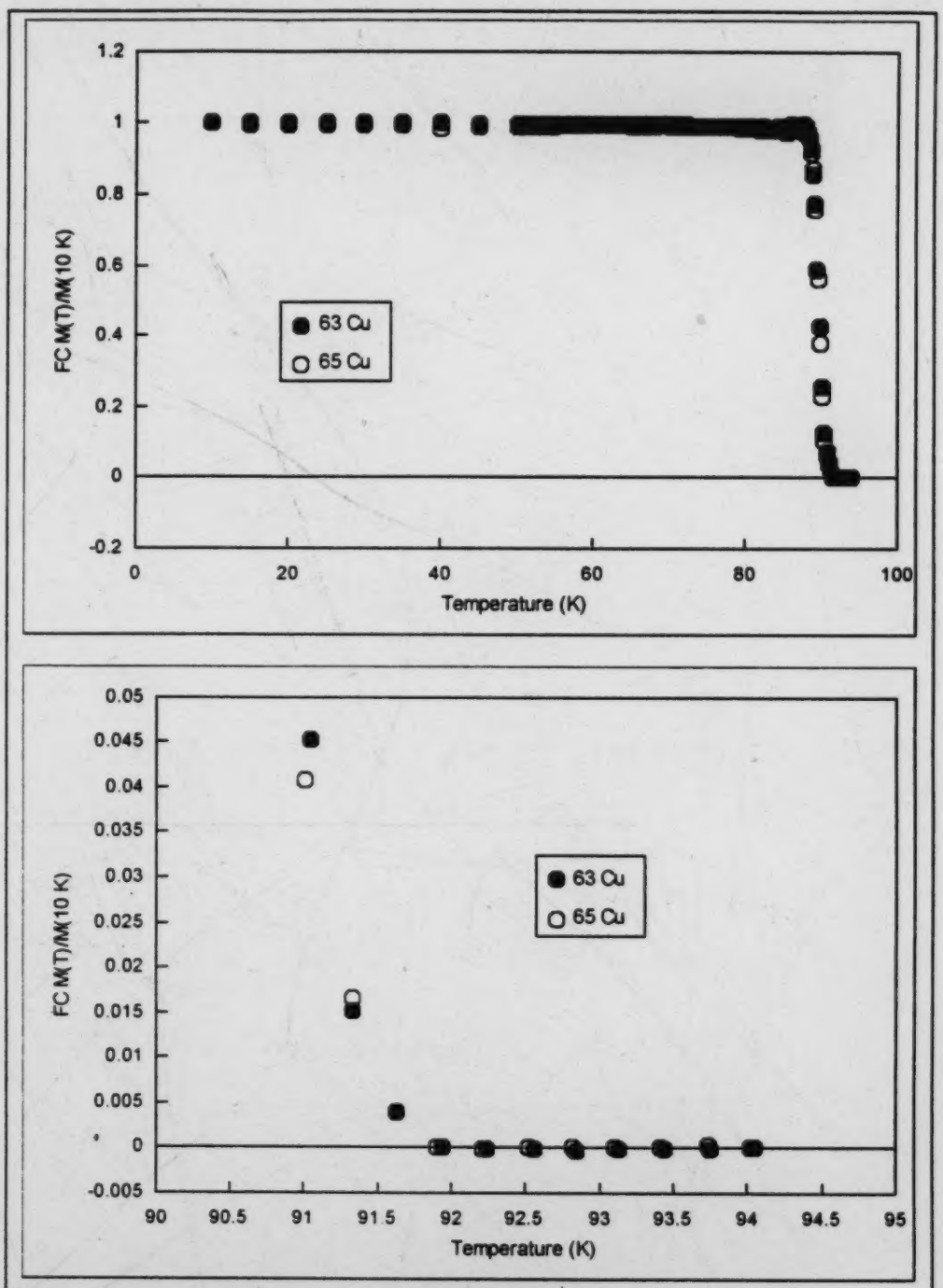

Figure 6.3.7 Normalized Field Cooled Magnetization for Pair 2, after re-oxygenation. Upper – Full temperature range. Lower – Enlargement showing the transition.

The results of all measurements are summarized in tables 6.3.2 and 6.3.3. Plots of the data are shown in figures 6.3.8 ($T_c(\delta)$) and 6.3.9 ($\alpha_{Cu}(\delta)$).

Table 6.3.2 Isotopic Shifts for Pair 1.

δ	T_c (K)	ΔT_c	α_{Cu}
0.06	91.20	< 0.04	< 0.013
0.32	66.92	-0.84 ± 0.07	-0.40 ± 0.03
0.36	62.25	-0.32 ± 0.06	-0.16 ± 0.03
0.39	61.30	-0.30 ± 0.05	-0.16 ± 0.03
0.38	60.90	-0.24 ± 0.06	-0.13 ± 0.03
0.39	61.38	-0.27 ± 0.05	-0.14 ± 0.03
0.45	59.90	-0.30 ± 0.05	-0.16 ± 0.03
0.48	61.34	-0.21 ± 0.05	-0.11 ± 0.03
0.39	61.25	-0.35 ± 0.05	-0.18 ± 0.04
0.24	85.23	-0.58 ± 0.05	-0.22 ± 0.02
0.32	67.40	-0.67 ± 0.05	-0.32 ± 0.02
0.25	83.65	-0.67 ± 0.05	-0.25 ± 0.02
0.27	80.00	-0.67 ± 0.05	-0.27 ± 0.02
0.30	73.62	-0.73 ± 0.06	-0.32 ± 0.03
0.51	59.53	-0.15 ± 0.05	-0.08 ± 0.03
0.63	40.87	-0.49 ± 0.05	-0.38 ± 0.04
0.59	49.50	-0.26 ± 0.05	-0.17 ± 0.03
0.06	91.40	< 0.04	< 0.013

Table 6.3.2 Isotopic Shifts for Pair 2.

δ	T_c (K)	ΔT_c	α_{Cu}
0.06	91.50	< 0.04	< 0.014
0.37	60.40	-0.68 ± 0.07	-0.36 ± 0.03
0.47	57.16	-0.80 ± 0.06	-0.44 ± 0.03
0.44	58.42	-0.65 ± 0.05	-0.35 ± 0.03
0.41	59.32	-0.60 ± 0.06	-0.32 ± 0.03
0.37	60.33	-0.58 ± 0.05	-0.31 ± 0.03
0.34	61.65	-0.64 ± 0.05	-0.33 ± 0.03
0.32	63.69	-0.67 ± 0.05	-0.33 ± 0.03
0.28	67.04	-0.91 ± 0.08	-0.43 ± 0.04
0.25	72.90	-0.90 ± 0.09	-0.39 ± 0.02
0.23	78.71	-1.27 ± 0.08	-0.51 ± 0.02
0.52	55.16	-0.96 ± 0.05	-0.55 ± 0.02
0.06	91.48	< 0.04	< 0.014

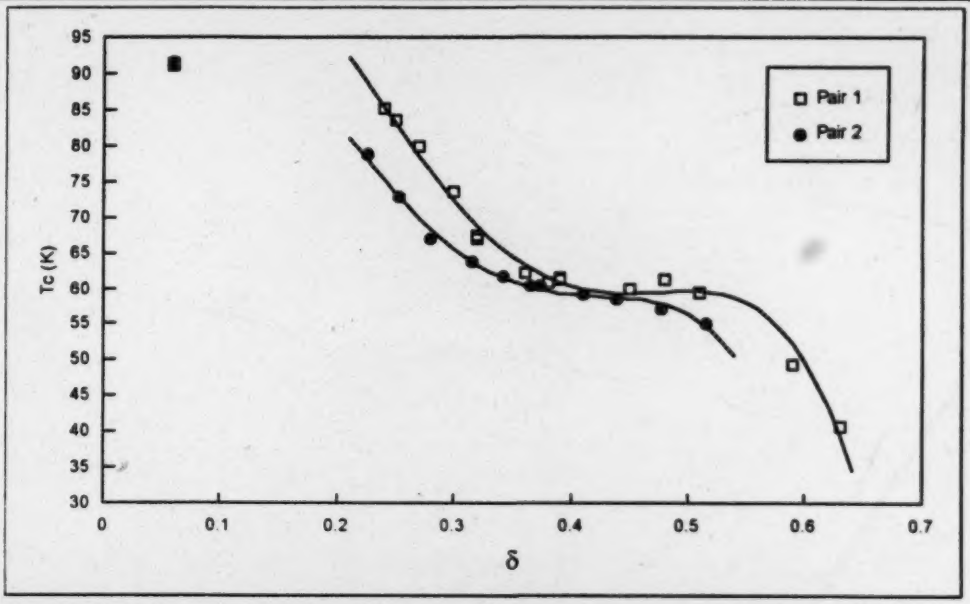

Figure 6.3.8 T_c as a function of δ for both sample pairs. The lines are 4th order polynomial fits to the data for the purpose of estimating $dT_c/d\delta$, see text. The solid square is the overlap of the two symbols.

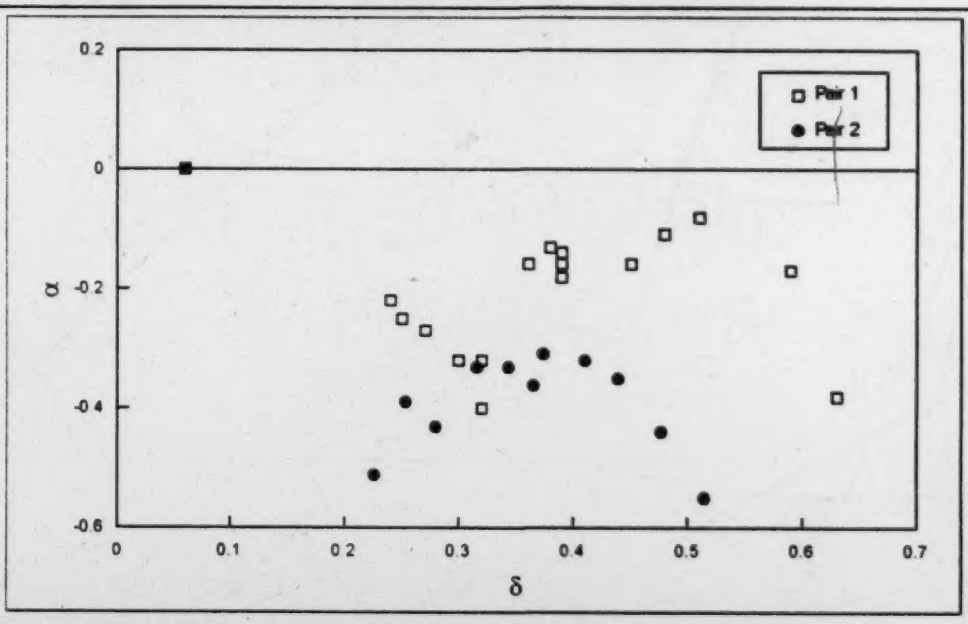

Figure 6.3.9 α_{Cu} as a function of δ for the two sample pairs. The solid square is the overlap of the two symbols.

6.4 Discussion

The time evolution of T_c shown in figure 6.3.1 and the different values of $T_c(\infty)$ resulting from different storage temperatures suggests that $T_c(\delta)$ is controlled by two factors. The first is the usual dependence on hole concentration determined directly by the oxygen content. The second is ordering of the oxygen in the Cu-O chains (Jorgensen *et al.*, 1990). It is important to remember that the changes in T_c associated with room temperature annealing occur without any changes in mass. This indicates that the total oxygen content remains constant. Yet T_c changes. If the total oxygen content is unchanged, the only possibility is changes in the position of various oxygen atoms. The decrease of $T_c(\infty)$ with increasing storage temperature supports this idea if higher storage temperatures are identified with more random oxygen distributions. It also suggests that the final $t = \infty$ equilibrium state is a dynamic one where at least some oxygen atoms have a high degree of mobility. It is unclear if the relaxation times for the two copper isotopes (^{63}Cu - 740 minutes, ^{65}Cu – 800 minutes) are significantly different. There is no obvious reason they should be different if the relaxation time is concerned with oxygen ordering.

The $T_c(\delta)$ dependence shown in figure 6.3.8 is generally similar for both sample pairs, but there are slight differences. Pair 2 shows a less pronounced plateau region and somewhat lower T_c values at a given value of δ compared to pair 1. As was discussed in the introduction to this chapter, the form of $T_c(\delta)$ is believed to be related to oxygen ordering in the Cu-O chains. These differences reflect the different preparation conditions, and suggest that the use of higher annealing temperatures in the preparation of pair 2 leads to more disorder in the Cu-O chains.

The most striking feature of the results of this section is that α_{Cu} has been found to be negative ($T_c(^{65}Cu) > T_c(^{63}Cu)$). It also shows a non-monotonic variation as a function of δ. Both sample pairs show larger negative values in the regions out side of the plateau areas, with smaller values occurring in the plateau region. At optimal doping the effect is very small ($\alpha_{Cu} < 0.01$) for both sample pairs, in agreement with previous work (table 6.1.1). There are differences in the actual values between the sample pairs however, with pair 2 consistently showing larger negative values. In the plateau region, α_{Cu} reaches values near – 0.14 and – 0.34 for pairs 1 and 2 respectively.

In order to more clearly illustrate the relationship between α_{Cu} and the form of $T_c(\delta)$, $\alpha_{Cu}(\delta)$ and $dT_c(\delta)/d\delta$ are plotted together in figure 6.4.1. $dT_c(\delta)/d\delta$ was estimated from the 4th

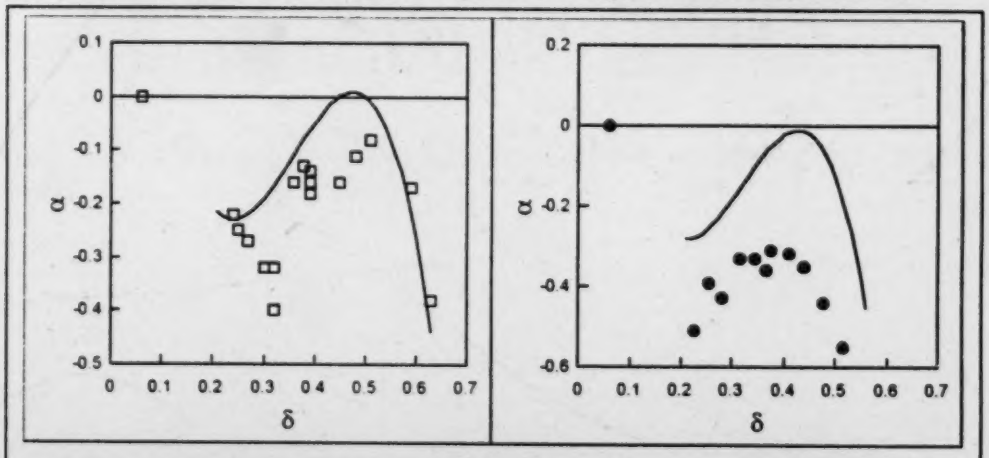

Figure 6.4.1 $\alpha_{Cu}(\delta)$ compared with $dT_c(\delta)/d\delta$. left – pair 1, right pair 2. The solid lines are $dT_c(\delta)/d\delta$ (see text for units), derived from the polynomial fits of figure 6.3.8.

order polynomial fits to $T_c(\delta)$ shown in figure 6.3.8. More elaborate fits were not attempted due to the lack of data in the region $0 < \delta < 0.2$, and lower order polynomials did not give good agreement. The fits are approximate, and disagree strongly with the data for $0 < \delta < 0.2$. However they do give a reasonable functional form for $T_c(\delta)$ in the region $0.23 < \delta < 0.65$ (pair 1) and $0.23 < \delta < 0.53$ (pair 2), and are sufficient for comparison purposes. $dT_c(\delta)/d\delta$ in figure 6.4.1 has been scaled for both pairs to lie in the region $0.1 < dT_c(\delta)/d\delta < -0.6$. Scaling factors are 1/1000 and 1/700 for pairs 1 and 2 respectively. Units are K. Fitting parameters are listed in table 6.4.1.

Table 6.4.1 Fitting parameters for $T_c(\delta) = a\,\delta^4 + b\,\delta^3 + c\,\delta^2 + d\,\delta + e$

Coefficient	Pair 1	Pair 2
a	- 9222.4	- 9529.6
b	13201	12155
c	- 6325.2	-5151.7
d	1035.9	711.41
e	49.225	64.866

There is clearly a strong correlation between rapid changes in T_c and large values of α_{Cu}. The results for pair 1 clearly show that α_{Cu} is smallest in the 60 K plateau region, i.e. in the region of smallest $dT_c(\delta)/d\delta$. The smallest values for pair 2 occur at slightly lower values of δ than the lowest values of $dT_c(\delta)/d\delta$, but this may be an artifact of the fitting.

In YBCO, there is no simple relation between δ and the hole concentration n in the Cu-O planes, but the two are connected. The connection between α_{Cu} and $dT_c(\delta)/d\delta$ suggests a connection between α_{Cu} and dT_c/dn. This is reminiscent of models suggested by Schneider and Keller (1992 and 1993) and by Kresin and Wolf (1994). Both groups have proposed that the measured isotope coefficient may be written as

$$\alpha_{OBS} = \alpha_\omega + \alpha_n \qquad \textbf{(6.4.1a)}$$

$$= -\left(\frac{\partial \ln T_c}{\partial \ln \omega}\right)\left(\frac{\partial \ln \omega}{\partial \ln m}\right) - \left(\frac{\partial \ln T_c}{\partial \ln n}\right)\left(\frac{\partial \ln n}{\partial \ln m}\right) \qquad \textbf{(6.4.1b)}$$

$$= -\frac{m}{T_c}\left(\frac{\partial T_c}{\partial \omega}\right)\left(\frac{\partial \omega}{\partial m}\right) - \frac{m}{T_c}\left(\frac{\partial T_c}{\partial n}\right)\left(\frac{\partial n}{\partial m}\right) \qquad \textbf{(6.4.1c)}$$

The first term is the usual isotope exponent due to a change in the phonon spectrum as a result of mass changes. ω is a characteristic phonon frequency for mass m. α_ω does not depend on n. The second term is the isotope effect in T_c due to changes in the hole concentration n as a result of the dependence of n on m. At optimal doping and in the plateau region $dT_c(\delta)/d\delta$, and equivalently dT_c/dn are zero, and in these regions one observes α_ω. At optimal doping, $\alpha_{Cu} = 0$, and this implies that the variation in $\alpha_{Cu}(\delta)$ is determined solely by α_n. One would then expect $\alpha_{Cu} \approx 0$ in the plateau region, contrary to the results found here. Further consideration is required however.

There is a structural phase transition at $\delta \approx 0.65$ (orthorhombic to tetragonal, Jorgensen *et al.*, 1990) and the a and b lattice parameters approach each other in size (b decreases, a increases) as $\delta \rightarrow 0.65$. This suggests that the characteristic phonon frequency ω may also be changing with δ, and therefore that α_ω itself varies with δ. In this case, one would expect larger observed isotope exponents ($\alpha_\omega(\delta) + \alpha_n$) outside the plateau region but not necessarily zero in the plateau ($\alpha_\omega(\delta)$), in agreement with the findings of this section. It is important to emphasize that

this dependence of α_∞ on δ is not related to changes in the hole concentration but is a result of structural changes that take place as δ varies.

With these considerations it is interesting to attempt to obtain values for $\partial \ln n/\partial \ln m$. This has been done by Schneider and Keller and by Kresin and Wolf by fitting to data for α_O. The two groups find $\partial \ln n/\partial \ln m_O$ = - 0.125 and - 0.13 respectively.

Equation 6.4.1b can be rearranged to give

$$\frac{\partial \ln n}{\partial \ln m_{Cu}} = \frac{(\alpha_\infty - \alpha_{OBS})}{\left(\frac{\partial \ln T_c}{\partial \ln \delta}\right)\left(\frac{\partial \ln \delta}{\partial \ln n}\right)} \qquad \textbf{(6.4.2)}$$

$\partial \ln n/\partial \ln \delta$ has been shown to be essentially constant for $\delta \geq 0.2$ by Zimmerman *et al.* (1995) based on μSR measurements of the penetration depth, with a value of about – 0.43. Values for $\partial \ln T_c/\partial \ln \delta$ can be obtained from the fits to $T_c(\delta)$. These are shown in figure 6.4.2.

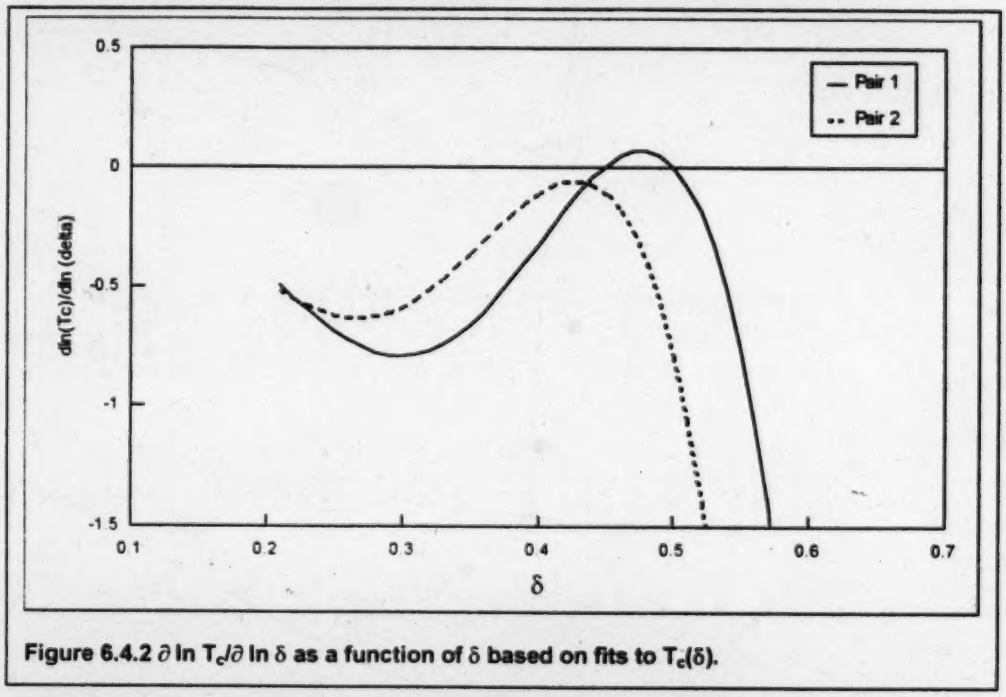

Figure 6.4.2 $\partial \ln T_c/\partial \ln \delta$ as a function of δ based on fits to $T_c(\delta)$.

As a first estimate, $\partial \ln n/\partial \ln m_{Cu}$ will be calculated with the assumption that α_∞ is zero in the plateau region. In this case values of + 1.07 (pair 1 with α_{OBS} = - 0.14) and + 0.70 (pair 2 with α_{OBS} = - 0.34) are obtained. These values are much larger than the equivalent oxygen values and are of the opposite sign. Given the comments above on the possible dependence of α_∞ on δ, the assumption that α_∞ is zero in the plateau region is probably unwarranted.

The other alternative is to assume that α_n is zero in the plateau, in line with the original conjecture. The observed isotope exponents are then α_∞, and equation 6.4.2 can again be used to attempt to determine $\partial \ln n/\partial \ln m_{Cu}$ in the regions outside the plateau. In this case, there is the problem of determining α_∞ outside the plateau. As an approximation, the values of α_{OBS} in the

plateau can be used. Since $\alpha_n = 0$ at optimal doping and assumes finite values in the plateau, this is probably not that reasonable an assumption, but is good enough for an estimate for comparison purposes. Proceeding in this manner, at $\delta = 0.24$, $\partial \ln n/\partial \ln m_{Cu} = 0.059$ (pair 1, $\alpha_n = -0.14$, $\alpha_{OBS} = -0.23$) and 0.093 (pair 2 $\alpha_n = -0.34$, $\alpha_{OBS} = -0.47$). These values are smaller than the equivalent oxygen values and again are of opposite sign. The relative difference between the pairs is about the same (35 %).

Clearly, the results for the two pairs cannot be fitted to equation 6.4.1 using the same value of $\partial \ln n/\partial \ln m_{Cu}$, at least as far as the simple assumptions made above are concerned. Even so, this analysis does qualitatively account for the general form of $\alpha_{Cu}(\delta)$. Large values of α_{Cu} outside the plateau are due to $\alpha_n + \alpha_n$, while finite values in the plateau, where $\alpha_n = 0$, are due to α_n that has changed from the optimal value ($\alpha_n = 0$) due to structural changes associated with the change in δ. An important question to ask is if it is reasonable to assume that the results for both pairs should be explainable by a single value of $\partial \ln n/\partial \ln m_{Cu}$. Given the different preparation conditions and the resulting differences in oxygen ordering it may not be.

A more fundamental question concerns the sign of α_{Cu}. These results are the first time a large negative isotope effect has been reported for any HTSC. A similar investigation has now been completed by Zhao *et al.*, (1996), and while they find similar absolute values for α_{Cu}, the reported values are positive ($T_c(^{63}Cu) > T_c(^{65}Cu)$). Figure 6.4.3 is a reproduction of 6.3.9 with the data of Zhao *et al.* added for comparison. The reason for this difference in sign is not known, but

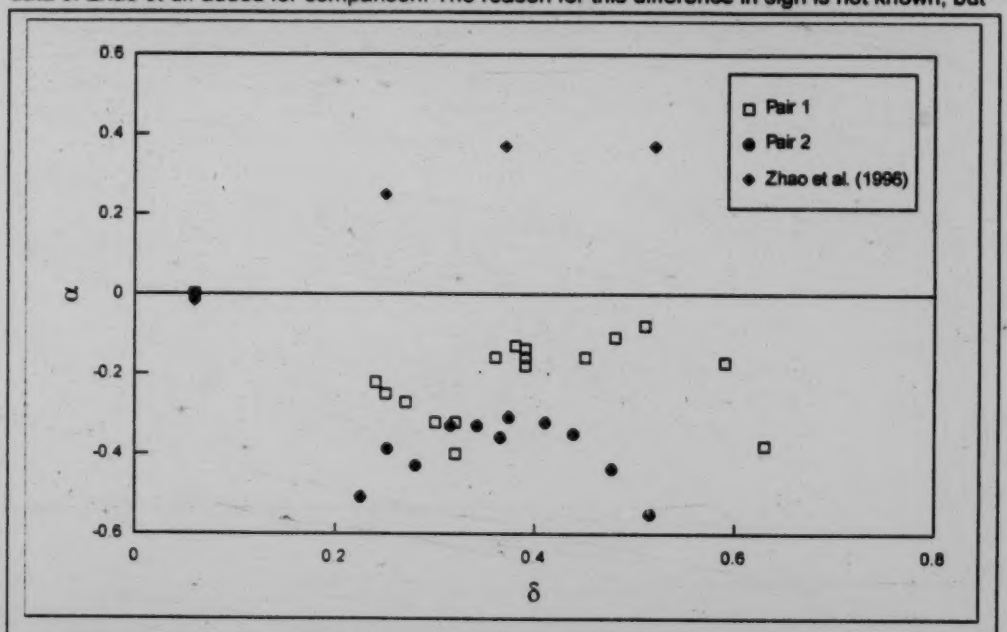

Figure 6.4.3 Reproduction of figure 6.3.9 with data of Zhao *et al.* (1996) added for comparison.

may be due to differences in ordering of Cu-O chains due to different sample production methods. Mass spectrometry was used to check that the samples used in this investigation had the expected isotopic composition. Zhao *et al.* do not report if a similar test was made on their samples.

The only other copper isotope effect studies in HTSC materials are those of Franck (1993) on $La_{(2-x)}Sr_xCuO_4$. In this case, a positive effect was found, with small relatively small

values at optimal doping (α_{Cu} = 0.15, at x = 0.15) but much larger values (α_{Cu} = 0.93) at lower doping (x = 0.125).

Until more copper isotope experiments are done (both on YBCO and other HTSCs) the sign of the effect will remain in question. YBCO and related compounds, such as $YBa_2Cu_4O_8$, are relatively unique among the HTSC materials in that the charge reservoir layers also contain copper. Copper isotope effect studies on these materials therefore simultaneously probe the effect of isotopic substitution on both the Cu-O planes and the charge reservoir layers. This fact may offer a starting point for an explanation of observed difference in sign of α_{Cu} between $La_{(2-x)}Sr_xCuO_4$ and $YBa_2Cu_3O_{7-\delta}$.

Finally, the pressure dependence of T_c in YBCO shows a qualitatively similar behaviour (Kraut *et al.*, 1993) as a function of δ to α_{Cu}. dT_c/dP is close to zero for optimally doped material and small (1.5 K/GPa) in the 60 K plateau. It becomes large (5 K/Gpa) in the region between optimal doping and the 60 K plateau, and below the plateau. Franck (1996 and 1998) has discussed these observations in detail.

6.5 Summary for Chapter 6

This chapter reports results for $\alpha_{Cu}(\delta)$ for $YBa_2Cu_3O_{7-\delta}$ for $0.06 \leq \delta \leq 0.60$. Measurements were performed on two sets of highly enriched (99.67 % ^{63}Cu and 99.72 % ^{65}Cu) sample pairs. Oxygen depletion was achieved by annealing at either constant temperature and various oxygen partial pressures; or constant oxygen partial pressure and various temperatures, followed in both cases by quenching in LN_2.

Results for the two preparation methods are similar, but show slight differences. The principle observations are:

1. α_{Cu} is negative for all values of δ.
2. α_{Cu} = 0 for optimal doping (δ = 0.06).
3. It is a non-monotonic function of δ, being large (up to – 0.55) in the region between optimal doping and the 60 K plateau, smaller, but not zero, in the plateau, and large beyond the plateau.

Chapter 7

Oxygen Isotope Effect in $Bi_2Sr_2CaCu_2O_{8+y}$

7.1 Background

The bismuth family of HTSCs consists of three closely related materials having the chemical formula $Bi_2Sr_2Ca_{(n-1)}Cu_nO_{2(n+2)+y}$, where n = 1, 2 or 3. The n value determines the number of adjacent CuO planes as described in the introduction. A shorthand notation has developed and the materials are commonly referred to as BSCCO 22(n-1)n, or simply 22(n-1)n, for example this chapter is concerned with BSCCO 2212. The idealized tetragonal structure for 2212 is shown in figure 7.1.1. All three materials usually have a slight orthorhombic distortion. The excess oxygen is located in the BiO layers, where there are two inequivalent oxygen sites. One site is always occupied and the other shows variable occupation. The structure shown is for y = 0. In addition, a long-range incommensurate structural modification has been observed in electron diffraction experiments (Martin and Lee, 1995 and references therein). These modifications are ignored in the figure, for simplicity. Note again that the oxygen content (y) is somewhat variable, and the T_c value is for the optimal composition. Lattice parameter values are for the idealized tetragonal structure (Maeda *et al.*, 1990 and Braun *et al.*, 1991).

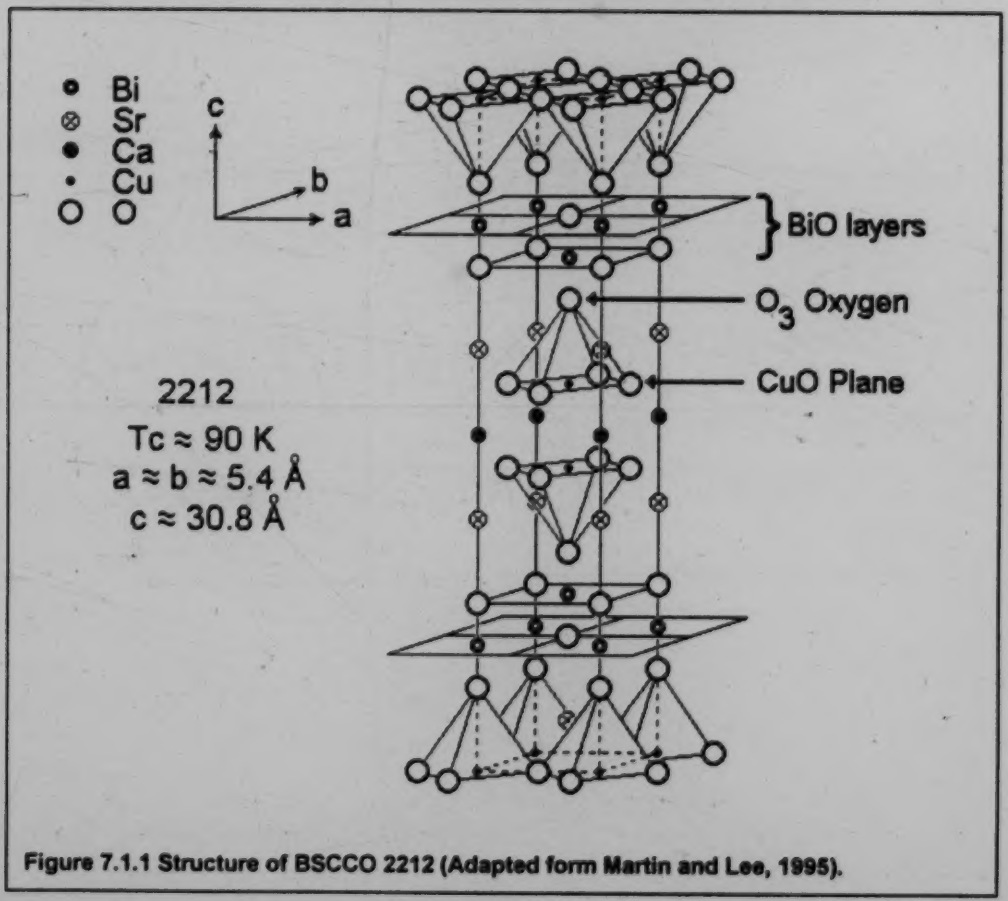

Figure 7.1.1 Structure of BSCCO 2212 (Adapted form Martin and Lee, 1995).

The BSCCO materials may be synthesized by the solid-state reaction method, but the existence of three closely related phases complicates matters considerably. It is very difficult to produce good single phase samples, and pure single phase 2223 does not seem to have been produced to date. The use of PbO in the synthesis procedure is generally cited as improving the 2223 fraction (Takano *et al.*, 1988; many others); but in this case there seems to be some substitution of Pb for Bi, so it is unclear if the final material is "pure" 2223. In addition, the structural modifications mentioned above lead to a complex powder x-ray diffraction pattern, making the determination of small amounts (5-10 %) of additional phases difficult. Finally, T_c is determined by the excess oxygen content y, which is a function of annealing temperature and oxygen partial pressure.

Only a few investigations have been conducted on the oxygen isotope effect in the BSCCO system. Results are summarized in table 7.1.1. No investigations seem to have been made for other isotope effects or on the 2201 phase at all.

Table 7.1.1 Oxygen Isotope Effect results in the BSCCO system

Material	T_c (K)	α_O	Reference
$Bi_2Sr_2Ca_2Cu_3O_x$	110	0.03	Katayama-Yoshida *et al.* (1988)
	75	0.03 to 0.05	
$Bi_{1.6}Pb_{0.4}Sr_2Ca_2Cu_3O_{10}$	108	-0.013 ± 0.002	Bornemann *et al.* (1991)
$Bi_2Sr_2Ca_{(1-x)}Y_xCu_2O_8$			Bornemann *et al.* (1992)
x = 0.00	75.5	0.03	
0.063	78.0	0.012	
0.250	71.3	0.065	
0.350	45.2	0.109	
$Bi_2Sr_2CaCu_{(2-x)}Fe_xO_8$			Bornemann *et al.* (1992)
x = 0.01	74.1	0.079	
0.02	71.5	0.000	
0.04	65.7	-0.101	

A few comments are in order. First it should be noted that all of the results in table 7.1.1 are for essentially different materials. That being said, the differences for nominally similar materials are most likely due to differences in oxygen content and the possible complications of additional phases. For example, the inconsistent 2223 results were obtained on mixed phase (2212 & 2223) samples, and an extrapolation procedure was used to obtain T_c. Katayama-Yoshida *et al.* found $\alpha_O = 0.03$, but the 2223 phase was probably only about 10 % of the total sample. Bornemann *et al.* (1991) found $\alpha_O = -0.013 \pm 0.002$, with the 2223 phase about 75 % of the total. They report a composition of $Bi_{1.6}Pb_{0.4}Sr_2Ca_2Cu_3O_{10}$, while the Katayama-Yoshida group did not use Pb in their synthesis.

The variation of T_c as a function of y in 2212 has been well studied, and there is general qualitative agreement (Allgeier *et al.*, 1990; Triscone *et al.*, 1991; Moodenbaugh *et al.*, 1996). $T_c(y)$ is approximately parabolic, with a maximum T_c around 90 K. The width and optimum y value vary between investigations, and this is probably due to variations in both sample preparation and the procedure used to determine y values. Data from Allgeier *et al.* are shown in figure 7.1.2. The y values were determined by careful weight loss measurements following an initial iodometric titration. Different T_c and y values were obtained by heating the starting material (y = 0.24) to various temperatures in vacuum, resulting in oxygen loss. The line is a parabolic fit to the data and can be written as

$$T_c = T_{cMax}\left[\, 1 - C(y - y_{opt})^2 \,\right] \qquad (7.1.1)$$

with values C = 31.72, $y_{opt} = 0.1531$ and $T_{c\,MAX} = 92.35$ K. This form will be useful for later discussion.

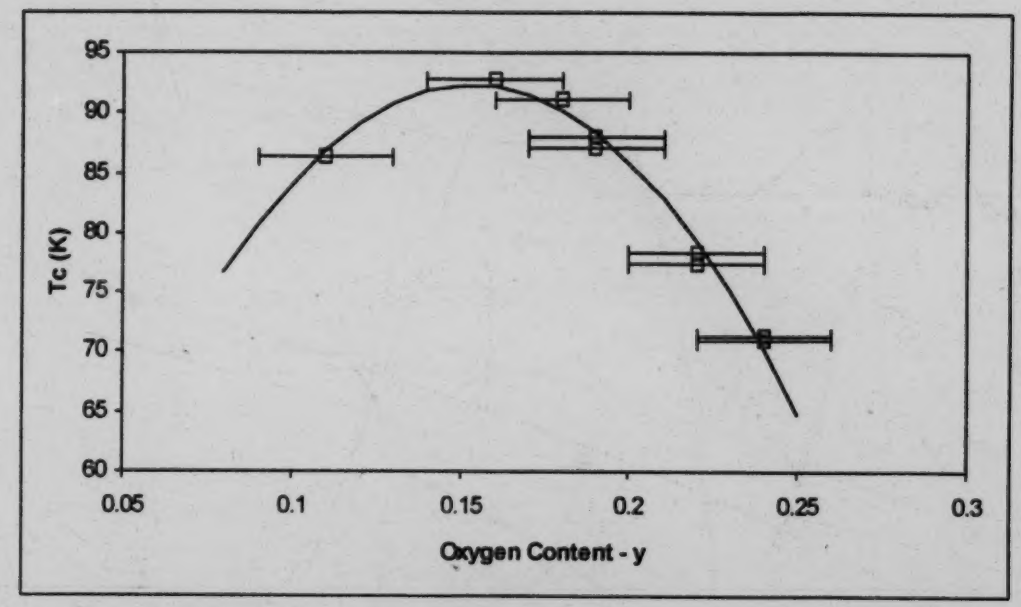

Figure 7.1.2 T_c as a function of y in $Bi_2Sr_2CaCu_2O_{8+y}$. Data are from Allgeier *et al.* (1990). The line is a fit to the data, see text.

This variation of T_c with y places stringent requirements on oxygen isotope effect studies, assuming that materials with different isotopes obey the same $T_c(y)$ relationship. Using equation 7.1.1, the difference in Tc for two samples with different y values can be estimated as

$$\Delta T_c(y, \Delta y) \approx \frac{dT_c}{dy} \Delta y = -2T_{cMax}\, C\,(y - y_{opt})\, \Delta y \qquad \textbf{(7.1.2)}$$

This relation is plotted in figure 7.1.3, using the listed fitting parameters. ΔT_c is defined (by the choice of Δy positive) as $T_c(y_>) - T_c(y_<)$.

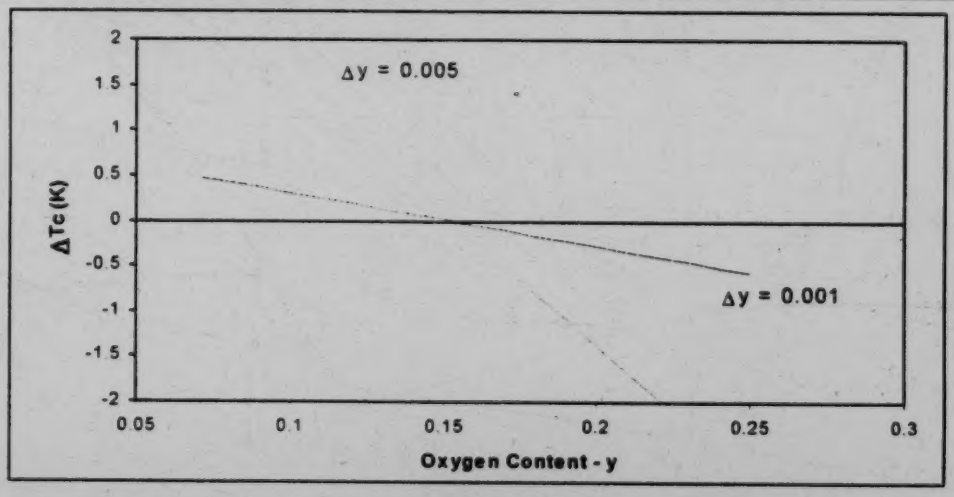

Figure 7.1.3 Change in T_c due to changes in y as a function of y for $Bi_2Sr_2CaCu_2O_{8+y}$.

As can be seen from the figure, very small changes in y can cause large changes in T_c. It is therefore essential that comparison samples have the same oxygen content. The most reliable comparisons are probably made on samples with T_c very close to the optimal value. The behavior of α_O as a function of hole doping (effectively y) is an interesting question however, and there are (at least) two possible approaches to dealing with uncertainties in y values.

Bornemann *et al.* (1992) approached the problem by first preparing Y substituted 2212 ($Bi_2Sr_2Ca_{1-x}Y_xCu_2O_{8+y}$) and exchanging all samples at 1 bar of $^{16}O_2$ or $^{18}O_2$ pressure. Pure 2212 prepared under these conditions is overdoped ($y \approx 0.25$, $Tc \approx 65$ K), and Y doping is believed to be similar to reducing the oxygen content. The T_c of samples prepared in this way first increases then decreases, with increasing Y content, even though the physical sample preparation procedures (annealing temperature and O_2 pressure) remain unchanged. Different amounts of Y doping were used to control the hole content and variations in the Y content of comparison samples was unlikely as the same starting material was used in the isotope exchange.

A more direct approach would be to measure the oxygen or hole content[1] independently. A variety of analytical techniques exist, but in general the best accuracy is on the order of $\delta y = 0.005$ with $\delta y = 0.01$ being typical. This is much greater than the accuracy required to rule out differences in y as a source of small shifts in T_c, making it questionable if isotope effect experiments on T_c are even possible in this material. For example shifts as large as 0.4 K in comparison samples with $Tc \approx 75$ K could be explained by a difference in y of only 0.001. This is generally addressed by extremely careful parallel processing, however it is not a guarantee. The fact remains that such studies are of interest and are done. The argument that differences in oxygen content between isotopic sample pairs (regardless of the isotope) can account for observed differences in T_c is one that plagues any investigation of isotope effects in HTSC materials and is virtually impossible to counter, given the strong dependence of T_c on oxygen content. A limited counter argument can be made that such slight differences would be expected to be random and therefore no consistent isotopic shifts would be observed. This assumes equillibrium conditions have been reached – i.e. differences in oxygen content could not be attributed to differences in the diffusion rates of ^{16}O and ^{18}O since the treatment was carried out for a long enough time to make the rate differences negligible. The book Solid State Chemistry – Techniques, edited by Cheetham and Day (1995) has several interesting comments in this regard, although it does not specifically address isotope effects in superconductors.

There have been suggestions that the hole concentration itself may depend on isotopic mass (Schneider and Keller, 1992 and 1993; and Kresin and Wolf 1994), and these ideas were discussed in the previous chapter with regard to the copper isotope effect in YBCO. This possibility indicates that direct measurements of n for isotopic samples would be of interest in and of themselves. The unique stoichiometry (y = n, assuming a constant Bi^{3+} valence) of BSCCO 2212 makes this system particularly attractive for such investigations. In addition, the entire doping range (under to over doped) can be reached simply by variations in total oxygen content. At the time of writing, no direct measurements have been made of variations in oxygen or hole content for any isotopically substituted HTSC material. Given this fact, this investigation is an attempt to directly probe the possible isotopic dependence of n for the first time. An experimental resolution of δy (= δn) $\leq 0.01$was achieved in most cases.

In this chapter I discuss my investigation of oxygen isotope effects in $Bi_2Sr_2CaCu_2O_{8+y}$. This investigation looks at the influence of isotopic oxygen (^{16}O / ^{18}O) substitution on T_c and y independently, for a number of y values.

Oxygen content, y, was determined by iodometric titration . A detailed description of the procedure is given in Appendix I.

---

[1] In 2212, n = the number of holes/Cu is identical to y due to stoichiometry. 2201 and 2223 have n = 2y and 2/3y respectively. This assumes a Bi valence of 3^+, see the discussion.

7.2 Experiment

A total of 17 pairs of comparison samples were investigated. In all cases the starting material was commercially produced melt textured BSCCO 2212, made by Hoechst A.G., Frankfurt, Germany. The material was very close to optimally doped and had been used in a previous specific heat investigation (Yu, 1991). X-ray diffraction measurements have shown the material to be essentially single phase 2212. The as received starting material was a polycrystalline cylinder approximately 2 cm in diameter and 2 cm high. Sections were cut from the cylinder, ground to a fine powder using an agate mortar and pestle and pressed into pellets 6 mm in diameter.

Isotopic substitution was achieved by gas phase thermal treatments using the OIES. The first treatments were designed to achieve as high a degree of substitution as possible. Samples were treated in 1 Atm. of high purity $^{16}O_2$ or $^{18}O_2$ (93.4 % isotopic purity) at a variety of temperatures and for varying amounts of time. Substitutions of > 80% were readily achieved, based on later Raman measurements. Under these conditions, the materials are overdoped and additional treatments in Ar or Ar / $^{16}O_2$, Ar / $^{18}O_2$ atmospheres were performed to make samples with lower oxygen content. Samples pairs were labeled as HBA through HBQ (HB for Hoechst BSCCO) and numbered as 1 and 2 for ^{16}O and ^{18}O enrichment respectively. Table 7.2.1 lists all the samples and treatments. In all cases, samples were heated to a certain temperature, held at that temperature for a given amount of time, then cooled in the oven to the ambient temperature. Slow heating and cooling (1 °C/min) were used to ensure equilibrium. In almost every case, susceptibility measurements were made after each and every thermal treatment.

Table 7.2.1 BSCCO annealing conditions.

Sample Series	Atmosphere	Hold Temperature (°C)	Hold Time (hours)
HBA	1 Atm. O_2	600	24
	"	650	36
	"	"	"
	1 Atm. Ar	450	24
HBB	1 Atm. O_2	650	72
	"	700	36
	"	650	24
HBC	1 Atm. O_2	625	36
	"	650	"
	"	"	"
	1 Atm. Ar	550	24
HBD	1 Atm. O_2	625	36
	"	650	"
	"	"	"
	1 Atm. Ar	"	24
	1 Atm. Ar + Ta	500	"
	"	600	"
	"	500	"
	"	650	"
	"	"	"
HBE	1 Atm. O_2	625	36
	"	650	"
	"	"	"
	1 Atm. Ar	"	"
HBF	1 Atm. O_2	625	36
	"	650	"
	"	"	"

Table 7.2.1 (con't.) BSCCO annealing conditions.

Sample Series	Atmosphere	Hold Temperature (°C)	Hold Time (hours)
HBG	1 Atm. O_2	600	36
	"	650	"
	"	"	"
HBH	1 Atm. O_2	300	48
HBI	1 Atm. O_2	350	48
	1 Atm. Ar	"	24
	Vacuum	"	"
HBJ	1 Atm. O_2	350	48
	"	"	"
	1 Atm. Ar	375	120
	"	350	"
HBK	1 Atm. O_2	350	48
HBL	1 Atm. O_2	350	48
	"	375	120
	0.4 % O_2, bal Ar	350	48
HBM	1 Atm. O_2	375	48
	"	"	120
	1 Atm. Ar	"	"
	"	350	"
HBN	1 Atm. O_2	350	120
	"	375	"
	0.4 % O_2, bal Ar	350	48
HBO	1 Atm. O_2	350	120
	"	375	"
	"	350	"
	20 % O_2, bal Ar	"	72
	3.4 % O_2, bal Ar	"	48
	7 % O_2, bal Ar	"	"
	0.5 % O_2, bal Ar	"	72
HBP	1 Atm. O_2	350	120
	"	375	"
	"	350	"
	1 Atm. Ar	"	48
HBQ	1 Atm. O_2	350	120
	"	375	"
	"	350	"

As can be seen from the table, two different heating regimes were used. The first experiments used higher temperatures, similar to those used in prior investigations (Katayama-yoshida *et al.*, 1988; Bornemann *et al.*, 1991 and 1992). X-ray diffraction measurements showed the formation of additional phases however. This is shown in figure 7.2.1. In general, diffraction patterns showed increasing degradation with increasing treatment time and temperature. It was not possible to conclusively identify the new phases, although some of the lines may be assigned to BSCCO 2201 or 2223, in addition to CuO and possibly $SrCuO_2$. Virtually no differences were observed between sample pairs (Both showed new peaks in the same positions).

These results agree with the findings of Wu *et al.* (1993) and Sun *et al.* (1997) who have reported evidence of decomposition of nominally phase pure BSSCO 2212 at elevated annealing temperatures. They find evidence for decomposition at temperatures as low as 450 °C.

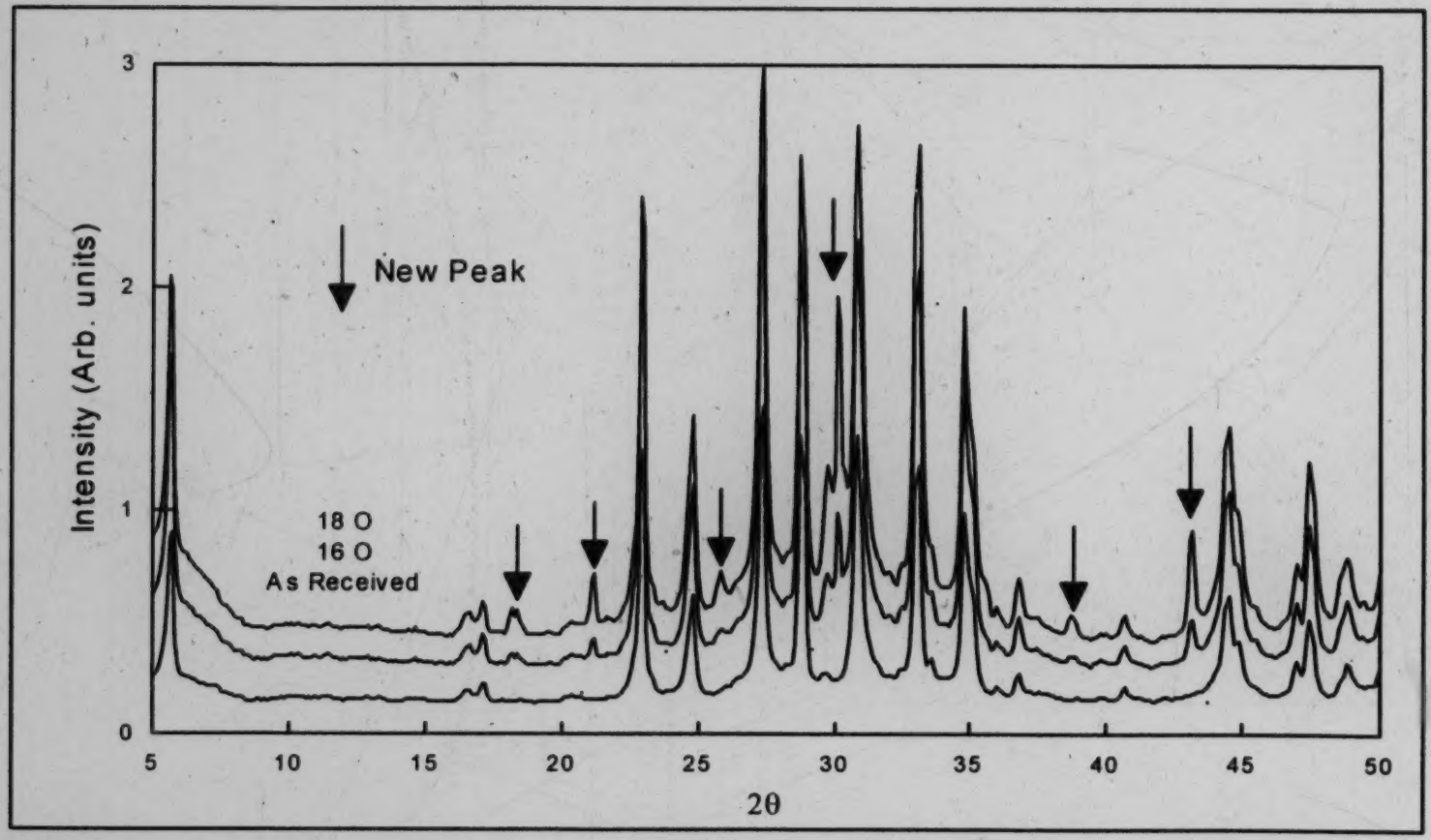

Figure 7.2.1 X-ray powder diffraction spectra comparison of samples before (As Received) and after oxygenation at 600 °C for 36 hours (HBG samples). Arrows indicate diffraction peaks appearing as a result of the treatment. All peaks in the As Received spectra can be indexed to BSCCO 2212.

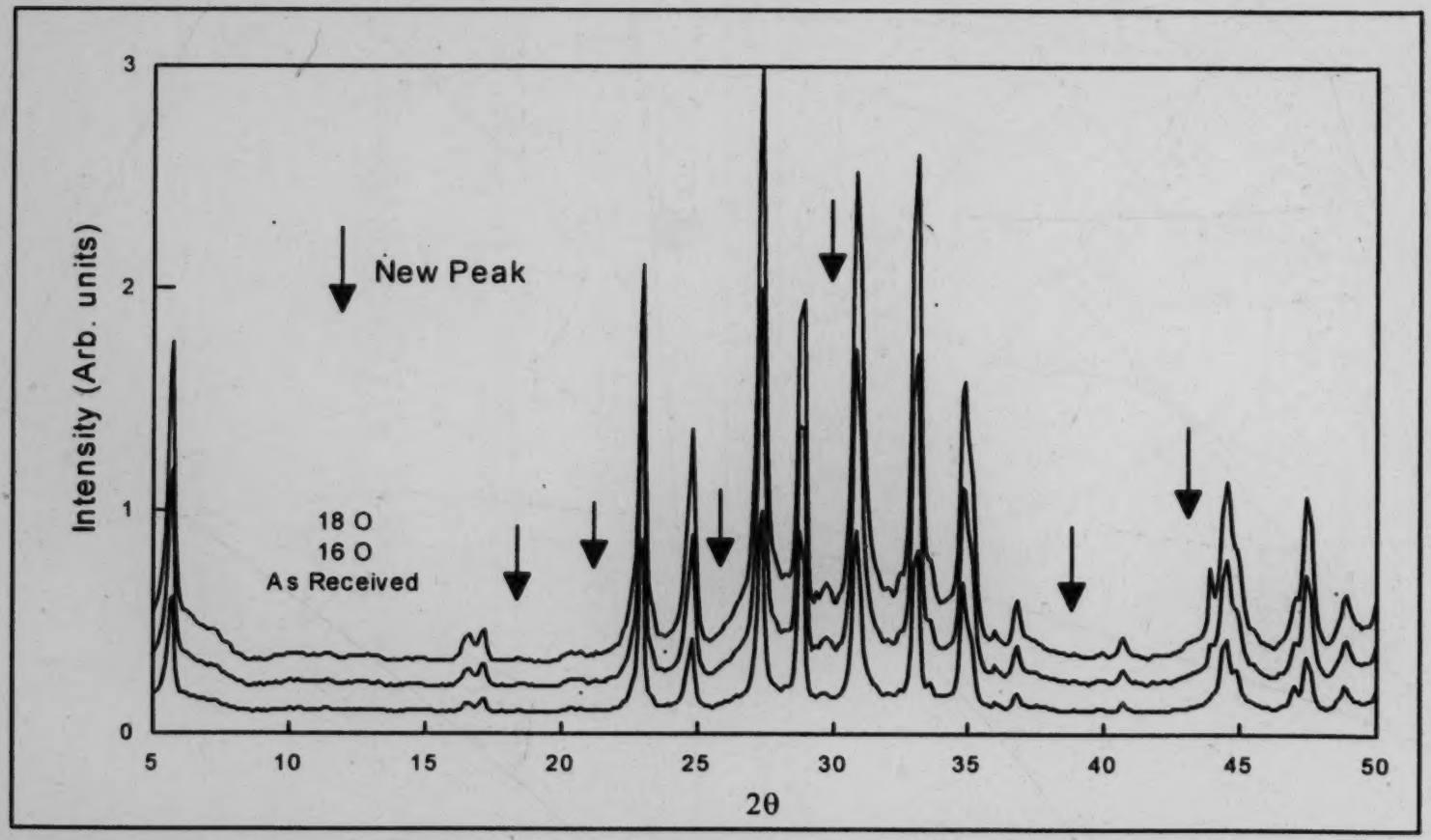

Figure 7.2.2 X-ray powder diffraction spectra comparison of samples before (As received) and after oxygenation at 350 °C for 48 hours (HBI samples). Arrows, indicating new peaks due to the high temperature treatment, are in the same positions as in figure 7.2.1. In contrast to the 600 °C treatment, the 350 °C treatment does not cause any perceptible change to the diffraction spectra.

In a 1991 paper investigating the properties of 2212 annealed in vacuum at temperatures ranging from 200 – 650 °C, Nagoshi *et al.* showed that oxygen was evolved in two steps. A peak in oxygen production was observed around 350 °C, followed by increased production above 500 °C. Given this result and those of Sun *et al.* and Wu *et al.*, it was decided to attempt a much lower annealing temperature of 350 °C. Samples treated in this way showed no differences from the untreated diffraction pattern. Typical results are shown in figure 7.2.2. Results for oxygen depletion in Ar were essentially identical.

Such a low treatment temperature raises questions about the effectiveness of isotopic exchange. Attempts to determine ^{18}O substitution from mass changes were hampered by the readiness with which BSCCO 2212 absorbs moisture and CO_2 from the atmosphere. In general, the first oxygenation showed a mass gain for the ^{18}O sample, but a loss for the ^{16}O sample (as a result of driving off adsorbed gases). The oxygen content of both samples increased however, as shown by the change in T_c (~ 91 K → ~ 65 K) corresponding to an increase in y of about 0.1. Subsequent treatments typically showed small losses for both samples. As a result, there was no observable correlation between changes in mass and T_c. Determinations of total oxygen content and the degree of ^{18}O substitution therefore could not be made, as has been done in other investigations (chapter 6). This is not as much of drawback as it might seem, since independent measurements of the isotopic substitution (Raman) and total oxygen content (iodometric titration) were made.

Raman results are given in Table 7.2.2 for both high and low temperature treatments. The Raman spectra for the HBI samples were shown in figure 3.2.4 of chapter 3 with the discussion of Raman measurements of isotopic content.

Table 7.2.2 Isotopic substitution determined from Raman measurements

Sample Series	Treatment Temperature	ν ^{16}O (cm^{-1})	ν ^{18}O (cm^{-1})	% ^{18}O
HBB	650 °C	612	578	97
		471	449	82
		300	287	76
HBH	300 °C	630	618	33
		473	463	37
		298	292	35
HBI	350 °C	630	606	67
		473	451	81
		298	285	80
HBK	350 °C	624	600	67
		464	440	91
		not measured	not measured	/

Data are presented for 3 different oxygen Raman modes, corresponding to three different oxygen positions. According to Martin and Lee (1995), the modes correspond to vibrations along the c-axis of oxygen in the BiO layers (~627 cm^{-1}), SrO layer (~458 cm^{-1}, the O_3 oxygen in figure 7.1.1) and CuO planes (~290 cm^{-1}). The results are for a single oxygenation, and show that similar levels of substitution can be achieved for the two treatments. Based on these results, a single exchange at 350 °C gives at least 60 % substitution at all oxygen sites. The majority of samples underwent more than one oxygenation and so the total ^{18}O substitution is estimated to be $\gtrsim$ 80 % for those samples. Mass changes were virtually identical for the two samples in a pair after three oxygenation treatments. This suggests that equillibrium conditions had been reached, or at least that no additional exchange of ^{16}O was occurring, in the final treatment, which is essentially the same situation, as far as this investigation is concerned.

These observations suggest that the criteria outlined in chapter 3 for good isotopic comparison samples are only met by the sample series HBI to HBQ. As such, the following discussion focuses only on those sample series. To summarize, samples HBA to HBG underwent thermal treatments that resulted in the formation of additional phases. In addition to violating the criteria outlined in chapter 3 for good isotopic comparison samples, the presence of additional phases meant that oxygen content could not be accurately determined by iodometric titration (see appendix). This last point eliminates these samples for consideration in the investigation of the influence of isotopic substitution on total oxygen content. The HBH sample pair underwent only a single oxygenation and showed only a moderate degree of substitution (less than 40 %) of ^{18}O for ^{16}O for this particular (and unique) thermal treatment. Subsequent samples were prepared using the more efficient process (in terms of oxygen isotope exchange) used to prepare sample series HBI. The HBH sample pair is not included in the interest of consistency, in agreement with the requirements outlined in chapter 3 for good isotopic comparison samples. Had the final results for maximal substitution been more consistent, the HBH results would have been included in the final analysis. In this case, they would have played a role analogous to the deliberately mixed $^{10}B/^{11}B$ samples used in the borocarbide investigations discussed in chapter 4.

7.3 Results

Typical normalized FC susceptibility data is shown in figure 7.3.1. T_c was found by fitting a straight line to the approximately linear portion from 5-30 % M/Mo and determining the M/Mo = 0 intercept. This criterion was chosen to reduce the effect of broadening of the transition due to the weakly sintered nature of the samples. In preliminary investigations a 1% M/Mo criterion was

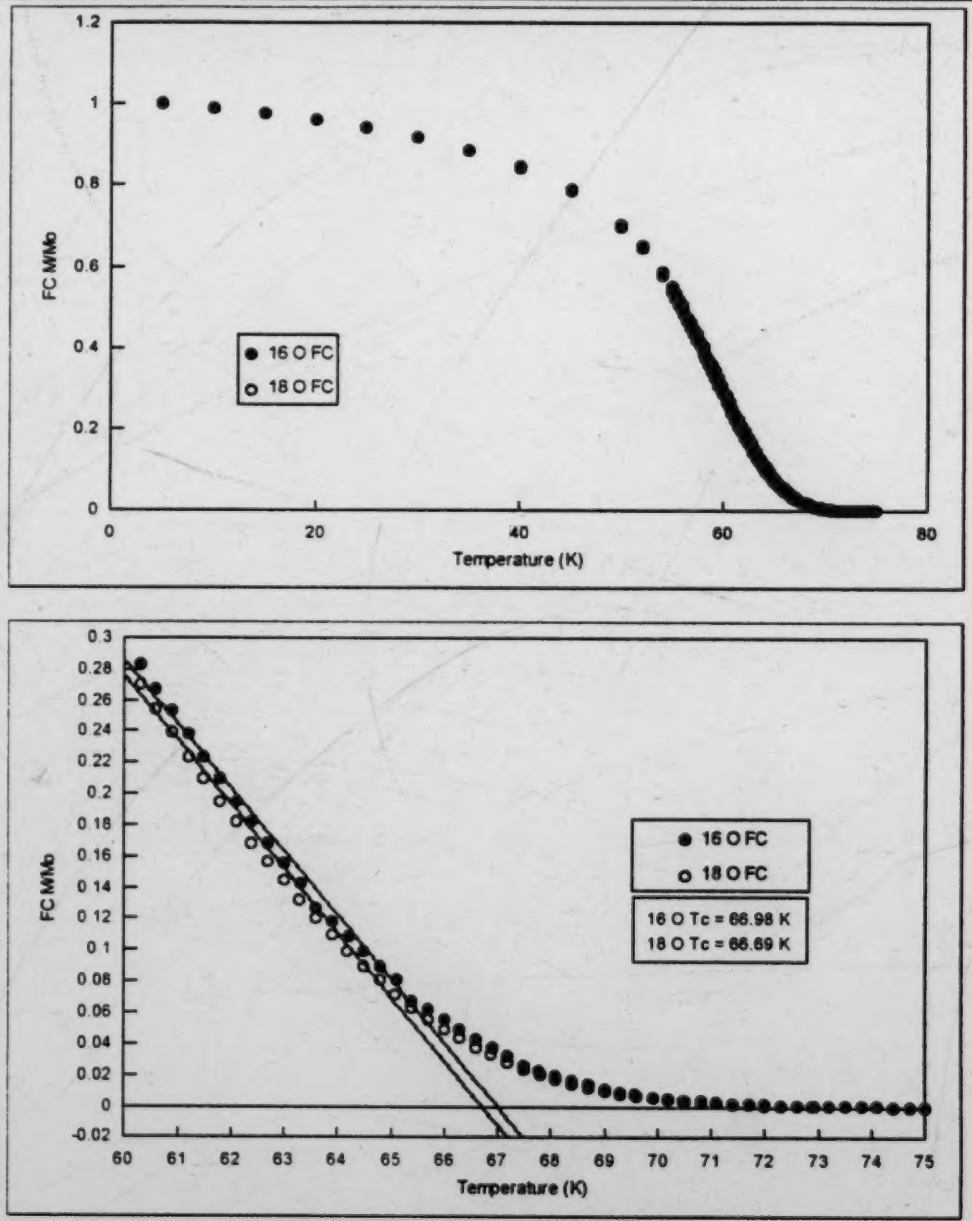

Figure 7.3.1 Typical BSCCO normalized FC susceptibility (HBQ°02 samples)

used, as described in chapter 6 for the determination of T_c in YBCO. It was observed that for a number of samples (in the HBA to HBG series) that the portion of the magnetization curve from about 5 – 30 % of M/Mo was fairly linear. A linear fit to this region, when extrapolated to M/Mo = 0 yielded T_c values consistent with (if margrinally smaller than) the those determined from the 1 % criterion. A large number of T_c values (≈ 80) for many different sample series (HBC to HBN) were determined by both methods. The result was that the two methods are equivalent, even with the "bowing" of the curve shown in figure 7.3.1. A linear regression of T_c(5-30 %) versus T_c(1%) gives T_c(5-30 %) = 0.97 T_c(1%), so if anything, the 5-30 % criterion minimizes differences in T_c. The ultimate reason for adopting the 5-30 % criterion over the 1 % criterion was that the former could be more readily automated in the computer analysis of the data. It should be remembered that 17 different sample pairs were examined, most of which underwent at least two thermal treatments. More than 180 separate determinations of T_c were made in this particular investigation, and a process which reduced the labour and time involved was of great use. Franck (1994) gives a detailed discussion regarding the choice of the definition of T_c in his review.

Tables 7.3.1 to 7.3.6 summarize the results of measurements on the BSCCO sample series HBI to HBQ. The mass change is defined as the percentage increase after treatment compared to the pre-treatment mass. $\Delta T_c = T_c(^{16}O) - T_c(^{18}O)$. Oxygenation conditions were similar for all samples and are reported together.

Table 7.3.1 BSCCO results after first oxygenation.

Sample	Mass Change (%)	^{16}O T_c (K ± 0.02 K)	^{18}O T_c (K ± 0.02 K)	ΔT_c (K ± 0.04 K)
HBI101	- 0.605	66.32		
HBI201	1.014		66.06	+ 0.26
HBJ101	- 0.290	66.51		
HBJ201	0.670		66.82	- 0.31
HBK101	- 0.326	66.85		
HBK201	1.038		66.53	+ 0.32
HBL101	- 0.443	66.40		
HBL201	0.812		67.43	- 0.03
HBM101	-0.055	66.34		
HBM201	1.145		66.64	- 0.30
HBN101	-0.409	66.25		
HBN201	1.015		66.18	+ 0.07
HBO101	-0.442	65.93		
HBO201	0.842		66.17	- 0.24
HBP101	0.022	65.96		
HBP201	0.030		66.17	- 0.21
HBQ101	-0.418	66.64		
HBQ201	0.335		66.26	+ 0.40

Table 7.3.2 BSCCO results after second oxygenation.

Sample	Mass Change (%)	^{16}O T_c (K ± 0.02 K)	^{18}O T_c (K ± 0.02 K)	ΔT_c (K ± 0.04 K)
HBJ102	- 0.615	63.86		
HBJ202	0.002		63.86	0.00
HBM102	- 0.155	64.24		
HBM202	- 0.306		64.25	- 0.01
HBN102	- 0.004	64.20		
HBN202	- 0.251		64.38	- 0.18
HBO102	0.018	66.03		
HBO202	0.016		66.55	- 0.52
HBP102	- 0.032	66.30		
HBP202	0.062		66.23	+ 0.07
HBQ102	0.001	66.98		
HBQ202	0.100		66.69	+ 0.29

Table 7.3.3 BSCCO results after third oxygenation.

Sample	Mass Change (%)	^{16}O T_c (K ± 0.02 K)	^{18}O T_c (K ± 0.02 K)	ΔT_c (K ± 0.04 K)
HBO103	- 0.484	64.11		
HBO203	- 0.356		63.20	+ 0.91
HBP103	- 0.576	63.83		
HBP203	- 0.556		63.16	+ 0.67
HBQ103	- 0.494	64.06		
HBQ203	- 0.545		63.63	+ 0.43

After oxygenation, the samples are over-doped ($y \approx 0.25$) and oxygen must be removed in order to reach other y values. Two approaches were used. The majority of samples were reduced in a pure Ar atmosphere while the HBO samples were treated in O_2-Ar mixtures. Results are listed separately below.

Table 7.3.4 BSCCO results after first reduction.

Sample	Mass Change (%)	^{16}O T_c (K ± 0.02 K)	^{18}O T_c (K ± 0.02 K)	ΔT_c (K ± 0.04 K)
HBI102	- 0.118	not measured		
HBI202	- 0.219		not measured	/
HBJ103	- 0.345	74.28		
HBJ203	- 0.731		74.50	- 0.22
HBM103	- 0.156	74.97		
HBM203	- 0.599		75.02	- 0.05
HBP101	- 0.272	77.58		
HBP201	- 0.357		76.48	+ 1.10

Table 7.3.5 BSCCO results after second reduction.

Sample	Mass Change (%)	^{16}O T_c (K ± 0.02 K)	^{18}O T_c (K ± 0.02 K)	ΔT_c (K ± 0.04 K)
HBI103	- 0.169	67.10		
HBI203	- 0.102		66.48	+ 0.62
HBJ104	- 0.587	74.33		
HBJ204	- 0.862		72.94	+ 0.39
HBM104	- 0.919	73.22		
HBM204	- 1.563		72.47	+ 0.75

Table 7.3.6 HBO reduction results.

Sample	Mass Change (%)	^{16}O T_c (K ± 0.02 K)	^{18}O T_c (K ± 0.02 K)	ΔT_c (K ± 0.04 K)
HBO104	- 0.062	70.87		
HBO204	- 0.458		70.40	- 0.47
HBO105	- 0.587	74.15		
HBO205	- 0.862		72.19	+ 1.96
HBO106	- 0.919	73.22		
HBO206	- 1.563		68.79	+ 4.43
HBO107	- 0.672	73.93		
HBO207	- 0.351		74.03	- 0.10

As can be seen from the tables, wide variations in both T_c and mass change were encountered. Variations in mass changes can most likely be traced to variations in adsorbed gas (water, CO_2) content, as has been mentioned. The relatively large variations in T_c are harder to explain. Small differences in oxygen content could be responsible, particularly when samples were prepared in different treatment runs. The HBO, HBP and HBQ samples were all treated together for the three oxygenations however. The variations for these three sample sets may reflect systematic difficulties with the procedure. Since the samples were treated under identical conditions, it is appropriate to use this variation as a measure of the resolvable differences in T_c. This comparison is presented in Table 7.3.7. Average T_c values are given, together with an uncertainty defined as the maximum deviation from the mean for each set of samples.

Table 7.3.7 Averaged results for 3 identical oxygenations.

Isotope	Average Transition Temperature (K)		
	1st Oxygenation	2nd Oxygenation	3rd Oxygenation
^{16}O	66.18 ± 0.46	66.44 ± 0.54	64.00 ± 0.17
^{18}O	66.20 ± 0.06	66.36 ± 0.19	63.33 ± 0.30

Clearly there is no resolvable difference in T_c for the first two oxygenations. The third shows a shift of $\Delta Tc = 0.77 \pm 0.47$ K, which suggests a possible isotope effect ($\alpha_O = 0.089 \pm 0.009$), but could be explained by variations in oxygen content between the samples (see figure 7.1.3). A slightly higher oxygen pressure during treatment probably explains the slightly lower T_c values for the third oxygenation.

I have presented the results for each treatment in detail to emphasize the variation that was encountered, and hence the importance of independently determining the oxygen content of the samples. The analysis procedure is described in Appendix I and results are given in table 7.3.8. As an aside, it can be noted that an accurate determination of y for a single pair of samples required, on average, two days of wet chemical analysis.

Table 7.3.8 Summary of T_c and y values.

Sample	Isotope	Tc (K)	y	δy
As Received	/	91.94	0.148	0.010
HBI103[1]	16	75.77	0.092	0.030
HBI203[1]	18	75.34	0.119	0.019
HBIR101[1]	16	67.10	0.241	0.013
HBIR201[1]	18	66.48	0.229	0.011
HBJ104	16	76.97[2]	0.095	0.006
HBJ204	18	72.02	0.092	0.007
HBK101	16	66.78	0.248	0.005
HBK201	18	66.57	0.235	0.006
HBM104	16	73.22	0.197	0.006
HBM204	18	72.47	0.198	0.007
HBO107	16	73.93	0.222	0.007
HBO207	18	74.03	0.212	0.006
HBP104	16	77.58	0.103	0.009
HBP204	18	76.48	0.129	0.011
HBQ103	16	64.06[3]	0.169[3]	0.009
HBQ201	18	63.63	0.249	0.010

Notes: The uncertainty in y, δy, is the standard deviation, as described in Appendix I.

1. The HBI samples were divided in half after the first oxygenation. One set (HBIR) was used for Raman measurements, and the other (HBI) underwent further treatment. The large uncertainties for the HBI samples are a result of the small amount of material remaining after the additional treatments.
2. This T_c does not correspond to the value listed in Table 7.3.5 as it changed as a result of drying at 130 °C. See text.
3. It is unlikely that this T_c and y value correspond due to drying. See text

A few comments are needed. The first concerns notes 2 and 3. In the iodometric analysis process, it is necessary to dry the powdered samples. In two cases (samples HBJ104 and HBQ103) this was accomplished by placing the powdered samples in a drying oven at 130 °C for over 24 hours, exposed to air. The HBQ analysis was completed first and a lower than expected y value was noted. The HBJ sample was therefore re-measured before oxygen analysis, and T_c was found to have increased by 2.64 K. Unfortunately, all of the HBQ sample had been consumed in the analysis, so re-measurement was not possible. The T_c and y values for HBQ103 are therefore not considered to be consistent and are not included in the following analysis. The HBJ values are considered reasonable however, at least in terms of individual T_c and y values. The ^{16}O sample (HBJ104) has a slightly different thermal history than the ^{18}O sample (HBJ204) due to the drying process. Prior to this discovery, drying had been done for much shorter periods of time (~ 2 hours or less). Subsequently samples were dried using a dessicator at room temperature for 24 hours.

Second it will be noted that oxygen determinations were not made for the HBL or HBN samples. These samples were subjected to thermal treatment together in a reduction run in 0.04 % O_2, balance Ar at 350 °C for 48 hours. Upon removal from the OIES, it was noted that ALL samples showed small patches of orange discolouration. A similar effect had been noted with HBD samples under much more extreme reducing conditions. It was concluded that the Pt mesh holding the samples might have been contaminated and that the samples were partially degraded, and therefore were not used for oxygen analysis.

Finally, the HBM samples are anomalous. The treatment process was similar to the HBJ samples and they show similar T_c values. The measured oxygen content is unexpectedly high, given the final reducing conditions used, compared to the HBI, HBJ and HBP samples. The reduction conditions should have produced under doped samples, but the oxygen analysis indicates that the HBM samples are overdoped. It is unclear if this is a real effect or represents some undetected error in the HBM oxygen analysis or measurement of T_c.

Figure 7.3.2 is a plot of the data in table 7.3.8, with the fit from figure 7.1.2 for comparison.

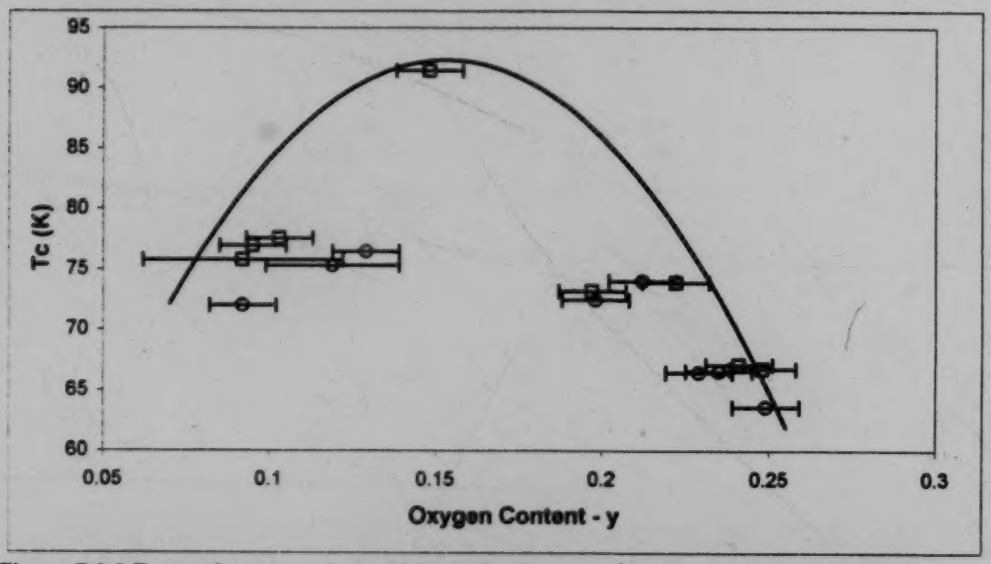

Figure 7.3.2 T_c as a function of y in $Bi_2Sr_2CaCu_2O_{8+y}$, as measured in this investigation. Squares – ^{16}O samples, circles – ^{18}O samples. The solid line is the fit to the data of Allgeier *et al.* from figure 7.1.2.

This concludes the presentation of results for this chapter. Table 7.3.8 and figure 7.3.2 represent the final summary of data found in this investigation.

7.4 Discussion

Perhaps the most striking feature of the results of this investigation are the difference in y values for isotopic sample pairs with similar T_c values (usually larger than the experimental uncertainty in y) and the difference in T_c for samples (usually not the same pair) with similar y values. The differences for sample pairs are summarized in table 7.4.1. Δy is defined as $\Delta y = y(^{16}O) - y(^{18}O)$ and ΔT_c is defined as $\Delta T_c = T_c(^{16}O) - T_c(^{18}O)$. The entries in the table are arranged in order of increasing oxygen content, from under to over doped.

Table 7.4.1 Observed values of Δy and ΔT_c.

Sample Set	Doping	Δy	ΔT_c (K)
HBI	Under	- 0.027	+ 0.43
HBJ	"	+ 0.003	+ 4.95
HBP	"	- 0.026	+ 1.10
HBM	?	- 0.001	+ 0.75
HBIR	Over	+ 0.012	+ 0.62
HBO	"	+ 0.010	- 0.10
HBK	"	+ 0.013	+ 0.21

If the observed differences in Tc are due to differences in total oxygen content (as discussed in section 7.1. See figure 7.1.3), there should be a relationship between the signs of Δy and ΔT_c. Using the definitions of Δy and ΔT_c given above, the general form of equation 7.1.1 implies the correlation shown in table 7.4.2.

Table 7.4.2 Expected Δy and ΔT_c correlation.

Doping	Δy	ΔT_c
Under	+	+
"	-	-
Over	+	-
"	-	+

Several of the sample pairs violate this correlation. Careful comparison of table 7.4.1 with figure 7.1.3 shows that the samples that do not (HBJ, HBM, HBO) display Δy and ΔT_c values inconsistent with the values expected from figure 7.1.3 [2]. This lack of correlation either with table 7.4.2 (or figure 7.4.1) suggests that some factor other than differences in oxygen content must be responsible for the observed differences in T_c, and that there is an observable isotope effect despite the wide scatter of the data.

Isotope exponents have been calculated for sample pairs with oxygen values that agree within experimental uncertainty in table 7.3.8, and are presented in table 7.4.2. It is difficult to estimate the uncertainty in α_O, since it is calculated from a single measured T_c for each sample. This measurement is, in itself, quite precise (± 0.02 K), but this is an unrealistic estimate given the variation shown in table 7.3.7 for nominally identical samples. The uncertainty in y was therefore used to estimate the uncertainty in T_c using the fit in figure 7.1.3 and equation 7.1.2. Admittedly

[2] A detailed comparison has not been made since it is clear from figure 7.3.2 that the fit to the Allgeier *et al.* data does not fit the observed data very well. Better fits are attempted later in this chapter.

the fit is not the best for the observed data, but it is satisfactory for a rough estimate of the uncertainty in α_O. The entries are in order of increasing oxygen content.

Table 7.4.3 Oxygen isotope exponents

Sample Series	Average y	α_O
HBJ	0.094 ± 0.007	0.564 ± 0.007
HBI	0.106 ± 0.025	0.048 ± 0.023
HBM	0.198 ± 0.007	0.087 ± 0.005
HBO	0.217 ± 0.007	- 0.011 ± 0.008
HBIR	0.235 ± 0.012	0.079 ± 0.020

With the exception of the HBJ result, these values are in rough agreement with previously reported results for the BSCCO system (table 7.1.1). Note that there is only one result in table 7.1.1 for BSCCO 2212, and that was for a mixed phase sample. The anomalous HBJ result is probably due to the shift in T_c of the ^{16}O sample due to drying, mentioned above. Essentially the ^{16}O and ^{18}O HBJ samples have undergone slightly different thermal treatments, and therefore do not meet the criteria outlined in chapter 3 for good comparison samples and the and are not included in the analysis that follows. b

It is of interest to attempt to fit equation 7.1.1 to the observed results. First, the HBM samples are anomalous, as discussed in the previous section. As a result, the HBM sample pair is not included in the following analysis. Second, no (equillibrium) process was found that could reproduce the original T_c and y values. The following analysis is therefore concerned only with samples that have a similar history of thermal treatments. This eliminates the As Received data from further consideration. Given these constraints, the data may be fitted as shown in figure 7.4.1.

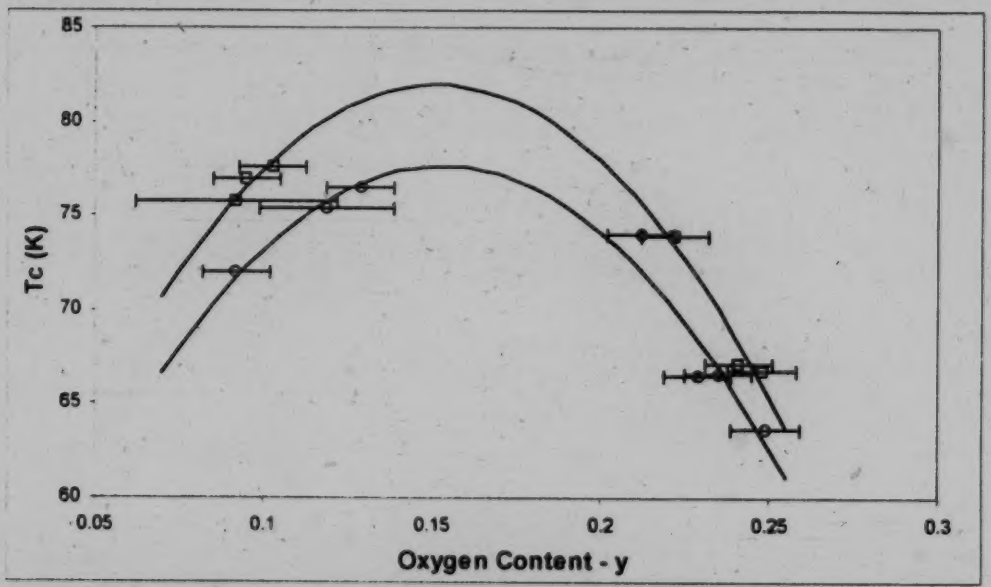

Figure 7.4.1 Fits to the data of table 7.3.8. Upper curve and squares – ^{16}O, lower curve and circles – ^{18}O.

For reference, equation 7.1.1 is

$$T_c = T_{cMAX}\left[1 - C(y - y_{opt})^2\right] \qquad (7.1.1)$$

and the fitting parameters are listed in the table below.

Table 7.4.4 Fitting parameters

	^{16}O Fit	^{18}O Fit
T_{cMAX} (K)	81.96	77.63
C	20.85	20.57
y_{opt}	0.1515	0.1531

These results show good agreement for the C and y_{opt} values. In particular the value of y_{opt} is in excellent agreement with many other results (eg. Tallon *et al.* 1995). The slight differences between the values may not be significant, given the accuracy of the data and the fitting procedure. If the values are not different, the definition of α_O and 7.1.1 imply an isotope exponent that is independent of doping.

$$\alpha_O = -\frac{\Delta \ln(T_c)}{\Delta \ln(m_O)} \qquad (2.1.3)$$

$$= -\ln\left[\frac{^{16}T_{cMax}\,[1-C(y-y_{opt})^2]}{^{18}T_{cMax}\,[1-C(y-y_{opt})^2]}\right] \Big/ \ln\left[\frac{16}{18}\right] \qquad (7.4.1)$$

$$= -\ln\left[\frac{^{16}T_{cMax}}{^{18}T_{cMax}}\right] \Big/ \ln\left[\frac{16}{18}\right] \qquad (7.4.2)$$

Using the T_{cMax} values gives $\alpha_O = 0.46$. This value should be treated with caution for two reasons. First, the HBM samples were not used in the fits. If they are included, the two fits differ significantly (^{16}O - T_{cMax} = 79.15 K, C = 10.60, y_{opt} = 0.1441; ^{18}O - T_{cMax} = 76.91K, C = 18.50, y_{opt} = 0.1505), and α_O is clearly not independent of y.

The second factor is the T_{cMax} values themselves. The value for the ^{18}O samples is quite a bit lower than the 91.94 K of the untreated starting material. No treatment was found that could reproduce this initial T_c. In addition, no samples with $0.14 < y < 0.16$ were produced, despite a number of different reducing conditions. A proprietary melt-texturing process was used to produce the original starting material. In this method the sample is partially melted in a controlled atmosphere, in a manner similar to travelling melt zone refining or crystal growth. It is NOT an equilibrium process, and this may explain the failure to achieve intermediate and optimal doping in the samples examined here.

It should be noted that an α_O that is independent of y does not necessarily contradict the proposals by Schneider and Keller and Kresin and Wolf mentioned in the introduction to this chapter, and discussed in chapter 6. There is evidence that Bi has a mixed valence (3+ and 5+) in 2212 (Idemoto and Fueki, 1990). If pentavalent Bi is present, there is no longer any direct correlation between the hole concentration in the planes and y. In other words, there are holes in both the Cu-O planes and the Bi-O layers. Bi^{5+} is indistinguishable from Cu^{3+} in iodometric titrations. This implies that while determinations of total oxygen content are unaffected (due to charge balance requirements), the measured value of y may not reflect the actual hole concentration in the Cu-O planes. The total oxygen content may therefore be the same for two isotopic samples, while the actual hole concentration in the Cu-O planes differs. The fact that different isotopes are chemically identical predicts that dy/dm = 0, assuming y is determined solely by chemical bonding considerations.

In conclusion, it is very difficult to make any definite statements given the variation in the data. There is evidence that the observed differences in T_c cannot be accounted for simply by differences in oxygen content between the isotopic samples. Direct calculation of α_O (Table 7.4.3) for samples with the same oxygen content shows variations, but the majority of samples suggest that it is small and positive. It is not possible to identify any correlation of the actual value and oxygen content from this data. Fitting of equation 7.1.1 to a selected set of samples seems to show that the $T_c(y)$ relationship is the same for both isotopes.

7.5 Summary for Chapter 7

This chapter discussed the investigation of the oxygen isotope effect in BSSCO 2212 as a function of oxygen content. It was found that high temperature (650 °C) annealing resulted in multi-phase samples as revealed by x-ray diffraction. A lower temperature (350 °C) process was therefore adopted and Raman measurements showed reasonable amounts of substitution. A wide variation in T_c values was encountered, even for samples treated under identical conditions. Oxygen content measurements showed that under ($y < 0.13$) and over ($y > 0.18$) doped samples were produced, but no samples with more intermediate values.

The large variations in the data prevent any definite statements about values of the oxygen isotope exponent, but the evidence suggests it is small ($\alpha_O < 0.1$), in agreement with previous work. There is also evidence that it does not vary much as a function of y. Finally, there is evidence that isotopic substitution does not affect the form of the $T_c(y)$ relationship.

8.1 Final Discussion

This thesis presents the results of isotope investigations on four different materials, only two of which can be properly classified as HTSC materials. Of the two non-HTSC materials, CuO is of obvious interest given the importance of the Cu-O planes to HTSC materials. The borocarbides are of interest for a number of reasons. First, they show relatively high T_c values for non-cuprate superconductors. They also exist in a large series of homologous compounds. A generalized chemical formula can be written for the entire class of materials as RM_2B_2C, where R = Y or a rare earth and M = Ni, Pd or Pt. A wide variety of magnetic ordering phenomena occur depending on the rare earth element (see Lynn, 1997 for a review), including reentrant superconductivity.

An important point is that these are stoichiometric compounds that, at least in the Ni based materials, are relatively easy to synthesize. There are essentially no complications due to variable doping. A second important point, as far as isotope effect studies are concerned, is that high purity enriched boron (^{10}B and ^{11}B) and carbon (^{12}C and ^{13}C) isotopes are readily available and are relatively inexpensive compared to other isotopes such as copper or oxygen. These facts mean that this is an excellent system for studying partial isotope effects.

The first investigation (chapter 4 – the borocarbides) shows a clear dependence of T_c on boron mass. Confirmation of the observed isotopic shifts in the Ni based compounds has come from the work of Cheon *et al.* (1998) on studies of the B isotope effect in single crystals of YNi_2B_2C. The values of $\alpha_B = 0.26 \pm 0.03$ and 0.32 ± 0.04 for the Ni and Pd based materials respectively, show that B phonon modes are important for superconductivity in these materials, as suggested by Mattheis *et al.* (1994). An indication of a smaller C isotope effect was found ($\alpha_C = 0.07 \pm 0.06$) for YNi_2B_2C, but is at the limit of experimental uncertainty. Single crystal work using enriched C offers the possibility of refining this value. The trend in values of α_B for YNi_2B_2C, $LuNi_2B_2C$ (Cheon *et al.*) and YPd_2B_2C was found to be qualitatively explicable in terms of the model of Mattheis *et al.* Extension of these ideas leads to the prediction that α_B should be relatively large (0.3 or greater) in YPt_2B_2C, but will probably be of the same size as that found for $LuNi_2B_2C$ for other (non-magnetic) rare earth elements.

The second investigation (chapter 5 – CuO) was concerned with the possibility of isotope effects in the magnetic ordering temperatures of pure CuO. No effect was found for either T_{N1} or T_{N2}, within the limits of experimental uncertainty. This result is in agreement with previous investigations (Zhao *et al.*, 1994). A calculation (Lawrie and Franck, 1998) based on the observed strong spin-phonon interaction in 240 cm-1 copper mode (Chen *et al.*, 1995) suggests that any possible isotopic shift is at or below the limit of experimental detection. In short, while there may be significant spin-phonon interactions in CuO, isotope effect investigations of the Néel temperatures are too crude to reveal any dependence, at least for sintered powder samples. It would be interesting to examine the possibility in isotopically enriched single crystals (consider figures 5.3.1 and 5.3.2). The high cost of sufficient enriched material and the difficulty involved in growing good CuO crystals probably makes this an impractical idea however.

The third investigation was concerned with the behaviour of the copper isotope exponent as a function of oxygen content, δ, in $YBa_2Cu_3O_{7-\delta}$. It was found that $\alpha_{Cu}(\delta)$ is zero at optimal doping ($\delta = 0.06$) and negative ($T_c(^{65}Cu) > T_c(^{63}Cu)$) for all other values of δ. It is a non-monotonic function of δ, showing large negative values (up to – 0.55) away from the 60 K plateau and smaller values (α_{Cu} = - 0.14 for pair 1 and – 0.34 for pair 2) in the plateau ($0.35 < \delta < 0.45$). Oxygen depletion was achieved by two different annealing procedures. Results for the two methods are qualitatively similar, but show noticeable quantitative differences. The preparation method of Jorgensen *et al.* (1990) resulted in a more sharply defined plateau region and slightly higher T_c values for a given value of δ than the method of Metzger *et al.* (1993).

The behaviour of $\alpha_{Cu}(\delta)$ can be qualitatively explained by the ideas of Schneider and Keller (1992 and 1993) and of Kresin and Wolf (1994) in terms of a two component isotope exponent, $\alpha_{BCS} = \alpha_e + \alpha_n$, where α_e is a usual type of phonon related isotope exponent. α_n is a measure of the mass dependence of the hole concentration. Large values of α_{Cu} outside the plateau are due to $\alpha_e + \alpha_n$, while finite values in the plateau, where $\alpha_n = 0$, are due to α_e that has changed from the optimal value ($\alpha_e = 0$) due to structural changes associated with the change in δ. The observation of room temperature annealing effects offers a possible explanation of the difference in T_c of samples with nominally identical values of δ. According to Veal *et al.* (1990), the most likely explanation for the change in T_c with age is due to ordering of oxygen in the chains, and this is a thermally activated process. The more extreme conditions of Metzger *et al.*'s process likely results in oxygen disorder that cannot be readily "annealed away" at room temperature. Finally, it is conjectured that the existence of a negative copper isotope effect may be related to the fact that YBCO (and related compounds) are relatively unique among the HTSCs in having copper in the charge reservoir layers.

Two interesting, but negative, results were obtained from the investigation of the oxygen isotope effect in $Bi_2Sr_2CaCu_2O_{8+y}$ as a function of y. First, it is not possible to determine changes in total oxygen content from changes in mass (as was done for the YBCO investigation) due to the ease with which BSCCO absorbs moisture and CO_2 from the atmosphere. Second, treatment of nominally phase pure material at temperatures $\gtrsim 500$ °C results in decomposition and the formation of additional phases.

These discoveries led to the use of lower temperature thermal treatments for oxygen exchange and the determination of y by iodometric titration. Raman results showed that a single treatment at 350 °C in 1 atm. O_2 gave substitutions of at least 60 % at all oxygen sites, and powder x-ray diffraction showed no change in spectra compared to the original starting material.

Over and under doped samples were produced, but no treatment was found that could reproduce the optimally doped state of the starting material. A wide range of variation was seen in the data and a number of results for nominally identical samples are inconsistent. These facts limit what can be said about the behaviour of α_O in BSCCO 2212.

There are a number of potential explanations for the observed inconsistencies. One possibility is oxygen-ordering effects similar to those observed in YBCO. This possibility was considered and measurements made months apart showed no change in T_c, so this is unlikely.

A related possibility concerns the Bi valence and the iodometric titrations. There is evidence that Bi has a mixed valence in 2212 (Idemoto and Fueki, 1990). The stoichiometry involved means that Cu^{3+} and Bi^{5+} are indistinguishable in iodometric titrations. This implies that the measured value of y may not reflect the actual hole concentration in the Cu-O planes. This scenario is essentially the same as that discussed above for YBCO, but fails to fully explain the variation seen in identically prepared samples.

Overall, the BSCCO results are suggestive, but not very satisfactory. More work is needed. The most important feature of new work would be the development of a process to consistently produce single-phase BSCCO samples showing a full range of y values.

8.2 Conclusions

The principle results of the thesis are summarized below.

1. There is a boron isotope effect in both YNi_2B_2C and YPd_2B_2C with isotope exponents of $\alpha_B = 0.26 \pm 0.03$ and 0.32 ± 0.04 respectively.

2. There is evidence for a carbon isotope effect, $\alpha_C = 0.07 \pm 0.06$ in YNi_2B_2C.

Points 1 and 2 indicate that the borocarbides (at least YNi_2B_2C and YPd_2B_2C) are fairly conventional superconductors.

3. There are no observable isotope effects (copper or oxygen) in the Néel temperatures of CuO, within experimental uncertainty.

This is a "null result", but is in agreement with previous work and theoretical expectations.

4. $\alpha_{Cu} = 0$ for $\delta = 0.06$ in $YBa_2Cu_3O_{7-\delta}$

5. α_{Cu} is negative for $0.06 < \delta \lesssim 0.60$,

6. α_{Cu} is a non-monotonic function of δ, being large (up to – 0.55) in the region between optimal doping and the 60 K plateau, smaller, but not zero, in the plateau, and large beyond the plateau.

More quantitative statements about the behaviour of $\alpha_{Cu}(\delta)$ are difficult due to variations in oxygen ordering. Essentially $T_c(\delta)$ is dependent on sample making conditions, even for identical values of δ.

7. It is not possible to determine changes in y in $Bi_2Sr_2CaCu_2O_{8+y}$ from changes in mass due to adsorption of atmospheric water and CO_2.

8. Thermal treatment of treatment of nominally phase pure BSCCO at temperatures $\gtrsim 500$ °C results in decomposition and the formation of additional phases, as determined by powder x-ray diffraction.

Further definite comments concerning the behaviour of $\alpha_O(y)$ in $Bi_2Sr_2CaCu_2O_{8+y}$ are hampered by the range of variation in the observed results. The majority of samples show $0 < \alpha_O < 0.1$. There is some evidence to suggest that the form of the $T_c(y)$ relationship is the same for both isotopes, with $y_{opt} \approx 0.15$.

Bibliography

Allgeier, C., and Schilling, J.S., Physica C **168** (1990) 499.

Appelman, E.H., Morss, L.R., Kini, A.M., Geiser, U., Umezawa, A., Crabtree, G.W., Carlson, K.D., Inorg.Chem. **26** (1987) 3237.

Altendorf, E., Chrzanowski, J., Irwin, J.C., Franck, J.P., Phys. Rev. B **43** (1991) 2771.

Åsbrink, S., Norrby, L.J., Acta Crystallogr. B **26** (1970) 8.

Bardeen, J., Cooper, L.N. and Schrieffer, J.R., Phys. Rev. B **108** (1957) 1175.

Bardeen, J., Phys. Rev. **79** (1950) 167.

Belger, A., Jaenicke-Rössler, U., Lipp, D. Wehner, B., Paufler, P., Behr, G., Physica C **306** (1998) 277.

Bednorz, J.G. and Müller, K.A., Z. Phys. **B64** (1986) 189.

Bednorz, J.G., Takashige, M., Müller, K.A., Europhys. Lett. **3** (1987) 379.

Bordet, P., Caponi, J.J., Chaillout, C., Chenavas, J., Hewat, A.W., Hewat, E.A., Hodeau, J.L., Marezio, M., Tholence, J.L., Tranqui, D., Physica C **156** (1988) 189.

Bornemann, H.J. and Morris, D.E., Phys. Rev. B **44** (1991) 5322.

Bornemann, H.J., Morris, D.E., Liu, H.B., Physica C **182** (1991) 132.

Bornemann, H.J., Morris, D.E., Liu, H.B., Sinha, A.P.B., Narwankar, P.K., Chandrachood, M., Physica C **185-189** (1991) 1359.

Bornemann, H.J., Morris, D.E., Liu, H.B., Narwankar, P.K., Physica C **191** (1992) 211.

Bornemann, H.J., Morris, D.E., Sinha, A.P.B., Chandrachood, M., Liu, H.B., (to be published)

Bourne, L.C., Zettl, A., Barbee, T.W., Cohen, M.L., Phys. Rev. B **36** (1987) 3990.

Braun, E., Schnelle, W., Broicher, H., Harnismacher, J., Wohlleben, D., Allgeier, C., Reith, W., Schilling, J.S., Bock, J., Preisler, E., Vogt, G.J., Z. Phys. B **84** (1991) 333.

Brockhouse, B.N. Phys. Rev. **94** (1954) 781.

Bucher, E., Müller, J., Olsen, J.L., Palmy, C., Phys. Letters **15** (1965) 303.

Burns, G., High-Temperature Superconductivity, Academic Press, San Diego, (1992).

Carter, S.A., Batlogg, B.B., Cava, R.J., Krajewski, J.J., Peck Jr., W.F., Takagi, H., Phys. Rev. B **50** (1994) 4216.

Cava, R.J., Batlogg, B.B., Seigrist, T., Krajewski, J.J., Peck Jr., Carter, S., Felder, R.J., Takagi, H., van Dover, R.B., Phys. Rev. B **49** (1994) 12384.

Cava, R.J., Takagi, Batlogg, B.B., H., Zandbergen, H.W., Krajewski, J.J., Peck Jr., W.F., Seigrist, T., van Dover, R.B., Felder, R.J., Mizuhashi, K., Lee, J.O., Eisaki, H., Carter, S.A., Uchida, S., Nature (London) **367** (1994) 146.

Cava, R.J., Takagi, H., Zandbergen, H.W., Krajewski, J.J., Peck Jr., W.F., Seigrist, T., Batlogg, B.B., van Dover,R.B., Felder, R.J., Mizuhashi, K., Lee, J.O., Eisaki, H., Uchida, S., Nature (London) **367** (1994) 252.

Chattopadhyay, T., McIntyre, G.J., Brown, P.J., Forsyth, J.B., Physica C **170**, (1990)

Cheetham, A.K., and Day, P., Editors, Solid State Chemistry – Techniques, Clarendon Press, Oxford 1995.

Chen, X.K., Irwin, J.C., Franck, J.P., Phys. Rev. B **52** (1995) R13130.

Cheon, K.O., Fisher, I.R., Canfield, P.C., Physica C **312** (1999) 35.

Claus, H., Yang, S., Paulikas, A.P., Downey, J.W., Veal, B.W., Physica C **171** (1990) 205.

Coehoorn, R., Physica C **228** (1994) 331.

Cooper, L.N., Phys. Rev. **104** (1956) 1189.

Culetto, F.J., Pobell, F., Phys. Rev. Lett. **40** (1978) 1104.

Eliashberg, G.M., Sov-Phys.-JETP **11** (1960) 696 and Sov-Phys.-JETP **12** (1961) 1000.

Finnemore, D.K., Mapother, D.E., Shaw, R.W., Phys. Rev. **118** (1960) 127.

Forsyth, J.B., Brown, P.J., Wanklyn, B.M., J. Phys. C-Solid State Phys. **21** (1988) 2917.

Franck, J.P., Jung, J., Mohamed, M.A-K., Gygax, S., Sproule, G.I., Phys. Rev. **44** (1991) 5318.

Franck, J.P., Gygax, S., Sorensen, G., Altshuler, E., Hnatiw, A., Jung, J., Mohamed, M.A-K., Yu, M.K., Sproule, G.I., Chrzanowski, J., Irwin, J.C., Physica C **185-189** (1991) 1379.

Franck, J.P., Hnatiw, A., Yu, M.K., Gygax, S., Sorensen, G., Altendorf, E., J. Irwin, J.C., in Lattice Effects in High-Tc Superconductors (World Scientific, Singapore 1992) ed. by Y. Bar-Yam, T. Egami J. Mustre-de Leon and A.R. Bishop, p. 148.

Franck, J.P., Jung, J., Salomans, G., Miner, W.A., Mohamed, M.A-K., Chrzanowski, J., Gygax, S., J. Irwin, J.C., Mitchell, D.F., Sproule, G.I., in High Temperature Superconductors, Materials Aspects (DGM Informations – Gessellschaft 1991) ed. by H.C. Freyhardt, R. Flükkiger and M. Peuckert, p. 885.

Franck, J.P., Harker, S., Brewer, J.H., Phys. Rev. Lett. **71** (1993) 283.

Franck, J.P., in Physical Properties of High Temperature Superconductors IV, D.M. Ginsberg (ed.), World Scientific, Singapore (1994) pp. 189-293.

Franck, J.P. and Lawrie, D.D., Journal of Superconductivity **8** (1995) 591.

Franck, J.P., Physica Scripta **T66** (1996) 220.

Franck, J.P. in Proceedings of the International School of Physics "Enrico Fermi" Course CXXXVI, G. Iadonisi, J.R. Schrieffer and M.L. Chiofalo (Eds.) IOS Press, Amsterdam (1998) 269.

Fröhlich, H., Phys. Rev. **79** (1950) 845. and Frölich, H., Proc. Phys. Soc. **A63** (1950) 778.

Geballe, T.H., Matthias, B.T., Hull, G.W., Corenzwit, E., Pys. Rev. Lett. **6** (1961) 275.

Gmelin, E. Köbler, U., Brill, W., Chattopadhyay, T., Jastri, J., Proceedings International Conference on Superconductivity, Bangalore, India, World Scientific, Singapore, 1990.

Handbook of Chemistry and Physics, 66th Edition, CRC Press Inc. Boca Raton (1986).

Harris, D.C. and Hewston, T.A., J. Solid State Chem. **69** (1987) 182.

Hazen, R.M., in Physical Properties of High Temperature Superconductors II, D.M. Ginsberg (ed.), World Scientific, Singapore (1990) pp. 121-198.

Hidaka, T., Matsui, T., Nakagawa, Y., Jpn. J. Appl. Phys. **27** (1988) L553.

Hikami, S., *et al.*, Jpn. J. Appl. Phys. **26** (1987) L314.

Holstein, T., Ann. Phys. **8** (1959) 238.

Hubbard, J. Proc. Roy. Soc. A **276** (1963) 238.

Idemoto, Y., and Fueki, K., Physica C **168** (1990) 167.

Inyushkin, A., Babushkina, N., Florintiev, V., Kopylov, A., Ozhogin, V., Kaul, A., Graboy, I., in High T_c Superconductors (Plenum Press, New York 1988) ed. by H.W. Weber, p.217.

Irwin, J.C., Wei, T., Franck, J.P., J. Phys.-Condens. Matter **3** (1991) 299.

Jorgensen, J.D., Veal, B.W., Paulikas, A.P., Nowichi, L.J., Crabtree, G.W., Claus, H., Kwok, W.K., Phys. Rev. B **41** (1990) 1863.

Junod, A., Eckert D., Triscone, G., Müller, J., Reichardt, W., J. Condens. Matter **1** (1989) 8021.

Kamerlingh Onnes, H., Leiden Comm. **120b, 122b, 124c** (1911).

Karppinen, M., Fukuoka, A., Niinsto, L., Yamauchi, H., Supercond. Sci. Technol. **8** (1995) 1.

Katayama-Yoshida, H., Hirooka, T., Mascarehnas, A.J., Okabe, Y., Takahashi, T., Sasaki, T., Ochiai, A., Suzuki, T., Pankove, J.I., Ciszek, T.F., Deb, S.K., Jpn. J. Appl. Phys **26** (1987) L2085.

Katayama-Yoshida, H., Hirooka, T., Oyamada, A., Okabe, Y., Takahashi, T., Sasaki, T., Ochiai, A., Suzuki, T., Mascarenhas, A.J., Pankove, J.I., Ciszek, T.F., Deb, S.K., Goldfarb, R.B., Li, Y., Physica C **156** (1988) 481.

Kishio, K., Shimoyama, J., Hasegawa, T., Kitazawa, K., Fueki, K., Jpn. J. Appl. Phys. **26** (1987) L1231.

Köbler, U. and Chattopadhyay, T., Z. Phys. B **82** (1991) 383.

Kondo, O., Ono, M., Sugiro, E., Sugiyama, K., Date, M., J. Phys Soc. Jpn. **57** (1988) 3293.

Kraut, O., Meingast, C., Bräuchle, G., Claus, H., Erb, A., Müller-vogt, G., Wühl, H., Physica C **205** (1993) 139.

Kresin, V.Z., and Wolf, S.A., Phys. Rev. B **49** (1994) 3652.

Lawrie, D.D. and Franck, J.P., Physica C **245** (1995) 159.

Lawrie, D.D., Franck, J.P., Beamish, J.R., Molz, E.B., Chen, Wei-min, Graf, M.J., J. Low Temp. Phys. 107 (1997) 491.

Lawrie, D.D., Franck, J.P., Lin, Cheng-Tain, Physica C **297** (1998) 59.

Lee, J.I., Zhao, T.S., Kim, I.G., Min, B.I., Youn, S.J., Phys. Rev. B **50** (1994) 4030.

Liu, Q. (C. Liu), Wei, Y., Yan, Q., Chen, G., Zhang, P., Shen, Z., Ni, Y., Yang, Q., Liu, C. Ning, T., Zhao, J-K., Shao, Y., Han, S., Li, J., Sol. State Comm. **65** (1988) 869.

Lockwood, D.J., and Cottam, M.G., J. Appl. Phys 64 (1988) 5876.

Loram, J.W., Mirza, K.A., Joyce, C.P., Osborne, A.J., Euro-phys. Lett **8** (1989) 263.

Lynn, J.W., Skanthakumar, S., Huang, Q., Sinha, S.K., Hossain, Z., Gupta, L.C., Nagarajan, R., Godart, C., Phys. Rev. B **55** (1997) 6584.

Maeda, A., Hase, M., Tsukada, I., Noda, K., Takebayashi, S., Uchinokura, K., Phys. Rev. B **41** (1990) 6418.

Maeno, Y. *et al.*, Nature **372** (1994) 532.

Marsiglio, F., J. Low Temp. Phys. **87** (1992) 659.

Martin, A.A., and Lee, M.J.G., Physica C **254** (1995) 222.

Mascarehnas, A.J., Katayama-Yoshida, Pankove, J., Deb, S.K., Phys. Rev. B **39** (1989) 4699.

Mattheiss, L.F., Phys. Rev. B **49** (1994) 13279.

Mattheiss, L.F., Seigrist, T., Cava, R.J., Solid State Commun. **91** (1994) 587.

Maxwell, E., Phys. Rev. **78** (1950) 477.

McMillan, W.L., Phys. Rev. **167** (1968) 331.

Metzger, J., Weber, T., Fietz, W.H., Grube, K., Ludwig, H.A., Wolf, T., Wühl, H., Physica C **214** (1993) 371.

Moodenbaugh, A.R., Fischer, D.A., Wang, Y.L., Fukumoto, Y., Physica C **268** (1996) 107.

Nagarajan, R., Mazumdar, C., Hossain, Z., Dhar, S.K., Gopalakrishnan, K.V., Gupta, L.C., Godart, C., Padalia, B.D. and Vijayaraghavan. Phys. Rev. Lett. **72** (1994) 274.

Nagoshi, M., Suzuki, T., Fukuda, Y., Terashima, K., Nakanishi, Y., Ogita, M., Tokiwa, A., Syono, Y., Tchiki, M., Phys. Rev. B **43** (1991) 10445.

Nazzal, A.I., Lee, V.Y., Engler, E.M., Jacowitz, R.D., Tokura, Y., Torrance, J.B., Physica C **153-155** (1988) 1367.

Nickel, J.H., The contributions of different oxygen sites to the oxygen isotope shift in $YBa_2Cu_3O_{7-\delta}$. PhD Thesis, University of California at Berkeley, (1992)

Phillips, N.E., Phys. Rev. **114** (1959) 676.

Pickett, W.E., Singh, D.J., Phys. Rev. Lett. **72** (1994) 3702.

Rainer, D. and Culetto, F.J., Phys. Rev. B **19** (1979) 2540.

Reynolds, C.A., Serrin, B., Wright, W.H. and Nesbitt, L.B., Phys. Rev. **78** (1950) 487.

Roden, B., Freimuth, A., Solid State Commun. **64** (1987) 1051.

Schneider, T., and Keller, H., Int. J. Mod. Phys. B **8** (1993) 487.

Schneider, T., and Keller, H., Phys. Rev. Lett. **69** (1992) 3374.

Schwarz, R.B., Pascal, Yvon J., Coffey, D., in Studies of High Temperature Superconductors, Volume 9, A. Naklikar (ed.), Nova Science Publishers, New York (1992) pp. 221 – 258.

Shafer, M.W., Penney, T. and Olson, B.L., Phys. Rev. B **36** (1987) 4047.

Sheng, Z.Z. and Hermann, A.M., Nature **232** (1988) 55.

Singh, D.J., Phys. Rev. B **50** (1994) 6486.

Sun, X., Wenbin, W., Zhao, X., Zheng, L., Zhou, G., Li, X-G., Zhang, Y., Physica C **279** (1997) 47.

Takagi, H., Uchida, S., Kitazawa, K., Tanaka, S., Jpn. J. Appl. Phys. **26** (1987) L123.

Takano, M., Takada, J., Oda, K., Kitaguchi, H., Miura, Y., Ikeda, Y., Tomii, Y., Mazaki, H., Jpn. J. Appl. Phys. **27** L1041 (1988).

Tallon, J.L., Bernhard, C., Shaked, H., Hitterman, R.L., Jorgensen, J.D., Phys. Rev. B **51** (1995) 12911.

Tinkham, M., Introduction to Superconductivity, McGraw Hill, New York, (1996).

Thomsen, C. and Cardona, M., in Physical Properties of High Temperature Superconductors I, D.M. Ginsberg (ed.), World Scientific, Singapore (1989) pp. 409-507.

Tokura, Y., et al. Phys. Rev. B **38** (1988) 7156.

Triscone, G., Genoud, J.-Y., Graf, T., Junod, A., Muller, J., Physica C **176** (1991) 247.

Uchida, S., Takagi, H., Kitazawa, K., Tanaka, S., Jpn. J. Appl. Phys. **26** (1987) L1.

Vasiliev, B.V., Lushikov, V.I., Physica C **153-155** (1988) 261.

Veal, B.W., You, H., Paulikas, A.P., Shi, H., Fang, Y., Downey, J.W., Phys. Rev. B **42** (1990) 6305.

Wu, M.K., Ashburn, A.J., Torng, C.J., Hor, P.H., Meng, R.L., Gao, L., Huang, Z.J., Wang, Y.Q., Chu, C.W. Phys. Rev. Lett. **58** (1987) 908.

Wu, W., Li, F., Li, X-G., Lei, S., Zhou, G., Qian, Y., Qin, Q., Zhang, Y., J. Appl. Phys **74** (1993) 4262.

Wu, W., Wang, L., Li, X-G., Zhou, G., Qian, Y., Qin, Q., Zhang, Y., J. Appl. Phys **74** (1993) 7388.

Yang, B.X., Thurston, T.M., Tranquada, G., Shirane, G., Phys. Rev. B **39** (1989) 4343.

Yang, B.X., Tranquada, G., Shirane, G., Phys. Rev. B **38** (1988) 174.

Yu, M.K., Specific Heat Measurements of HTSC, PhD Thesis, University of Alberta, (1991).

Zhao, G.M., Kirtikar, V., Singh, K.K., Singh, A.P.B., Morris,D.E., Inyushkin, A.V., Phys. Rev. B **41** (1990) 182.

Zhao, G.M., Singh, K.K., Morris, D.E., Phys. Rev. B **50** (1994) 4112.

Zhao, Z.X., et al., Kexue Tongbao **33** (1987) 661.

Zimmermann, P., et al., Phys. Rev. B **52** (1995) 541.

Appendix A Oxygen Content Analysis

The facts that all known HTSC materials can be doped over a certain range and that this doping level (hole content) determines T_c makes it of great interest to be able to determine this doping level. Since the oxygen content controls the doping in many materials, determinations of oxygen content are equivalent to determinations of doping levels, and vice-versa.

Iodometric titration determinations of oxygen content (Shafer *et al.*, Kishio *et al.*, Appelman *et al.*, Harris *et al.*, (all 1987); Nazzal *et al.* (1988), Karppinen *et al.* (1995)) are actually a determination of hole content and the oxygen content is calculated based on charge balance. The method relies on the following reactions:

$$2Cu^{2+} + 5I^- \rightarrow 2CuI + I_3^- \quad \text{(A.1)}$$

$$[CuO]^+ + 4I^- + 2H^+ \rightarrow CuI + I_3^- + H_2O \quad \text{(A.2)}$$

$$2[CuO]^+ + 2H^+ \rightarrow 2Cu^{2+} + H_2O + \tfrac{1}{2}O_2 \quad \text{(A.3)}$$

$$2Cu^+ + \tfrac{1}{2}O_2 + 2H^+ \rightarrow 2Cu^{2+} + H_2O \quad \text{(A.4)}$$

$$I_3^- + 2S_2O_3^{2-} \rightarrow 3I^- + S_4O_6^{2-} \quad \text{(A.5)}$$

A portion of the sample is dissolved under an inert atmosphere (to prevent reaction A.4) and reactions A.1 and A.2 produce iodine in proportion to the amount of Cu in the sample having a valence in excess of +1. The liberated iodine is titrated with a standardized thiosulphate solution using starch as an indicator, reaction A.5. This gives the "excess charge" of the copper per gram of sample. A second titration is performed, but the sample is dissolved in acid and boiled, and reactions A.3 and A.4 convert all Cu to Cu^{2+}. Reactions A.1 and A.5 then give the amount of copper per gram of sample. The two results are combined to give the excess charge (above 2^+) per copper atom in the sample. In this appendix I give a detailed account of the procedure used for determinations of oxygen (hole) content in BSCCO 2212 (Chapter 7).

Equipment Required

Chemicals: (All chemicals should be reagent grade quality or better.)

KI	Potassium Iodide
$Na_2S_2O_3 \cdot 5H_2O$	Sodium Thiosulphate Pentahydrate
HCl	Hydrochloric Acid
CuO	Copper Oxide
	Soluble Starch
	Good quality distilled H_2O

Glassware:

Volumetric Flasks:	2 each of 1000ml, 100 ml, 50 ml; 1 x 500 ml
Erlenmeyer Flasks:	1 x 5000 ml, 1 x 250 ml, 6 x 50 ml
Beakers:	4 x 30 ml, 1 x 250 ml

Miscellaneous:

Buret (described below)
Inert Atmosphere System (IAS) (described below)
syringes – 2 x 10 ml, 1 x 5 ml, 1 x 1 ml
magnetic stirrer and stirring bars (6)
Rubber septa to fit 50 ml Erlenmeyer flasks (several)

Balance accurate to at least 0.1 mg
Heat source capable of boiling water (Hot plate or Bunsen burner)
Dessicator / Drying oven

Experimental Setup

In order to prevent air oxidation of the various chemical species, the titrations are carried out in an inert atmosphere. This requires somewhat specialized apparatus. A schematic of the IAS is shown in figure A.1

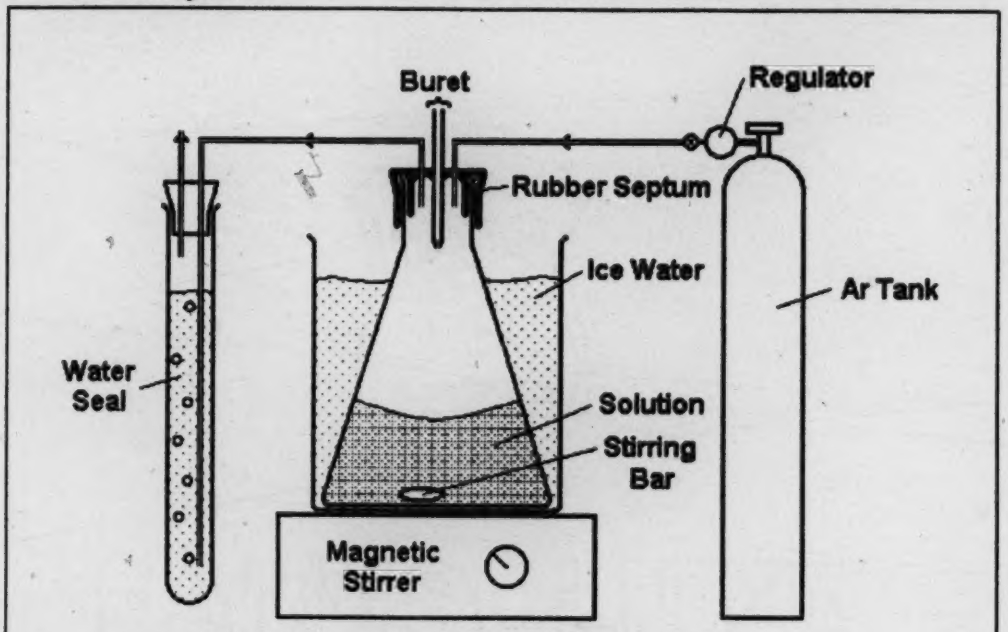

Figure A.1 Inert Atmosphere System (IAS) used for titrations.

The setup consists of a 50 ml Erlenmeyer flask sealed with a rubber septum. The tip of the buret passes through the septum along with two needles. One needle is connected to an Ar cylinder (N_2 could also be used) through a regulator. The other is connected to a water seal. Care should be taken to ensure that the needle tips do not interfere with the buret tip. The flow rate is adjusted to give roughly 1-2 bubbles per second. Higher rates are not required and can cause problems with excess pressure in the flask. Bubbling for 5 minutes is usually sufficient to flush air from the flask. The various solutions are added using syringes through the septum. The flask contains a magnetic stirring bar and is placed in a 250 ml beaker on top of a magnetic stirrer. In the final stage of the titration, the solution is cooled by adding ice water to the 250 ml beaker.

A Jencons 25 ml Digitrate digital buret was used. It consists of a large reservoir and a 25 ml cylinder fitted with a piston that dispenses the titrant. The dispensed volume is measured electronically based on the piston position. Stated accuracy was 0.01 ml, but 0.02 is probably more reasonable. It is designed to allow refilling of the cylinder during use, but a variable backlash error of 0.06 to 0.15 ml was noted and so the maximum dispensed volume was therefore 25 ml in a single titration. This limit, combined with the sample size available, determines the optimal thiosulphate solution concentration (see below). A conventional buret could be used, but care must be taken that the Ar pressure in the flask is low enough to allow the thiosulphate solution to enter.

Solutions Required:

2 M HCl — About 250 ml distilled water is placed in a 1000 ml volumetric flask, 165 ml of full strength (39.6 M) HCl is added, and diluted to 1000 ml with distilled water.

1M HCl — 250 ml of 2 M HCl is placed in a 500 ml volumetric flask and diluted to 500 ml with distilled water.

If stored in closed containers, these solutions are stable more or less indefinitely.

All the remaining solutions need to be prepared using freshly boiled distilled water (to remove dissolved CO_2).

2 M KI — 16.60 (33.20) g of KI are placed in a 50 (100) ml volumetric flask and diluted to the required volume with distilled water.

0.7 M KI — 5.810 (11.620) g of KI are placed in a 50 (100) ml volumetric flask and diluted to the required volume with distilled water.

The KI solutions are not air stable and decompose according to the reaction:

$$6I^- + O_2 + 4H^+ \rightarrow I_3^- + 2H_2O \qquad \textbf{(A.6)}$$

They therefore need to be prepared fresh for each investigation. 50 ml of each are sufficient to analyze one sample (Approximately ½ day work) 100 ml is sufficient for two samples. There is not much point in preparing larger amounts. The solutions should be clear and colourless, any trace of orange indicates decomposition. Adding a small amount of starch solution to a portion of the solution can check this. Decomposition will be indicated by a blue colour.

Starch — ~1 g of soluble starch is mixed with a small quantity of distilled water to form a paste. This paste is washed into 100 ml of boiling distilled water. Boiling is continued for a couple of minutes. The cooled solution should be clear and colourless, with no suspended particles. The solution is reasonably stable, but should not be used if it appears cloudy.

Thiosulphate — The optimal concentration is determined by two factors. With the buret used, ~ 20 ml of titrant could be reliably dispensed. A total of six titrations were carried out on a given sample and the starting mass was ~250 mg. This gives an average sample size (allowing for grinding losses) of about 40 mg. 40 mg of $Bi_2Sr_2CaCu_2O_{8+y}$ contains ~ 0.09 mmol of Cu. Combining these gives a thiosulphate concentration of ~ 0.005 M, and this was used.

0.005 M $S_2O_3^{2-}$ — 1.2409 g of $Na_2S_2O_3 \cdot 5H_2O$ is placed in a 1000 ml volumetric flask and diluted to 1 l with freshly boiled (and cooled) distilled water.

Thiosulphate solutions are subject to oxidation through the reaction

$$S_2O_3^{2-} + H^+ \rightarrow HSO_3^- + S_{(s)} \qquad \textbf{(A.7)}$$

where H^+ can come from dissolved CO_2. Despite A.7, the solution was found to be stable for a month or more, based on standardizations with CuO, when stored in the brown reservoir bottle of the buret. Solutions that had been prepared with distilled water that had not been freshly boiled were not stable.

Procedure

A standardized analysis of a BSCCO sample consisted of 9 titrations. The sample was first ground and placed in a dessicator overnight. The next day, 3 CuO standardizations (Titration IIS) were made for practice, followed by 3 each of Titrations I and II. Blank determinations (Titration IA) were made infrequently as previous work had shown reasonable consistency. The titrations are outlined below.

Titration I – Excess charge determination

Required materials: syringes containing
- 10 ml 2 M KI
- 10 ml 2 M HCl
- 4 ml distilled water (freshly boiled)
- 1 ml starch indicator

1. ~ 40 mg of sample is accurately weighed into a 50 ml flask, a stirring bar is added and the flask is connected to the IAS. Ar flow is started.
2. After 5 minutes of Ar flow, the KI is added and stirring begun.
3. Within 30 seconds of adding the KI, the HCl is added.

   The timing of 2 and 3 are critical. The Bi in BSCCO reacts with I^- in solution, and this forms a surface layer, which impedes the BSCCO dissolving[1]. Rapid addition of the HCl is therefore important. The KI and HCl cannot be added in reverse order due to reaction A.6. Reaction A.2 most likely occurs at the surface as the BSCCO dissolves, so it is essential to have I^- available.

   When done properly, a clear deep orange (due to Bi^{3+} – I^- and I_3^- complexes) solution is formed, with no suspended material or black material adhering to the stirring bar. Stirring can be stopped briefly to check. Full dissolution is usually achieved in about 5 minutes.
4. When fully dissolved, the water is added.
5. The titration is begun. The first 10 – 15 ml can be added fairly rapidly, but care is needed to avoid overshooting the endpoint.
6. A slight fading of the orange colour indicates the approach of the end point. The solution becomes more yellow.
7. The starch is added at this point and ice water is placed in the outer beaker. The solution is allowed to cool for about 5 minutes.

   If the endpoint has not been exceeded, the solution will be dark brown-black and opaque.
8. The titration is carried out dropwise until the endpoint, with short pauses between additions. The solution will change colour from dark brown-black to a dirty orange-brown to clear orange (close to the initial colour) and finally to a clear golden yellow (endpoint).
9. Further additions make no change in colour, so the endpoint is taken as the last addition that caused a change. The endpoint is characteristic and recognizable, with practice !

---

[1] This fact was finally discovered by attempting to dissolve Bi_2O_3 in a KI solution. The yellow Bi_2O_3 becomes dark reddish and fairly resistant to dissolving, even after HCl is added. In addition, Bi^{3+} forms BiOCl in dilute acid solution, which is sparingly soluble. Probably both these processes occur as the BSCCO is dissolving. It was found that if more than about a minute elapses before the addition of HCl, the BSCCO will not dissolve completely, even after an hour or more.

Titration IA – Blank determination

The entire procedure for Titration I is followed but no sample is used. It was generally found that the procedure had an offset of ~ 0.5 ml. (ie. 0.5 ml of thiosulphate were required to eliminate the blue colour formed on the addition of starch.

Titration II – Copper determination

Required materials: syringes containing 10 ml 0.7 M KI
1 ml starch indicator

1. ~ 40 mg of sample is accurately weighed into a 50 ml flask and 10 ml 1 M HCl is added.
2. The solution is boiled for ~ 10 minutes. Additional HCl is added as necessary to prevent the solution boiling dry.
3. The solution is allowed to cool, a stirring magnet added and connected to the IAS. Ar flow is started. At this point, there should be about 10 ml of clear pale blue solution.
4. After 5 min of Ar flow, the KI is added. A dark cloudy orange solution is formed.
5. The titration is begun. The first 10 – 15 ml can be added fairly rapidly, but care is needed to avoid overshooting the endpoint.
6. A slight fading of the orange colour indicates the approach of the end point. The solution becomes more yellow.
7. The starch is added at this point and ice water is placed in the outer beaker. The solution is allowed to cool for about 5 minutes.

   If the endpoint has not been exceeded, the solution will be dark brown-black and opaque.

10. The titration is carried out dropwise until the endpoint, with short pauses between additions. The solution will change colour from dark brown-black to a dirty orange-brown to cloudy orange (close to the initial colour) and finally to a cloudy golden yellow (endpoint).
11. Further additions make no change in colour, so the endpoint is taken as the last addition that caused a change. The endpoint is characteristic and recognizable, with practice !

Numerous blank determinations on Titration II failed to show a response. This is most likely due to the lower concentrations of HCl and KI used. A high I^- concentration for Titration I ensures reaction A.2 occurs in preference to A.3. Attempts to use a lower HCl concentration made the dissolution process even more problematic.

Titration IIS – $S_2O_3^{2-}$ Standardization

This is Titration II applied to a known amount of high purity CuO. The CuO should be dried before use (stored 24+ hours in a drying oven at over 100 °C).

Required materials: syringes containing 10 ml 0.7 M KI
1 ml starch indicator

1. ~ 9 mg of CuO is accurately weighed into a 50 ml flask and 10 ml 1 M HCl is added.
2. The solution is boiled for ~ 10 minutes. Additional HCl is added as necessary to prevent the solution boiling dry.

3. The solution is allowed to cool, a stirring magnet added and connected to the IAS. Ar flow is started. At this point, there should be about 10 ml of clear pale blue solution.
4. After 5 min of Ar flow, the KI is added. A cloudy orange solution is formed.
8. The titration is begun. The first 10 – 15 ml can be added fairly rapidly, but care is needed to avoid overshooting the endpoint.
9. A fading of the orange colour indicates the approach of the end point.
10. The starch is added at this point and ice water is placed in the outer beaker. The solution is allowed to cool for about 5 minutes.

    If the endpoint has not been exceeded, the solution will be dark blue-black.

12. The titration is carried out dropwise until the endpoint, with short pauses between additions. The solution will change colour from dark blue-black through purple to a cloudy light pink. The endpoint is indicated by the fading of pink to white.
13. Further additions make no change in colour, so the endpoint is taken as the last addition that caused a change.

Calculations

The reactions for Titration I, A.1, A.2 and A.5, can be rewritten as

$$x I^- + Cu^{(1+x)+} \rightarrow \tfrac{1}{2} x I_2 + Cu^+ \qquad \text{(A.8)}$$

$$\tfrac{1}{2} x I_2 + x S_2O_3^{2-} \rightarrow x I^- + \tfrac{x}{2} S_4O_6^{2-} \qquad \text{(A.9)}$$

which shows that the charge above 1^+ on the Cu, x, can be determined from the volume of thiosulphate, V_1, required to reach the endpoint. Per gram of sample, x_g, this is

$$x_g = \frac{CV_1}{M_1} \qquad \text{(A.10)}$$

where C is the thiosulphate concentration and the subscript 1 refers to Titration I. Similarly using A.2 and A.5, the number of moles of Cu per gram of sample, n, is

$$n = \frac{CV_2}{M_2} \qquad \text{(A.11)}$$

Hence the excess charge per Cu is

$$x = \frac{x_g}{n} = \frac{V_1M_2}{V_2M_1} \qquad \text{(A.12)}$$

The hole concentration, p, is defined as the charge in excess of 2^+ per Cu. Charge balance using valences of Bi^{3+}, Sr^{2+}, Ca^{2+}, $Cu^{(2+p)+}$ and O^{2-} shows that for $Bi_2Sr_2CaCu_2O_{8+y}$, the hole concentration, p, and the oxygen content, y, are identical, so that

$$p = y = x - 1 = \frac{V_1M_2}{M_1V_2} - 1 \qquad \text{(A.13)}$$

The hole concentration is always given by A.13, but other relations will apply for the oxygen content in materials like $YBa_2Cu_3O_{7-\delta}$.

The purpose of Titration II is precisely to allow the cancellation of the thiosulphate concentration in determining x. If the thiosulphate concentration is accurately known, A.11 can be used to determine the copper content of the sample, and this is one reason for performing so many standardizations with CuO. Others are monitoring the thiosulphate concentration for decomposition and to provide practice before performing titrations on "irreplaceable" samples. Using A.11, the percentage of copper by mass is

$$\% = (6354.9\,\%_{mol})\frac{CV_2}{M_2} \qquad \textbf{(A.14)}$$

In BSCCO 2212, this percentage varies slightly with y, but is generally ~ 14 %. The thiosulphate concentration is calculated as

$$C = \frac{M_{CuO}}{(79.549\,\%_{mol})V_{CuO}} \qquad \textbf{(A.15)}$$

where the CuO subscript refers to the results of Titration IIS.

Data Analysis

Typical raw data are given below. Experimental uncertainties in mass and volume are 0.1 mg and 0.02 ml respectively.

As Received Hoechst BSCCO

Table A.1 Titration I – Raw Data

Trial #	M_1 (mg)	V_1 (ml)	V_{1cor} (ml)	V_{1cor}/M_1 (ml/mg)	Uncertainty (ml/mg)
1	41.1	21.41	20.90	0.509	0.003
2	40.7	21.37	20.86	0.513	"
3	41.8	21.54	21.03	0.503	"

Table A.2 Titration II – Raw Data

Trial #	M_2 (mg)	V_2 (ml)	V_2/M_2 (ml/mg)	Uncertainty (ml/mg)
1	40.7	18.04	0.443	0.002
2	42.9	19.06	0.444	"
3	41.2	18.13	0.440	"

10 blank determinations (Titration IA) gave an average of 0.51 ± 0.04 ml offset. This value is subtracted from V_1 to give V_{1cor}. No corrections were made to V_2. Rather using the average result for each set of titrations to find y, nine separate calculations were made and averaged and the standard deviation found, as outlined below in table A.3. This method has no effect on the value of y, but does give a better estimate for the standard deviation.

Generally, the results from different titrations on the same sample showed a variation slightly above the estimated experimental uncertainty so it is possible that this uncertainty has been under estimated.

The standard deviation of the nine different calculations is therefore used as the final estimate of the uncertainty in y.

Table A.3 Calculation of y

V_{1cor}/M_1 (ml/mg)	V_2/M_2 (ml/mg)	y	y uncertainty
0.509	0.443	0.149	0.002
"	0.444	0.146	"
"	0.440	0.157	"
0.503	0.443	0.158	"
"	0.444	0.155	"
"	0.440	0.166	"
0.513	0.443	0.135	0.001
"	0.444	0.133	"
"	0.440	0.143	0.002
Average		0.149	0.002
Standard Deviation		0.010 -	

Thus for the as received Hoechst BSSCO, y = 0.149 ± 0.010.

Typical results of a standardization with CuO are given below.

Table A.4 CuO Standardization Data

Trial #	M_{CuO} (mg)	V_{CuO} (ml)	$[S_2O_3^{2-}]$ (mM)	Error (mM)
1	7.7	19.20	5.04	0.07
2	10.7	26.76	5.03	0.05
3	8.6	21.58	5.01	0.06
Average			5.03	0.06

Using A.14 and the data from Titration II, this gives a value of 14.1 ± 0.2 % Cu by mass for the as received Hoechst BSCCO. For y = 0.149, the expected value is 14.26 %, showing reasonable agreement. It was generally found that the Cu mass percentage was slightly lower than expected.